NUREG/CR-1318
RO

Analytical and Experimental Studies of a Beam with a Geometric Nonlinearity

Manuscript Completed: June 1980
Date Published: November 1980

Prepared by
Y. A. Mariamy, S. F. Masri, J. C. Anderson

Department of Civil Engineering
University of Southern California
Los Angeles, CA 90007

Prepared for
Division of Reactor Safety Research
Office of Nuclear Regulatory Research
U.S. Nuclear Regulatory Commission
Washington, D.C. 20555
NRC FIN No. B5976

8012080014

ABSTRACT

Analytical and experimental studies of the dynamic response of a system with a geometric nonlinearity that is encountered in many practical engineering applications are described. An exact solution for the steady-state motion of a viscously damped Bernoulli-Euler beam with an unsymmetric geometric nonlinearity, under the action of harmonic excitation, is derived. Experimental measurements with a mechanical model verify the analytical findings. The effect of various parameters on the system response is determined. Major conclusions based on this investigation are presented.

TABLE OF CONTENTS

LIST OF FIGURES

Figure		Page

NOMENCLATURE

$A_i^{(j)}$ = amplification ratio for the i^{th} mode and j^{th} solution region

C = a linear operator of L^* and M

$F(x,t)$ = harmonically varying load, $F(x,t)=F(x)\cos\Omega t$

$K_i^{(j)}$ = the i^{th} mode generalized stiffness for the j^{th} solution region

K_s, K_t = spring stiffness of striker and target, respectively

K^* = stiffness ratio of target to striker beam

L = length of beam

L^* = a linear differential operator

$M_i^{(j)}$ = the i^{th} mode generalized mass for the j^{th} solution region

$M(x)$ = uniform mass density of striker beam

$Q_i^{(j)}(x)$ = the i^{th} mode forcing function for the j^{th} solution region

S_o = amplitude of base motion

$S(t)$ = base excitation, $S(t) = S_o \cos\Omega t$

T_c^* = dimensionless contact time = $1 - \alpha_2/(2\pi)$

$W(x,t)$ = striker beam displacement

$\dot{W}(x,t)$ = striker beam velocity

$W''(x,t)$ = striker beam second derivative with respect to x

d = gap size

h = gap location along beam

t = time

α, β = coefficients of proportional damping

α_o = phase angle between excitation and response

α_2 = fraction of excitation period during which $W^{(1)}(h,t) \le d$

$\varepsilon_1, \varepsilon_2$ = strain of striker and target beams, respectively, at specified locations

$\zeta_i^{(j)}$ = the i^{th} mode of critical damping for the j^{th} solution region of the striker beam

$\omega_i^{(j)}$ = the i^{th} frequency of the striker beam for the j^{th} solution region

Ω = frequency of harmonic excitation

ACKNOWLEDGEMENTS

This study was supported in part by a contract with the U.S. Nuclear Regulatory Commission. The assistance of S. Beckwith, D. Oba, and J. Radler in the preparation of the report is appreciated.

Chapter 1

INTRODUCTION

1.1 Background

The problem of forced vibration of a dynamic system with motion limiting stops is of great importance in many practical engineering applications. Some cases in which this problem is encountered are (1) the effect of gapped supports on the response of nuclear piping subjected to postulated rupture conditions, (2) the vibration of mechanical equipment possessing deadspace nonlinearities, and (3) the vibration isolation of dynamic systems mounted on resilient supports with motion-limiting stops.

Several investigators have conducted analytical, numerical, and experimental studies of dynamic systems with geometric nonlinearities (present, in some cases, together with material nonlinearities). These studies may be classified into two main categories based on the method of investigation.

1.1.1 Analytical Studies

Investigators performing analytical studies have, in many cases, resorted to numerical techniques. For example, Anderson and Singh (1976) and Moreadith, et al. (1973) performed analytical studies on nuclear steam piping subjected to impulsive rupture loads. Anderson used a discretization technique to model the piping system with the application of a numerical procedure on finite element concepts.

Masri (1978) reported the results of an extensive analytical/experimental study of a system having a geometric nonlinearity. He developed an exact closed-form solution for the steady-state motion of a simplified mathematical model of a cantilever (striker) beam carrying a concentrated mass whose motion is limited on one side by a stop (target) beam and that is subjected to harmonic excitation.

Anderson and Masri (1979) recently reported the results of analytical and experimental studies of the dynamic response of a system consisting of a cantilever beam with a gapped support at the free end. The system, represented as a single-degree-of-freedom system having generalized properties, was subjected to a dynamic excitation of sinusoidal and impulsive base accelerations. Their study extended Masri's earlier work (1978) to systems having both material and geometric nonlinearity.

Den Hartog and Heiles (1936) presented an exact theory for the solution of some types of couplings having springs with an initial set. Quantitative results were obtained by performing numerical calculations. Iwan (1968) discussed the steady-state response of a system constrained by a limiting slip joint and excited by a trigonometrically varying external load.

Recently, Onesto (1979) evaluated the response sensitivity to various snubber parameters and established ranges for those parameters that will bound system response to acceptable limits. In his study, Onesto first used simple models with simple loadings to establish dimensionless response parameters permitting insight into the basic problem, after which he went on to study more sophisticated models and loading (multi-degree-of-freedom lumped mass models).

Kotwicki, Chang, and Johnson (1979) recently performed studies aimed at the demonstration of the effects of varying support parameters on the dynamic response of piping systems. The parameters evaluated were the stiffness of the supports, gap size, and single-acting versus double-acting supports. The dynamic loadings considered were seismic response spectra, relief-valve hydraulic thrust, and postulated pipe rupture. They concluded that varying these parameters changed the system response significantly for the cases considered.

In all of the previously mentioned studies, the system has usually been considered a single- or multiple-degree-of-freedom system but not a continuous system. For the vibration problem in a piping system, however, the piping should be treated as a beam -- that is, as a continuous system. Watanabe (1978) presented an approximate analytical solution for the problem of a cantilever beam with symmetric elastic stops on both sides of the beam by considering the beam a continuous system and neglecting the damping effects.

1.1.2 Experimental Studies

In addition to the analytical studies mentioned, some experimental work has been done on the problem of dynamic systems with gaps. All of the experimental studies were mainly designed to gain insight into the unknown, basic dynamic behavior of the type of systems mentioned and to verify the validity of the analytical models proposed. In the analytical/experimental work conducted by Masri (1976), the effects of various system parameters and model sizes were presented and the simplified analytical single-degree-of-freedom system proposed was found to satisfactorily agree with the experimental findings. Anderson and Masri (1979) investigated systems having both geometric and material nonlinearity, and they made critical comparisons between calculated and measured responses.

Although the investigations have added considerable knowledge to the subject, no results are available in the published literature regarding the exact response of continuous systems with inherent energy dissipation and a geometric nonlinearity under the action of an arbitrary dynamic environment.

1.2 Scope of Study

To better determine the dynamic response of realistic nonlinear structural systems, this study concerns the exact solution for the steady-state motion of a viscously damped Bernoulli-Euler beam with an symmetric geometric nonlinearity, which is subjected to harmonic excitation. The elastic beam is assumed to have uniform properties and arbitrary boundary conditions. The geometric nonlinearity is an elastic spring placed at some arbitrary location within the span of the beam and separated from the beam by a certain gap.

Chapter 2 describes the analytical studies, including the formulation of the problem and the solution algorithm. The experimental studies that were conducted are presented in Chapter 3. In Chapter 4 the analysis is applied to an example problem and the effects of system parameters are investigated. Major conclusions based on this investigation and recommendations for future work are presented in Chapter 5.

Chapter 2

ANALYTICAL STUDIES

2.1 Description of the Problem

The model under consideration consists of a continuous beam with an elastic stop placed at a specified distance h from its left end, as shown in Figure 2.1. Although the figure shows a propped beam with an elastic stop at a distance h from the support, the solution technique also applies to beams with arbitrary boundary conditions. The striker beam is modeled as a continous Bernoulli beam with viscous damping, and the target beam as a spring.

The exact closed-form solution for the steady-state motion of the system was based on the assumption that when the system is harmonically excited, the predominant response is one in which the beam contacts the elastic stop once per cycle, and the conditions of the system are repeated once per excitation cycle. This assumed motion reflects the motion found by investigators to dominate in most experimental studies of such systems.

2.2 Formulation

The system consists of a viscously damped beam of mass M(x) and stiffness EI, which is separated by a gap d from an elastic stop (spring) placed at a distance h from its support and having a stiffness K_t. The system is excited through harmonic base motion.

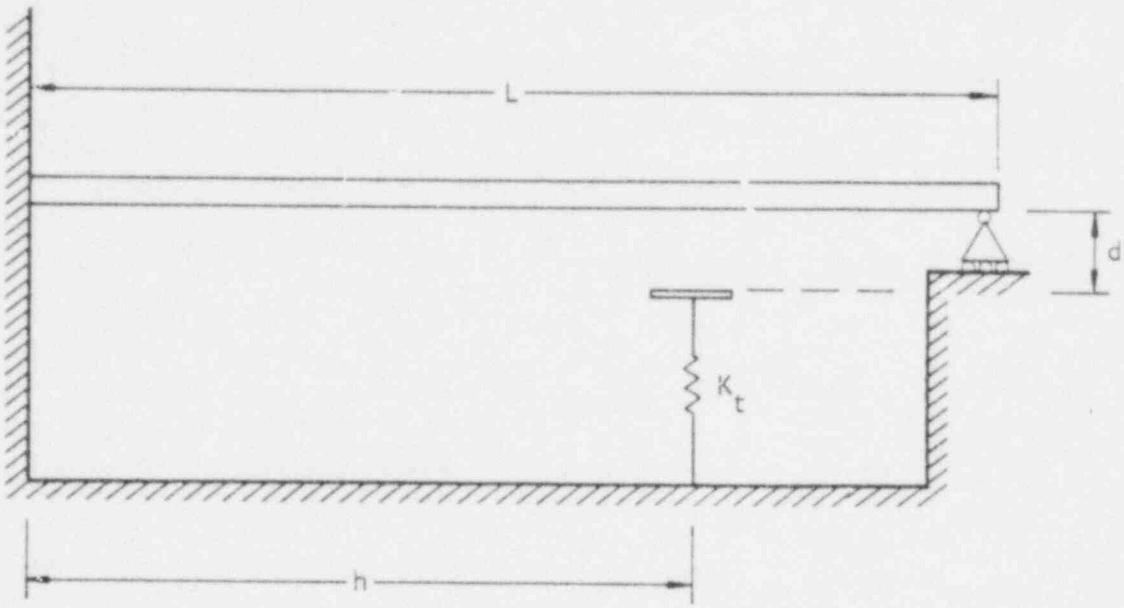

FIGURE 2.1 MODEL OF SYSTEM

The system is governed by the partial differential equation

$$L^*[W(x,t)] + \frac{\partial}{\partial t} C[W(x,t)] + M(x) \frac{\partial^2 W(x,t)}{\partial t^2} = F(x,t) \qquad (2.1)$$

over the length L of the beam, where

L^* = A linear, homogeneous, self-adjoint differential operator of order 2p with respect to spatial coordinate x that specifies the stiffness distribution of the beam.

C = An operator that is a linear combination of operator L^* and function M, viz.,

$$C = \alpha M + \beta L^* \qquad (2.2)$$

in which α and β are constant coefficients.

M = A function that specifies the mass distribution of the beam.

F(x,t) is a harmonically varying load equal to

$$F(x) \cos \Omega t \qquad (2.3)$$

with

$$F(x) = \Omega^2 S_o M(x) \qquad (2.4)$$

for base excitation.

2.3 Steady-State Solution

From the experimental studies of previous investigators (e.g., Masri, 1976) as well as from the experimental observations of Section 3, it has been found that the predominant type of response is that in which the beam contacts the elastic stop, and the conditions of the system are repeated once per cycle of the excitation.

The steady-state solution of the system shown in Figure 2.1 is developed using the normal-mode approach. The solution consists of two segments corresponding to $W^{(1)}(h,t) \leq d$, i.e., when there is no contact between the beam and the elastic stop (the spring), and $W^{(2)}(h,t) \geq d$, i.e., the solution region in which the beam and the elastic stop are in contact (see Figure 2.2). The solution should satisfy certain conditions of continuity of the displacement and velocity of the system at times of release and contact for one cycle. These conditions may be stated as follows:

(a) Everywhere along the beam, the displacement $W^{(1)}(x,\alpha_2)$ and velocity $\dot{W}^{(1)}(x,\alpha_2)$ at the end of the first region of solution (the no-contact solution region) should be equal to the corresponding displacement and velocity at the beginning of the second solution region.

(b) Everywhere along the beam, the displacement $W^{(1)}(x,\alpha_1)$ and velocity $\dot{W}^{(1)}(x,\alpha_1)$ at the beginning of the first solution region should equal the displacement $W^{(2)}(x,\alpha_3)$ and velocity $\dot{W}^{(2)}(x,\alpha_3)$ at the end of the second solution region (contact region).

(c) At the point of contact between the beam and the elastic stop, the displacements $W^{(1)}(h,\alpha_1)$, $W^{(1)}(h,\alpha_2)$, $W^{(2)}(h,\alpha_2)$, and $W^{(2)}(h,\alpha_3)$ at the beginning and the end of both solution regions should be equal to the gap d. All of these conditions are stated mathematically in Equations 2.15 to 2.20 of Section 2.3.2. Details of the solution are in the following sections.

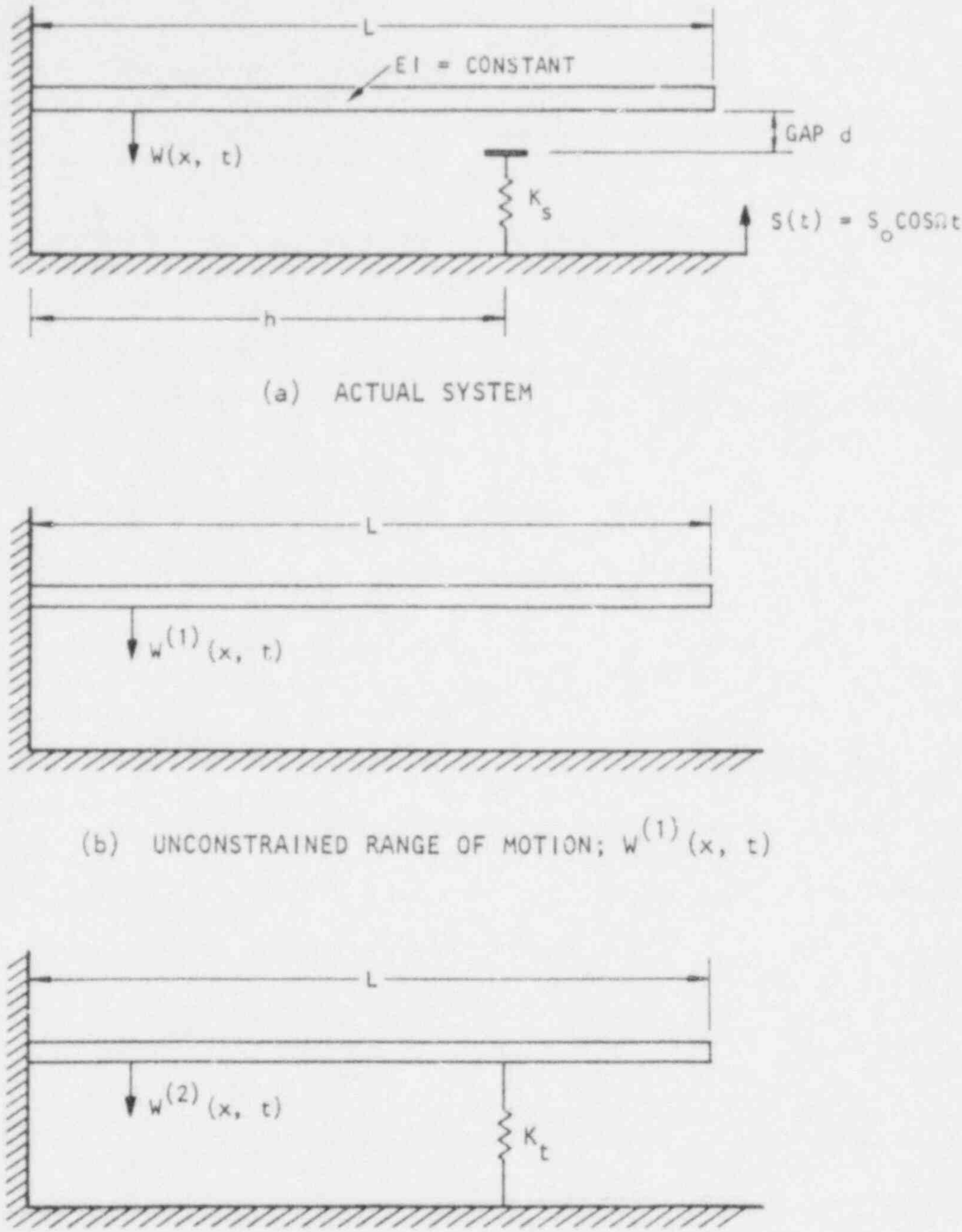

(a) ACTUAL SYSTEM

(b) UNCONSTRAINED RANGE OF MOTION; $W^{(1)}(x, t)$

(c) CONSTRAINED RANGE OF MOTION; $W^{(2)}(x, t)$

FIGURE 2.2 REGIMES OF MOTION OF ELASTIC BEAM WITH GEOMETRIC NONLINEARITY

2.3.1 Frequencies and Mode Shapes

In order to use the normal-mode method of analysis of the response of continuous systems, it is first necessary to determine the natural frequencies and modal configurations. Two types of frequencies and eigenfunctions are used in the solution of the problem (Figure 2.2a): (1) the frequencies and mode shapes of the elastic beam alone, which represents the system when there is no elastic stop (Figure 2.2b), and (2) those of the beam with the spring, i.e., the constrained beam (Figure 2.2c), which represents the case where the elastic stop is attached to the beam at all times.

Procedures for the derivation of the frequencies and modal shapes of beams such as those in Figure 2.2 may vary considerably depending on the type of system under consideration. Details on this subject are available in numerous publications (see, for example, Gorman (1975), Clough and Penzien (1975), Young (1948), McBride (1943), and Lee and Saibel (1952)). In the present work, the frequencies and mode shapes are derived through the solution of the homogeneous beam differential equation that expresses equilibrium between inertia forces and elastic restoring forces, subject to prescribed boundary conditions. A summary of the analysis is presented in Appendix A.

2.3.2 Solution Procedure

Referring to Figure 2.3, let $\phi_i^{(j)}(x)$ be the i^{th} eigenfunction associated with the homogeneous equation of the undamped system for the j^{th} solution region and assume that the eigenfunctions satisfy the orthogonality condition.

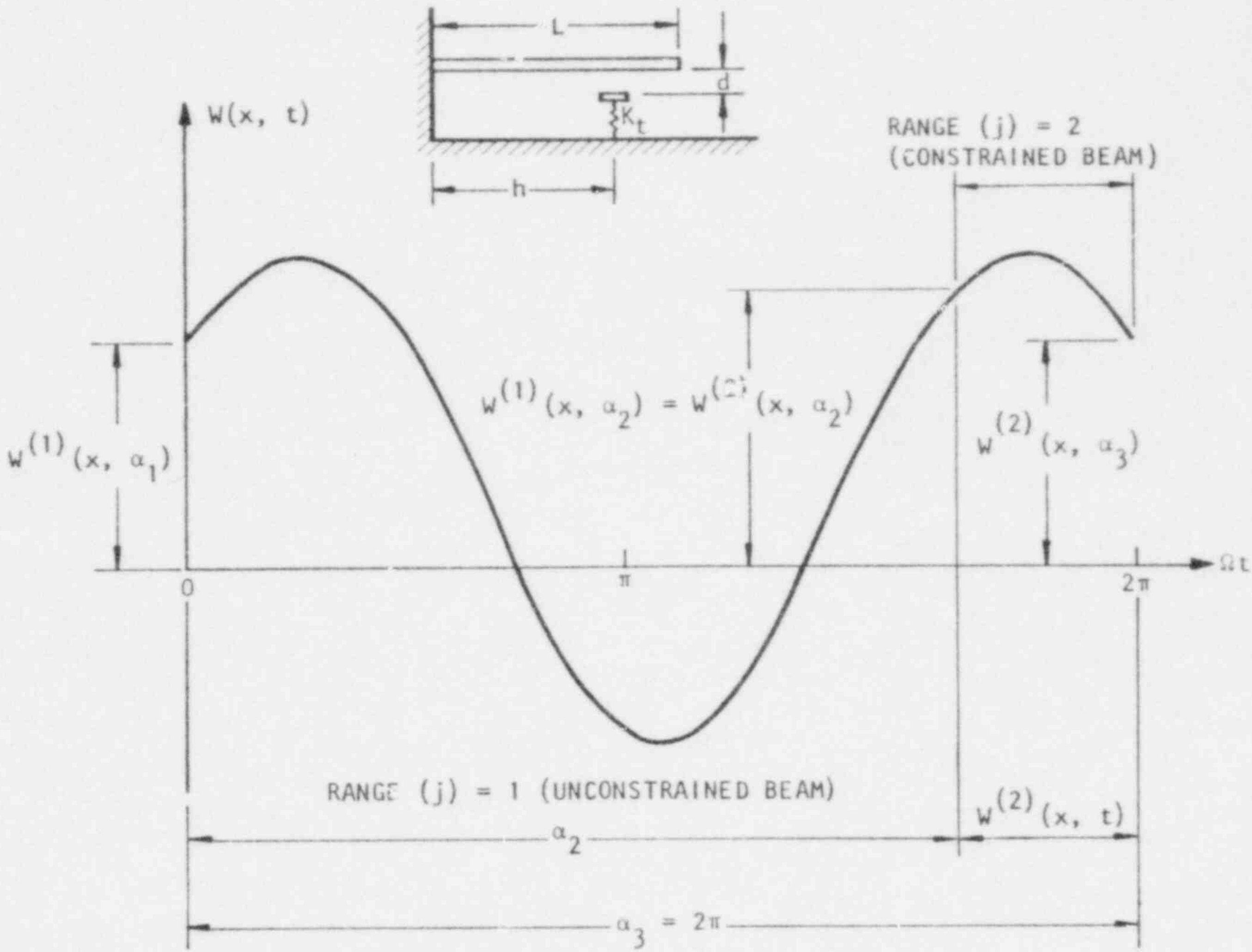

FIGURE 2.3 RANGES OF MOTION OF THE STEADY-STATE SOLUTION

$$\int_0^L \phi_i^{(j)}(x)\ M(x)\ \phi_s^{(j)}(x)dx \ = \ \delta_{is}M_i^{(j)} \tag{2.5}$$

and

$$\int_0^L \phi_i^{(j)}(x)\ L^*[\phi_s^{(j)}(x)]\ dx \ = \ \delta_{is}K_i^{(j)} \tag{2.6}$$

where δ_{is} is the Kronecker delta, and $M_i^{(j)}$ and $K_i^{(j)}$ are, respectively, the generalized mass and generalized stiffness of the i^{th} mode for solution region j.

Using the normal-mode approach, the solution for region j can be written as

$$W^{(j)}(x,t) \ = \ \sum_{i=1}^{\infty} \phi_i^{(j)}(x)\ q_i^{(j)}(t) \tag{2.7}$$

where $j = 1$ or 2, depending on the solution region.

Then substituting for $W^{(j)}(x,t)$ into Equation 2.1 leads to

$$M_i^{(j)}\ddot{q}_i^{(j)}(t) + C_i^{(j)}\dot{q}_i^{(j)}(t) + K_i^{(j)}q_i^{(j)}(t) = Q_i^{(j)}(t)$$

$$= \ \ [\int_0^L \phi_i^{(j)}(x)f_i^{(j)}(x)dx]\ \ \cos(\Omega t + \alpha_0) \tag{2.8}$$

where α_0 is a phase angle related to the origin t_0 by $\alpha_0 = \Omega t_0$.

The solution of Equation 2.8 is

$$q_i^{(j)}(t) = \exp\left[-\frac{\zeta_i^{(j)}}{r_i^{(j)}}(\Omega t - \alpha_j)\right]\Bigg\langle q_i^{(j)}(\alpha_j)$$

$$\left\{\frac{1}{\eta_i^{(j)}}\left[\zeta_i^{(j)} \sin \frac{\eta_i^{(j)}}{r_i^{(j)}}(\Omega t - \alpha_j)\right.\right.$$

$$\left.\left. + \eta_i^{(j)} \cos \frac{\eta_i^{(j)}}{r_i^{(j)}}(\Omega t - \alpha_j)\right]\right\}$$

$$+ \dot{q}_i^{(j)}(\alpha_j)\left\{\frac{1}{\omega_i^{(j)}\eta_i^{(j)}} \sin \frac{\eta_i^{(j)}}{r_i^{(j)}}(\Omega t - \alpha_j)\right\}$$

$$+ \sin \theta_i^{(j)}\left\{\frac{A_i^{(j)}}{\eta_i^{(j)}} r_i^{(j)} \sin \frac{\eta_i^{(j)}}{r_i^{(j)}}(\Omega t - \alpha_j)\right\}$$

$$+ \cos \theta_i^{(j)}\left\{-\frac{A_i^{(j)}}{\eta_i^{(j)}}\left[\zeta_i^{(j)} \sin \frac{\eta_i^{(j)}}{r_i^{(j)}}(\Omega t - \alpha_j)\right.\right.$$

$$+ \eta_i^{(j)} \cos \frac{\eta_i^{(j)}}{r_i^{(j)}} (\Omega t - \alpha_j) \Bigg] \Bigg\} \Bigg\rangle$$

$$+ A_i^{(j)} \cos (\Omega t + \tau_i^{(j)}) \tag{2.9}$$

where

$$\omega_i^{(j)} = \sqrt{K_i^{(j)} / M_i^{(j)}} \;, \quad \zeta_i^{(j)} = C_i^{(j)} \Big/ 2\sqrt{K_i^{(j)} M_i^{(j)}}$$

$$\eta_i^{(j)} = \sqrt{1 - [\zeta_i^{(j)}]^2} \;, \quad r_i^{(j)} = \Omega / \omega_i^{(j)}$$

$$A_i^{(j)} = \left(f_i^{(j)} \Big/ K_i^{(j)} \right) \Big/ \sqrt{\left(1 - [r_i^{(j)}]^2\right)^2 + \left(2\zeta_i^{(j)} r_i^{(j)}\right)^2}$$

$$f_i^{(j)} = \int_0^L \phi_i^{(j)}(x) \, f^{(j)}(x) \, dx$$

$$\tau_i^{(j)} = \alpha_0 - \gamma_i^{(j)} \;,$$

$$\gamma_i^{(j)} = \tan^{-1} \left\{ 2\zeta_i^{(j)} r_i^{(j)} \Big/ \left(1 - r_i^{(j)}\right)^2 \right\}$$

subject to the conditions $\alpha_j \leq \Omega t \leq \alpha_{j+1}$

where

$$\alpha_1 = 0 \quad , \quad \theta_i^{(j)} = \tau_i^{(j)} + \alpha_j$$

and

$$\alpha_j = \Omega t_j \quad , \quad \alpha_2 \equiv \text{unknown to be determined,}$$

$$\alpha_3 = 2\pi$$

The velocity of the system is given by

$$\dot{q}_i^{(j)}(t) = \exp\left[-\frac{\zeta_i^{(j)}}{r_i^{(j)}}(\Omega t - \alpha_j)\right] \Bigg\langle q_i^{(j)}(\alpha_j)$$

$$\left\{-\frac{\omega_i^{(j)}}{\eta_i^{(j)}} \sin \frac{\eta_i^{(j)}}{r_i^{(j)}}(\Omega t - \alpha_j)\right\}$$

$$+ \dot{q}_i^{(j)}(\alpha_j) \left\{-\frac{1}{\eta_i^{(j)}}\left[\zeta_i^{(j)} \sin \frac{\eta_i^{(j)}}{r_i^{(j)}}(\Omega t - \alpha_j)\right.\right.$$

$$\left.\left. - \eta_i^{(j)} \cos \frac{\eta_i^{(j)}}{r_i^{(j)}}(\Omega t - \alpha_j)\right]\right\}$$

$$+ \sin \theta_i^{(j)} \left\{ - \frac{\omega_i^{(j)} r_i^{(j)} A_i^{(j)}}{\eta_i^{(j)}} \left[\xi_i^{(j)} \sin \frac{\eta_i^{(j)}}{r_i^{(j)}} (\Omega t - \alpha_j) \right. \right.$$

$$\left. \left. - \eta_i^{(j)} \cos \frac{\eta_i^{(j)}}{r_i^{(j)}} (\Omega t - \alpha_j) \right] \right\}$$

$$\left. + \cos \theta_i^{(j)} \left\{ \frac{\omega_i^{(j)} A_i^{(j)}}{\eta_i^{(j)}} \sin \frac{\eta_i^{(j)}}{r_i^{(j)}} (\Omega t - \alpha_j) \right\} \right\rangle$$

$$- \Omega A_i^{(j)} \sin (\Omega t + \tau_i^{(j)}) \tag{2.10}$$

subject to the condition

$$\alpha_j \le \Omega t \le \alpha_{j+1} .$$

Evaluating Equations 2.9 and 2.10 at $\Omega t = \alpha_{j+1}$ yields

$$q_i^{(j)}(\alpha_{j+1}) = S1_i^{(j)} q_i^{(j)}(\alpha_j) + S2_i^{(j)} \dot{q}_i^{(j)}(\alpha_j)$$

$$+ S5_i^{(j)} \sin \theta_i^{(j)} + S6_i^{(j)} \cos \theta_i^{(j)}$$

$$+ S7_i^{(j)} \cos(\alpha_{j+1} + \tau_i^{(j)}) \tag{2.11}$$

and

$$\dot{q}_i^{(j)}(\alpha_{j+1}) = S3_i^{(j)} q_i^{(j)}(\alpha_j) + S4_i^{(j)} \dot{q}_i^{(j)}(\alpha_j) + S8_i^{(j)} \sin \theta_i^{(j)}$$

$$+ S9_i^{(j)} \cos \theta_i^{(j)} + S10_i^{(j)} \sin (\alpha_{j+1} + \tau_i^{(j)}) \quad (2.12)$$

where all the undefined symbols are as given in Appendix B.

The solution for j = 1 is subject to the condition

$$\alpha_1 \leq \Omega t \leq \alpha_2 \quad (2.13)$$

and the solution for j = 2 is subject to the condition

$$\alpha_2 \leq \Omega t \leq \alpha_3 \ . \quad (2.14)$$

The problem solution should satisfy the following conditions:

$$W^{(1)}(x,\alpha_2) = W^{(2)}(x,\alpha_2) \equiv W_2(x) \quad (2.15)$$

$$\dot{W}^{(1)}(x,\alpha_2) = \dot{W}^{(2)}(x,\alpha_2) \equiv \dot{W}_2(x) \quad (2.16)$$

$$W^{(2)}(x,\alpha_3) = W^{(1)}(x,\alpha_1) \equiv W_1(x) \quad (2.17)$$

$$\dot{W}^{(2)}(x,\alpha_3) = \dot{W}^{(1)}(x,\alpha_1) \equiv \dot{W}_1(x) \quad (2.18)$$

$$W^{(2)}(x,\alpha_3)\Big|_{x=h} = W^{(1)}(x,\alpha_1)\Big|_{x=h} = W_1(h) = d \qquad (2.19)$$

$$W^{(1)}(x,\alpha_2)\Big|_{x=h} = W^{(2)}(x,\alpha_2)\Big|_{x=h} = W_2(h) = d \qquad (2.20)$$

Equations 2.15 through 2.20 provide six equations to solve for the unknowns $W_1(x)$, $W_2(x)$, $\dot{W}_1(x)$, $\dot{W}_2(x)$, α_0, and α_2.

Multiplying both sides of Equations 2.11 and 2.12 by $\phi_i^{(j)}(x)$ and summing over i with j = 1, 2 yields the following:

$$\sum_i \phi_i^{(1)}(x)\left\{ S1_i^{(1)} q_{i1} + S2_i^{(1)} \dot{q}_{i1} + S5_i^{(1)} \sin\theta_i^{(1)} \right.$$
$$\left. + S6_i^{(1)} \cos\theta_i^{(1)} + S7_i^{(1)} \cos\left(\alpha_2 + \tau_i^{(1)}\right) \right\}$$
$$= W_2(x) = \sum_i \phi_i^{(2)}(x) q_{i2} \qquad (2.21)$$

$$\sum_i \phi_i^{(1)}(x)\left\{ S3_i^{(1)} q_{i1} + S4_i^{(1)} \dot{q}_{i1} + S8_i^{(1)} \sin\theta_i^{(1)} \right.$$
$$\left. + S9_i^{(1)} \cos\theta_i^{(1)} + S10_i^{(1)} \sin\left(\alpha_2 + \tau_i^{(1)}\right) \right\}$$
$$= \dot{W}_2(x) = \sum_i \phi_i^{(2)}(x) \dot{q}_{i2} \qquad (2.22)$$

$$\sum_i \phi_i^{(2)}(x)\left\{ S1_i^{(2)} q_{i2} + S2_i^{(2)} \dot{q}_{i2} + S5_i^{(2)} \sin\theta_i^{(2)} \right.$$

$$+ S6_i^{(2)} \cos \theta_i^{(2)} + S7_i^{(2)} \cos \left(\alpha_3 + \tau_i^{(2)}\right)\Bigg\}$$

$$= W_1(x) = \sum_i \phi_i^{(1)}(x) q_{i1} \tag{2.23}$$

$$\sum_i \phi_i^{(2)}(x) \Bigg\{ S3_i^{(2)} q_{i2} + S4_i^{(2)} \dot{q}_{i2} + S8_i^{(2)} \sin \theta_i^{(2)}$$

$$+ S9_i^{(2)} \cos \theta_i^{(2)} + S10_i^{(2)} \sin \left(\alpha_3 + \tau_i^{(2)}\right)\Bigg\}$$

$$= \dot{W}_1(x) = \sum_i \phi_i^{(1)}(x) \dot{q}_{i1} \tag{2.24}$$

where

$$q_{i1} = q_i^{(1)}(\alpha_1) \tag{2.25a}$$

$$q_{i2} = q_i^{(2)}(\alpha_2) \tag{2.25b}$$

$$\dot{q}_{i1} = \dot{q}_i^{(1)}(\alpha_1) \tag{2.25c}$$

$$\dot{q}_{i2} = \dot{q}_i^{(2)}(\alpha_2) \tag{2.25d}$$

Using Equations 2.7, 2.11, and 2.12 together with Equations 2.19 and 2.20 yields

$$\sum_i \phi_i^{(2)}(h) q_i^{(2)}(\alpha_3) = \sum_i \phi_i^{(2)}(h) \Bigg\{ S1_i^{(2)} q_{i2} + S2_i^{(2)} \dot{q}_{i2}$$

$$+ S5_i^{(2)} \sin \theta_i^{(2)} + S6_i^{(2)} \cos \theta_i^{(2)}$$

$$+ S7_i^{(2)} \cos\left(\alpha_3 + \tau_i^{(2)}\right)\Bigg\} \quad = \quad d \qquad (2.26)$$

$$\sum_i \phi_i^{(1)}(h) q_i^{(1)}(\alpha_2) \quad = \quad \sum_i \phi_i^{(1)}(h) \Bigg\{ S1_i^{(1)} q_{i1} + S2_i^{(1)} \dot{q}_{i1}$$

$$+ S5_i^{(1)} \sin\theta_i^{(1)} + S6_i^{(1)} \cos\theta_i^{(1)}$$

$$+ S7_i^{(1)} \cos\left(\alpha_2 + \tau_i^{(1)}\right)\Bigg\} \quad = \quad d \qquad (2.27)$$

Using Equation 2.22, together with the orthogonality condition of Equations 2.5 and 2.6, yields

$$\dot{q}_{\ell 2} \quad = \quad \frac{1}{M_\ell^{(2)}} \sum_m \Bigg[C1_{\ell m} q_{m1} + C2_{\ell m} \dot{q}_{m1} + C3_{\ell m} \sin\theta_m^{(1)} + C4_{\ell m} \cos\theta_m^{(1)}$$

$$+ C5_{\ell m} \sin\left(\alpha_2 + \tau_m^{(1)}\right)\Bigg] \qquad (2.28)$$

Similarly, Equation 2.21 yields

$$q_{\ell 2} \quad = \quad \frac{1}{M_\ell^{(2)}} \sum_i \Bigg[C6_{\ell i} q_{i1} + C7_{\ell i} \dot{q}_{i1} + C8_{\ell i} \sin\theta_i^{(1)}$$

$$+ C9_{\ell i} \cos \theta_i^{(1)} + C10_{\ell i} \cos \left(\alpha_2 + \tau_i^{(1)}\right) \Big] \quad (2.29)$$

Substituting for $\dot{q}_{\ell 2}$ and $q_{\ell 2}$ from Equations 2.28 and 2.29 into Equations 2.23 through 2.26 yields

$$\sum_j \Big[h1_j q_{j1} + h2_j \dot{q}_{j1} + h3_j \sin \theta_j^{(1)} + h4_j \cos \theta_j^{(1)}$$

$$+ h5_j \cos\left(\alpha_2 + \tau_j^{(1)}\right) + h6_j \sin\left(\alpha_2 + \tau_j^{(1)}\right)$$

$$+ h7_j \sin \theta_j^{(2)} + h8_j \cos \theta_j^{(2)} + h9_j \cos\left(\alpha_3 + \tau_j^{(2)}\right) \Big]$$

$$= \sum_i \phi_i^{(1)}(x) q_{i1} = w_1(x) \quad (2.30)$$

$$\sum_p \Big[h10_p q_{p1} + h11_p \dot{q}_{p1} + h12_p \sin \theta_p^{(1)} + h13_p \cos \theta_p^{(1)}$$

$$+ h14_p \cos\left(\alpha_2 + \tau_p^{(1)}\right) + h15_p \sin\left(\alpha_2 + \tau_p^{(1)}\right)$$

$$+ h16_p \sin \theta_p^{(2)} + h17_p \cos \theta_p^{(2)} + h18_p \sin\left(\alpha_3 + \tau_p^{(1)}\right) \Big]$$

$$= \sum_p \phi_p^{(1)}(x) \dot{q}_{p1} = \dot{w}_1(x) \quad (2.31)$$

and

$$\sum_k \Big[h19_k q_{k1} + h20_k \dot{q}_{k1} + h21_k \sin \theta_k^{(1)} + h22_k \cos \theta_k^{(1)}$$

$$+ h23_k \cos\left(\alpha_2 + \tau_k^{(1)}\right) + h24_k \sin\left(\alpha_2 + \tau_k^{(1)}\right)$$

$$+ h25_k \sin \theta_k^{(2)} + h26_k \cos \theta_k^{(2)}$$

$$\left. + h27_k \cos\left(\alpha_3 + \tau_k^{(2)}\right)\right] = d \tag{2.32}$$

Also, Equation 2.26 can be written as:

$$\sum_i \left[h28_i q_{i1} + h29_i \dot{q}_{i1} + h30_i \sin \theta_i^{(1)} + h31_i \cos \theta_i^{(1)}\right.$$

$$\left. + h32_i \cos\left(\alpha_2 + \tau_i^{(1)}\right)\right] = d \tag{2.33}$$

From the definition of $\tau_i^{(j)}$ and $\theta_i^{(j)}$,

$$\theta_i^{(j)} = \alpha_o + (\alpha_j - \gamma_i^{(j)}) . \tag{2.34}$$

Making use of trigonometric identities to express sin and cos of $\theta_i^{(j)}$ in terms of α_o and α_j, then Equations 2.30 through 2.33 become

$$\sum_j \left[h1_j q_{j1} + h2_j \dot{q}_{j1} + h50_j \sin \alpha_o + h51_j \cos \alpha_o\right]$$

$$= \sum_j \phi_j^{(1)}(x) q_{j1} \tag{2.35}$$

$$\sum_p \left[h10_p q_{p1} + h11_p \dot{q}_{p1} + h52_p \sin \alpha_o + h53_p \cos \alpha_o\right]$$

$$= \sum_p \phi_p^{(1)}(x) q_{p1} \qquad (2.36)$$

$$h19_k p_{k1} + h20_k \dot{q}_{k1} + h60_1 \sin \alpha_o + h61_k \cos \alpha_o = d \qquad (2.37)$$

$$h28_i q_{i1} + h29_i \dot{q}_{i1} + h62_i \sin \alpha_o + h63_i \cos \alpha_o = d \qquad (2.38)$$

Note that Equations 2.35 through 2.38 provide four equations through which the unknowns q_{i1}, $\dot{q}_{i1}$, α_o, and α_2 can be determined.

The orthogonality conditions of Equations 2.5 and 2.6 can be further used with Equations 2.35 and 2.36 to yield

$$q_{\ell 1} = \sum_j [H1_{\ell j} q_{j1} + H2_{\ell j} \dot{q}_{j1} + H3_{\ell j} \sin \alpha_o + H4_{\ell j} \cos \alpha_o] \qquad (2.39)$$

$$q_{m1} = \sum_p [H5_{mp} \dot{q}_{p1} + H6_{mp} q_{p1} + H7_{mp} \sin \alpha_o + H8_{mp} \cos \alpha_o] \qquad (2.40)$$

2.3.3 Equation Solution

The solution for the unknowns α_o, α_2, q_{i1}, and $\dot{q}_{i1}$ in Equations 2.37 through 2.40 involves expanding each equation in the number of modes chosen and forming a matrix of the coefficients of q_{i1}, $\dot{q}_{i1}$, $\sin \alpha_o$, and $\cos \alpha_o$ ($i = 1, 2, \ldots,$ number of modes). An iteration scheme that is initiated by assuming a value for α_2 between reasonable limits based on physical properties of the problem gives a solution of the set of equations, thus determining the values of α_2, α_o, q_{i1}, and $\dot{q}_{i1}$. The rest of the unknowns can then be found by back substitution.

2.3.4 Iteration Scheme

The iteration procedure is started by assuming a range of α_2 between an initial and a final value. The assumed range is chosen based on the physical properties of the problem and on experience developed by solving different cases. A value of an increment $\Delta\alpha_2$ is then found by dividing the assumed solution range by the number of increments chosen for iteration. At each value of α_2 in the range $(\alpha_2)_{initial}$ to $(\alpha_2)_{final}$, the set of equations is solved and a test is performed to see if the parameter ε_0 satisfies the convergence criterion ε_0 where:

$$\varepsilon_0 = \text{Minimum value of } \left[\sin \alpha_0 \pm \sqrt{1 - \cos^2 \alpha_0} \right] \qquad (2.41)$$

At this point a new range for the solution is determined around the α_2 corresponding to ε_0. For this new range, the initial value of α_2 is set as the maximum value of either the old initial α_2 or the minimum value of $(\alpha_2 - \Delta\alpha_2)$, and the maximum range value is set as the minimum value of either the ld final value of α_2 or the minimum of $(\alpha_2 + \Delta\alpha_2)$. The iteration is then repeated for the new range and the equations are again solved and a new test value of ε_0 is found. This procedure is repeated as many times as needed up to the maximum number of iteration steps. If the ε_0 value is within the specified tolerance limits, convergence is reached and the solution is found. In the case where convergence could not be reached, the iteration procedure is modified to find an approximate solution. A back substitution for the rest of the unknowns is then carried out using the values of the unknowns $q_i^{(1)}$, $\dot{q}_i^{(1)}$, α_0, and α_2 found from iteration, and the equations that determine the solution are checked to see whether the solution is acceptable. Figure 2.4 shows the flow chart corresponding to this iteration scheme.

2.3.5 Stresses

Considering small deformations, the stresses $\sigma(x, t)$ at any point along the beam can be evaluated using the standard stress-strain relationships derived in structural analysis books:

$$\sigma^{(j)}(x,t) = E \sum_{i=1}^{\infty} \frac{\partial^2 \phi_i^{(j)}(x)}{\partial x^2} q_i^{(j)}(t) \tag{2.42}$$

where

$$\frac{\partial^2 \phi_i^{(j)}(x)}{\partial x^2} = \phi_i^{''(j)}(x) \tag{2.43}$$

denotes the second spatial derivative of the i^{th} mode shape function for the j^{th} solution region.

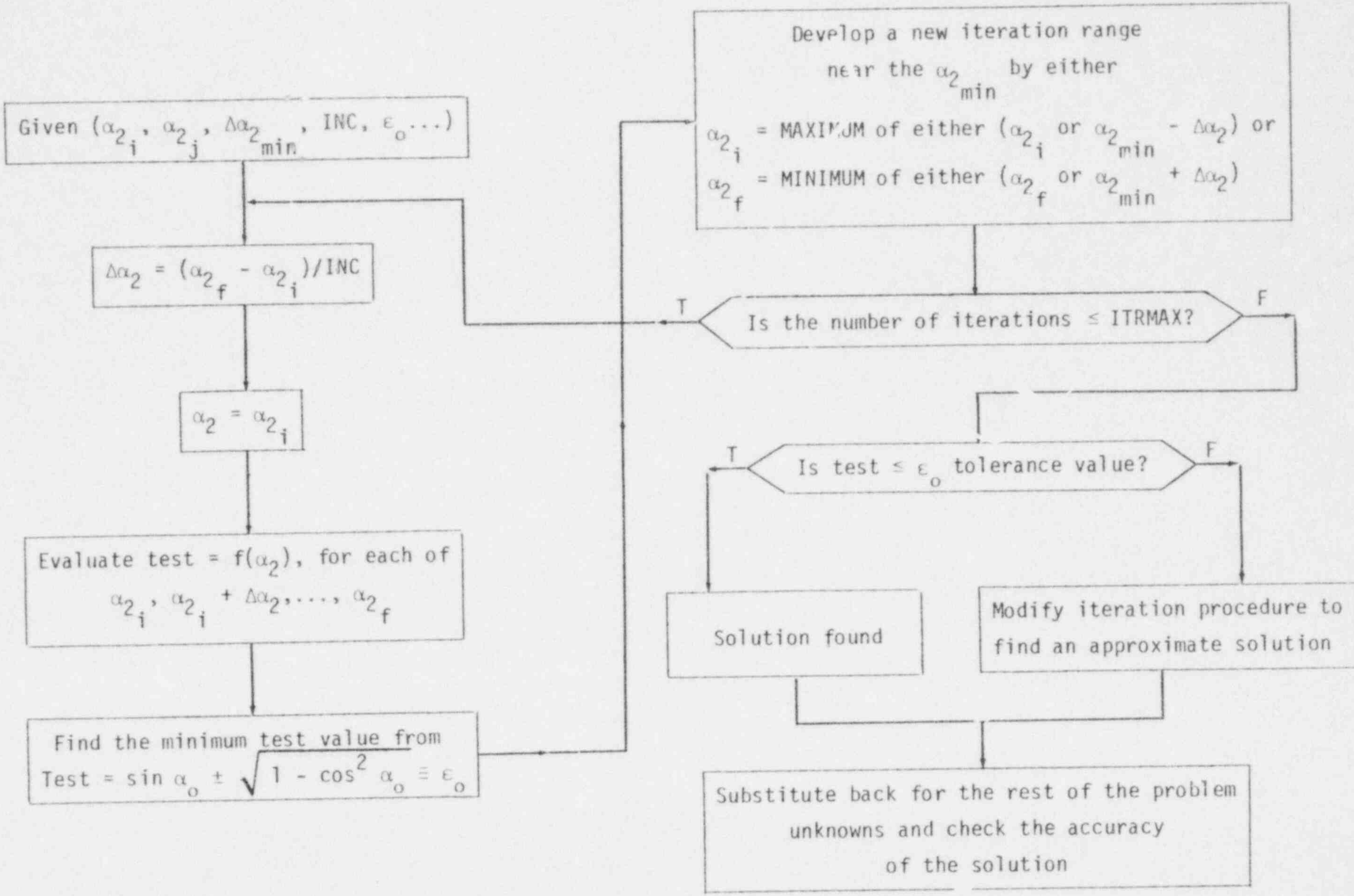

FIGURE 2.4 FLOW CHART FOR ITERATION SCHEME

Chapter 3

EXPERIMENTAL STUDIES

The objectives of the experimental studies reported herein are

(1) To verify the validity of the analytical results described in Section 2, and

(2) To investigate the effects of system parameters.

3.1 Description of Apparatus

A scale model of a cantilever (striker) beam with a one-sided motion-limiting stop (target) was mounted on a vibration exciter and subjected to sinusoidal vibration at several different magnitudes of excitation.

3.1.1 Beam Models

The striker and target beams were made from sheets of mild steel. Details of the striker and target beams are shown in Figure 3.1.

3.1.2 Test Fixtures

Figure 3.2 shows the lightweight yet rigid fixtures that simulate a fixed-free boundary condition for the striker beam and a clamped-free boundary condition for the target beam.

3.1.3 Instrumentation

In addition to a number of strain gages that were mounted on the striker and target beam models, several vibration pickups were attached to the test fixtures and the vibration exciter to monitor the excitation being furnished to the system. A model of the system under consideration is shown in Figure 3.3.

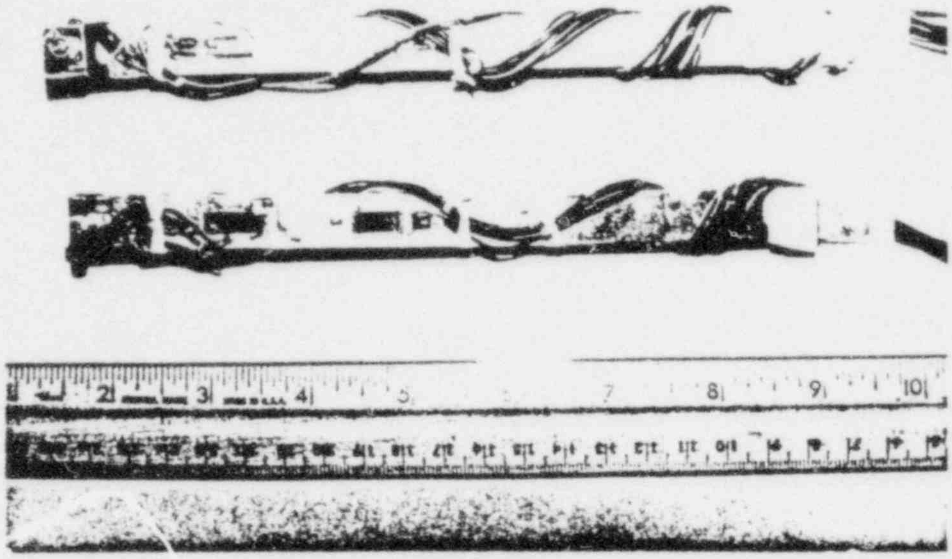

(a) STRIKER BEAM

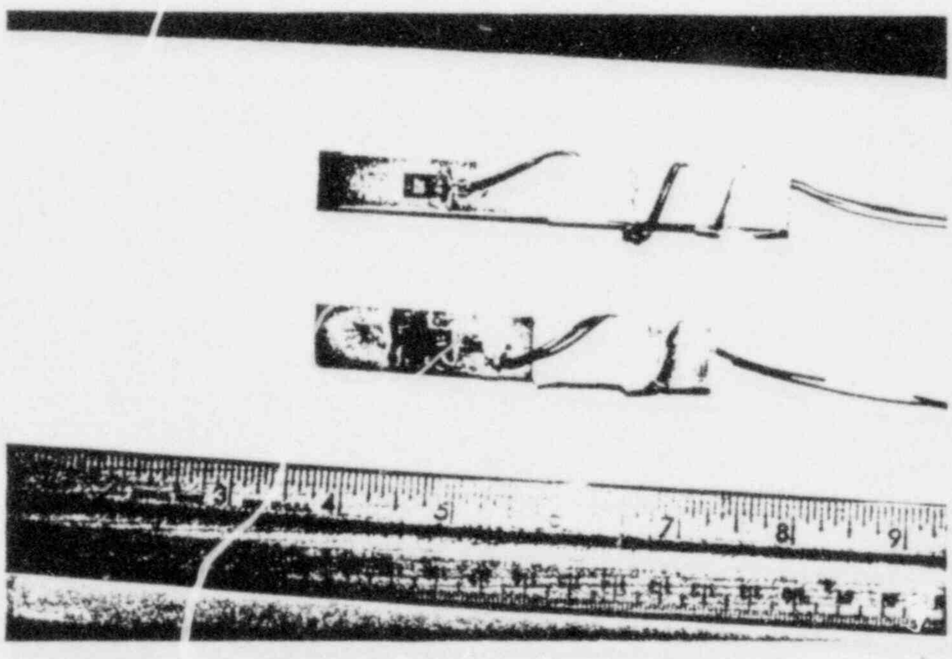

(b) TARGET BEAM

FIGURE 3.1 BEAM MODELS

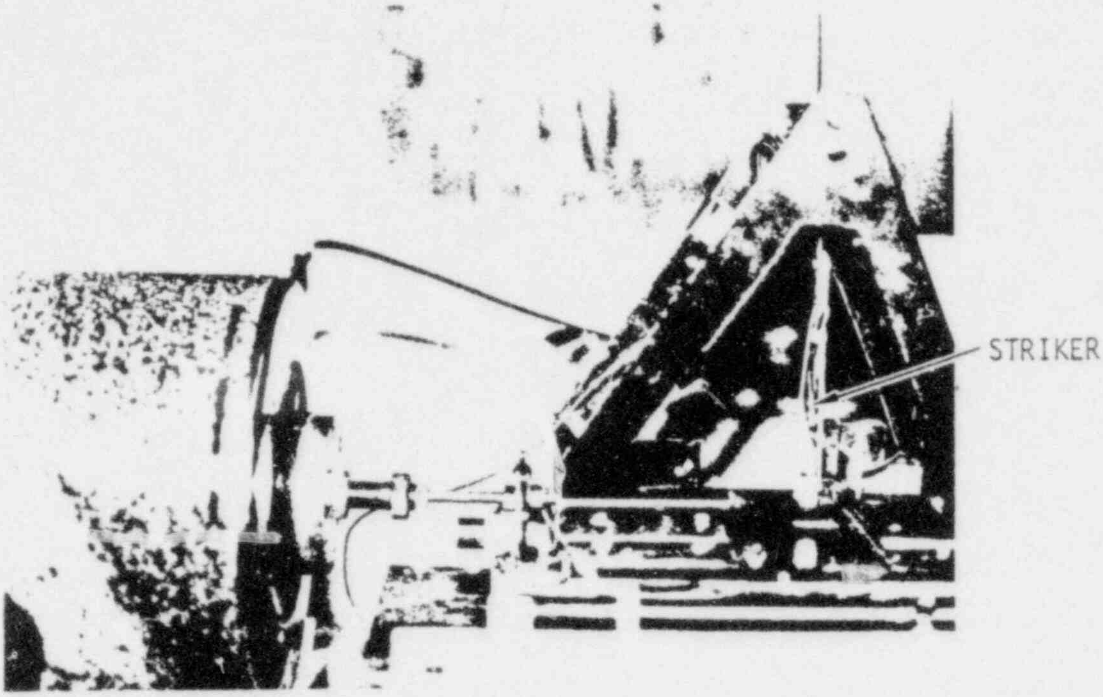

(a) STRIKER BEAM

(b) TARGET BEAM

FIGURE 3.2 TEST FIXTURES

3.2 Test

3.2.1 Vibration Test Setup

Figure 3.4 shows the setup of the test in which the system was subjected to a base excitation of the form $S(t) = S_o \sin \Omega t$.

3.2.2 Description of Vibration Machine

The vibration exciter was an electrodynamic shaker (Figure 3.5) capable of generating arbitrary motion. It was used to generate harmonic excitation in a horizontal plane.

3.2.3 Vibration Test Procedure

In a typical test, the gap clearance d was set to a specific value, the shaker base amplitude level S_o was selected, and the shaker frequency was set to a given frequency value Ω. The excitation and the system response were then measured and recorded. Measurements were made of the following quantities:

$\ddot{S}(t)$ = sinusoidal base acceleration = $-\Omega^2 S_o \sin \Omega t$

$W(x,t)$ = displacement at chosen stations along the beam

$\dot{W}(x,t)$ = velocity at chosen station along the beam

$\varepsilon_1(x,t)$ = striker beam strain at the chosen stations

$\varepsilon_2(x,t)$ = target beam strain at a station chosen along the target beam

Sample records of the measured quantities are shown in later figures.

The excitation frequency Ω was then increased to some value Ω_1 and the same response parameters were measured and recorded again. Due to the nonlinearity of the system parameters, the response [illegible] determined for both increasing and decreasing excitation frequency values that spanned a range of ±50% with respect to ω_1, the fundamental frequency of the striker beam.

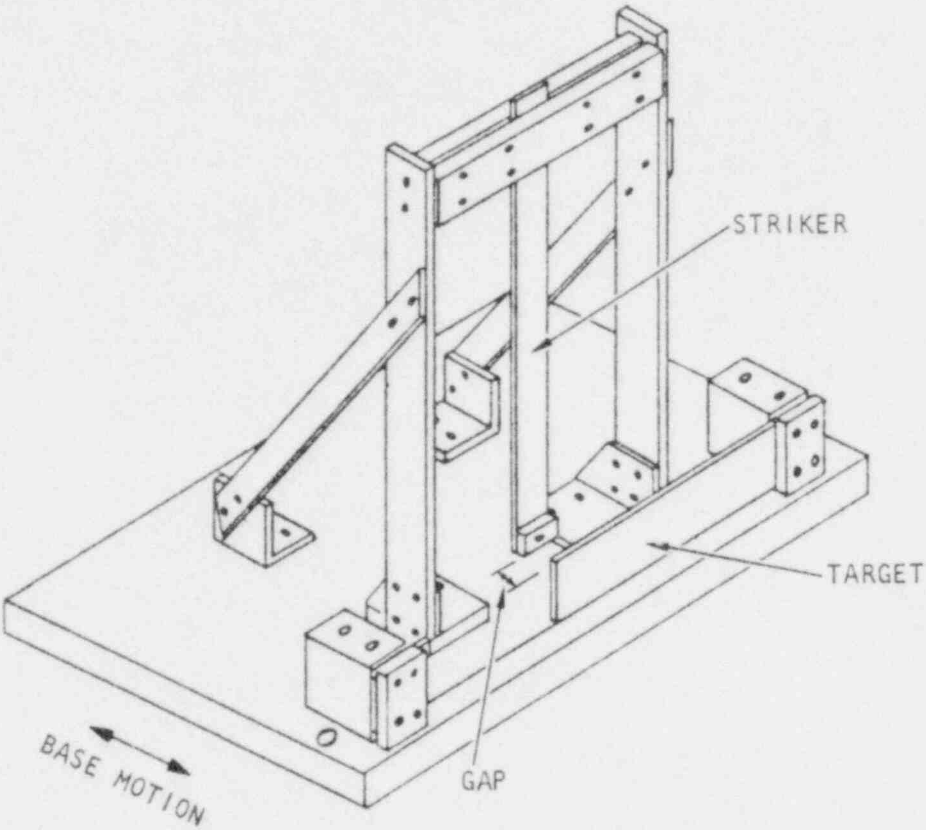

FIGURE 3.3 MODEL CONFIGURATION

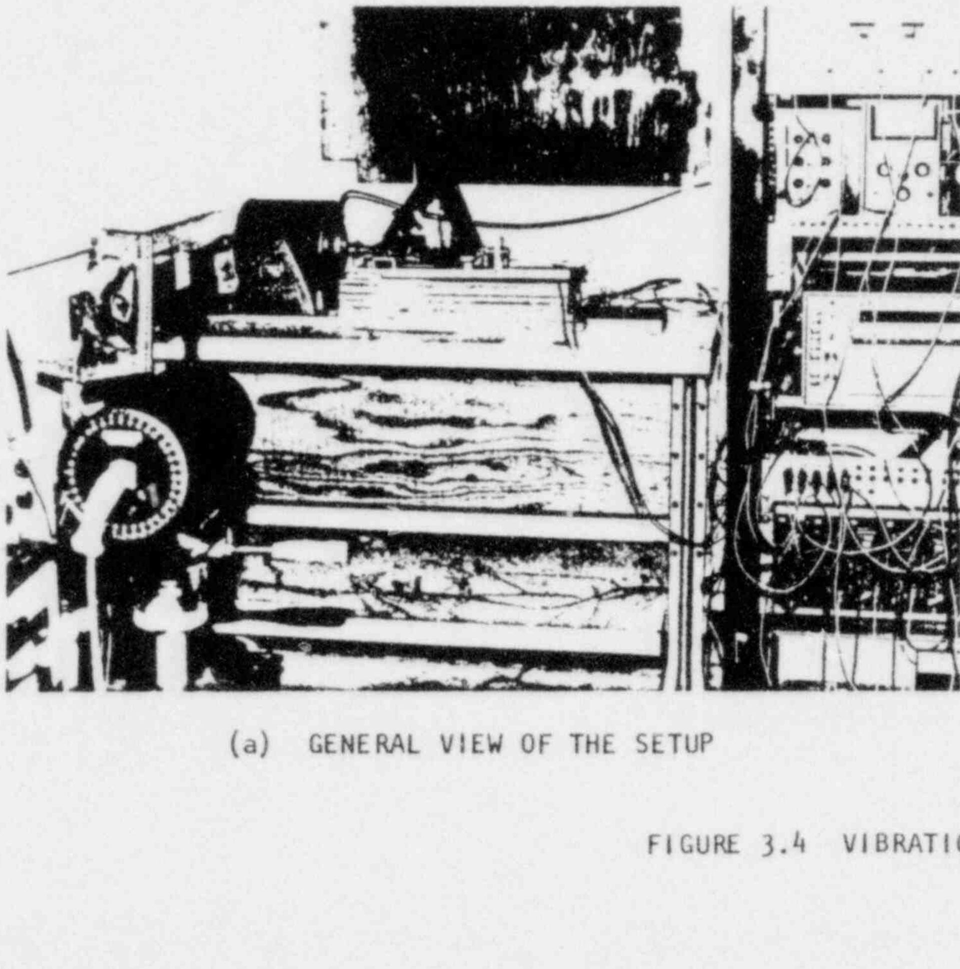

(a) GENERAL VIEW OF THE SETUP

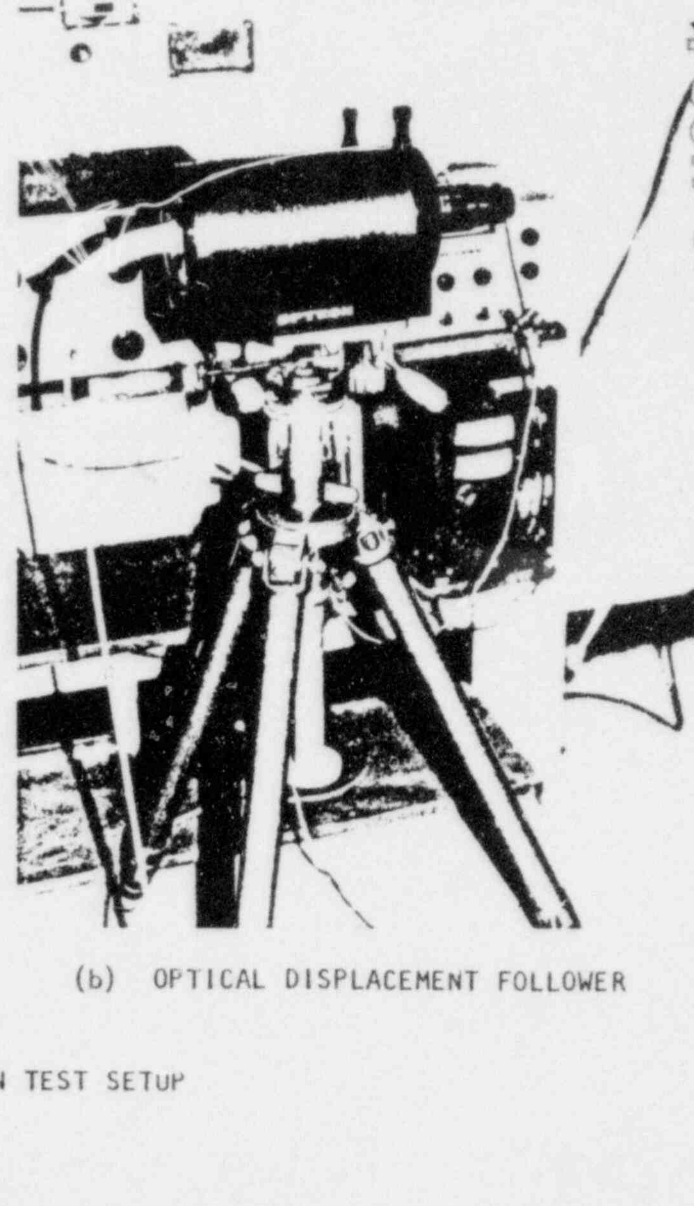

(b) OPTICAL DISPLACEMENT FOLLOWER

FIGURE 3.4 VIBRATION TEST SETUP

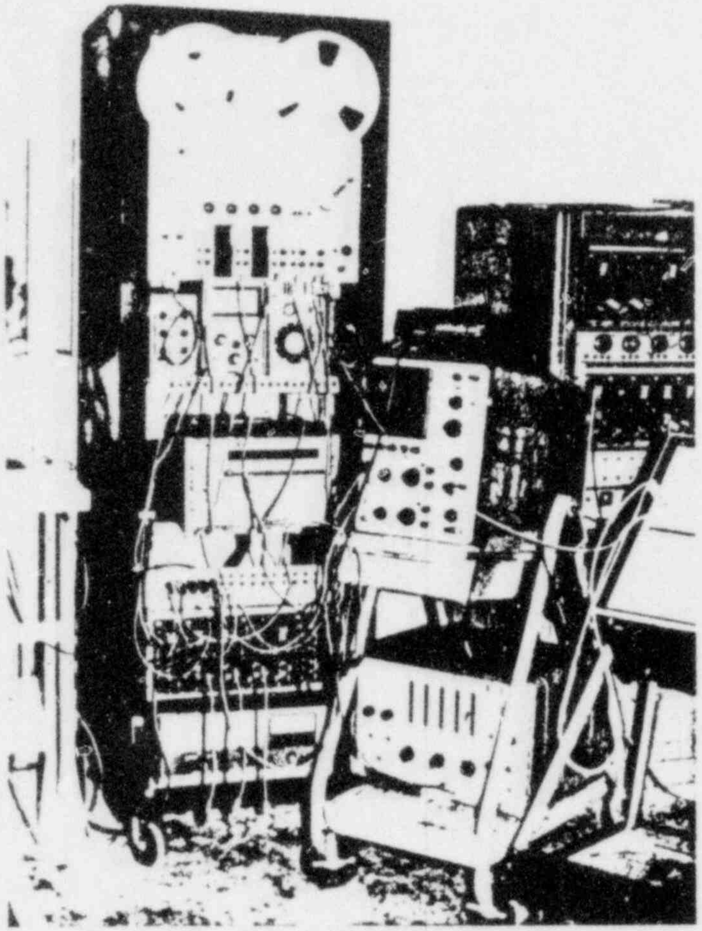

(c) INSTRUMENTATION

FIGURE 3.4 VIBRATION TEST SETUP (CONCLUDED)

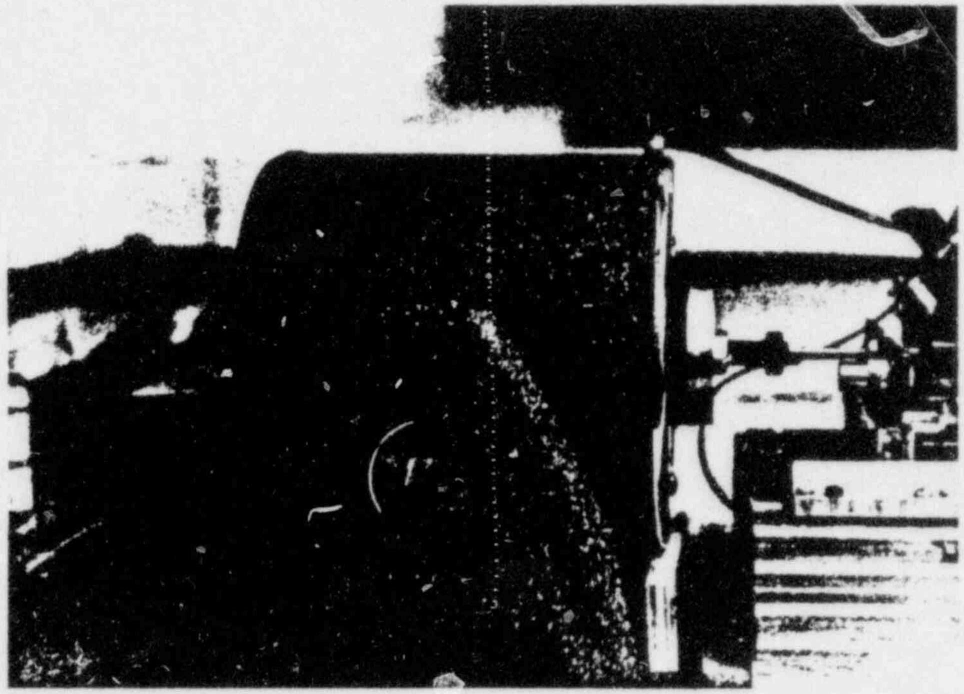

FIGURE 3.5 VIBRATION EXCITER

3.2.4 Vibration Data Gathered

Free vibration (logarithmic decrement; see Figure 3.6) and steady-state (half-power method) tests were conducted on the striker beam model in order to determine its natural frequency and ratio of critical damping. A summary of the beam characteristics is given in Table 3.1.

The beam was tested with two different gaps at a specific level S_o and frequency Ω. For each value of d, the frequency was varied from Ω_{min} to Ω_{max} and then back to Ω_{min}. This was repeated for each of two different striker- to target-beam ratios, which were produced by either changing the target beam dimensions or altering its boundary conditions to simulate a certain elastic-stop stiffness. The peak values of the steady-state response were measured and recorded.

3.2.5 Reduced Vibration Data

The data discussed in Section 3.2.4 were reduced to a more meaningful form by introducing the following dimensionless ratios:

$$\frac{\Omega}{\omega_1} = \text{excitation frequency ratio}$$

$$= \frac{\text{exciting frequency}}{\text{natural frequency of striker beam}}$$

$$\frac{d}{S_o} = \text{clearance ratio}$$

$$= \frac{\text{size of gap between striker and target beam}}{\text{amplitude of sinusoidal base motion}}$$

$$\frac{K_t}{K_t} = \text{stiffness ratio} = \frac{\text{target beam stiffness}}{\text{striker beam stiffness}} = K^*$$

$$\frac{A}{S_o} = \text{amplification ratio} = \frac{\text{peak S-S amplitude of striker beam}}{\text{amplitude of sinusoidal base motion}}$$

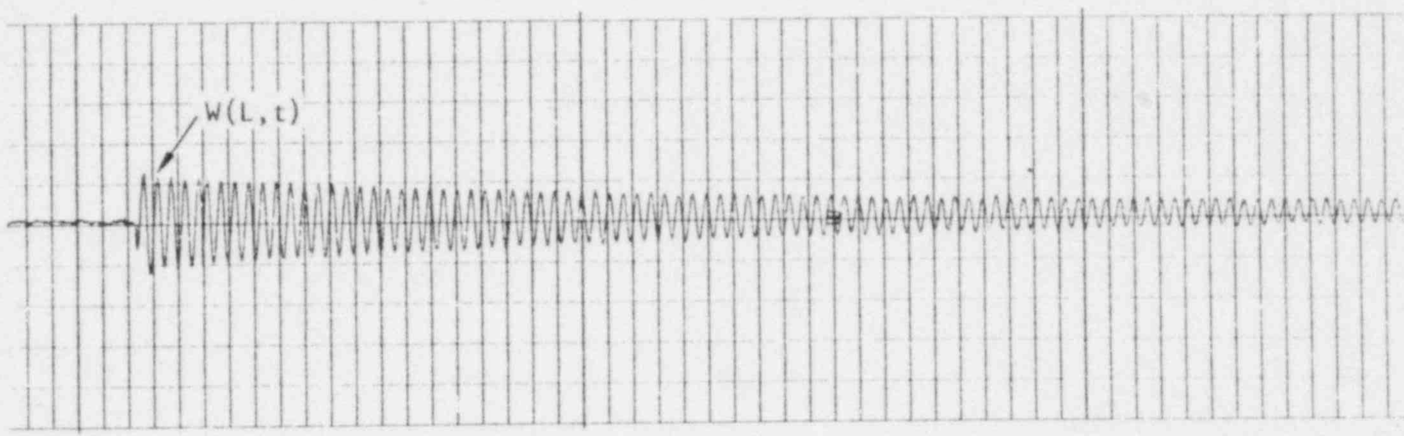

FIGURE 3-6. FREE VIBRATION OF SYSTEM

TABLE 3.1 BEAM DIMENSIONS AND WEIGHT

	Dimension, in.
Striker Beams	
Length	8.0
Thickness	0.057
Width	0.533
Target Beams	
Length	3.72
Thickness	0.057 - 0.025
Width	0.535 - 0.585
Striker Beam Concentrated Weight	
(with accelerometer)	32.0 gm

Sample reduced data are plotted in Figures 3.7 and 3.8 in the form of amplification ratio versus excitation frequency ratio for various excitation levels, and for clearance ratios, including the case where d/S_0 is very large.

3.2.6 Discussion of Vibration Results

Figures 3.9 to 3.16 represent sample time histories of the vibration response of the system for certain chosen parameter combinations. These figures show the displacement and the velocity at the tip of the striker beam, in addition to the base acceleration $\ddot{S}$ and the strain ε_1 at three-fourths of the striker beam length, and the strain ε_2 at the middle of the target beam for different levels of excitation $\ddot{S}$.

The electronic instrumentation used to measure and record the analog signals introduced extraneous phase shifts that tended to distort the actual phase relationships between the recorded dynamic measurements. Consequently, the time histories shown in Figures 3.9 to 3.12 do not show accurate phase relationships.

Figure 3.9 shows the response for the case of an excitation level $\ddot{S} = \ddot{S}_1$, for which the maximum peak displacement is such that the maximum relative deflection at the contact point is less than the gap d. This results in a simple harmonic response of the system at a frequency Ω corresponding to the exciting frequency of the base motion, $S(t) = S_0 \sin \Omega t$. The response shown in Figure 3.10 with a base excitation $\ddot{S} = \ddot{S}_2 > \ddot{S}_1$ corresponds to the limiting case where the maximum relative deflection is equal to the gap d (note the effect that hitting makes on the curves for velocity and strains ε_1 and ε_2).

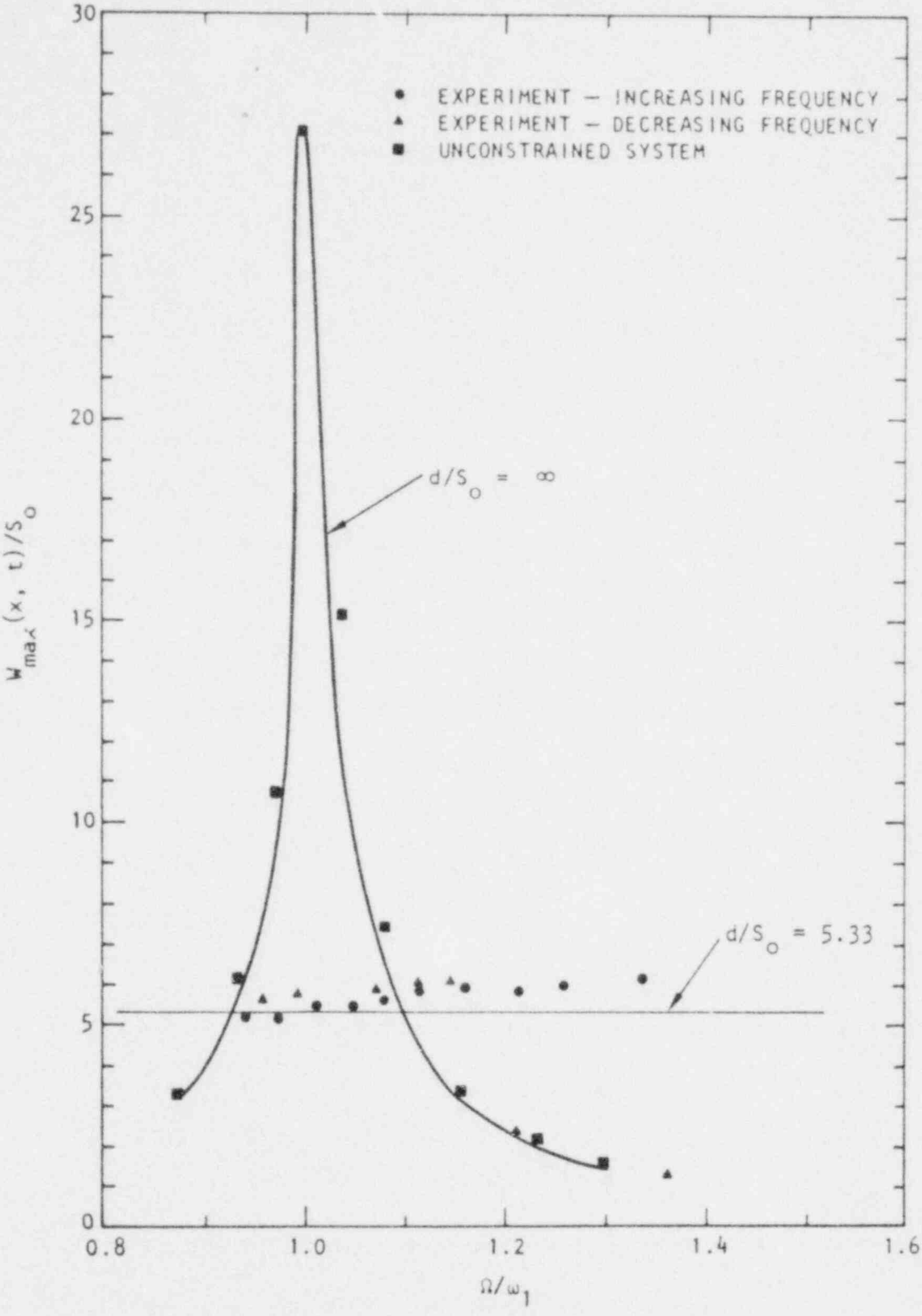

FIGURE 3.7 REDUCED VIBRATION DATA FOR $K^* = 25$, $\zeta = 0.04$, CLEARANCE RATIOS $d/S_o = 5.33$ AND ∞

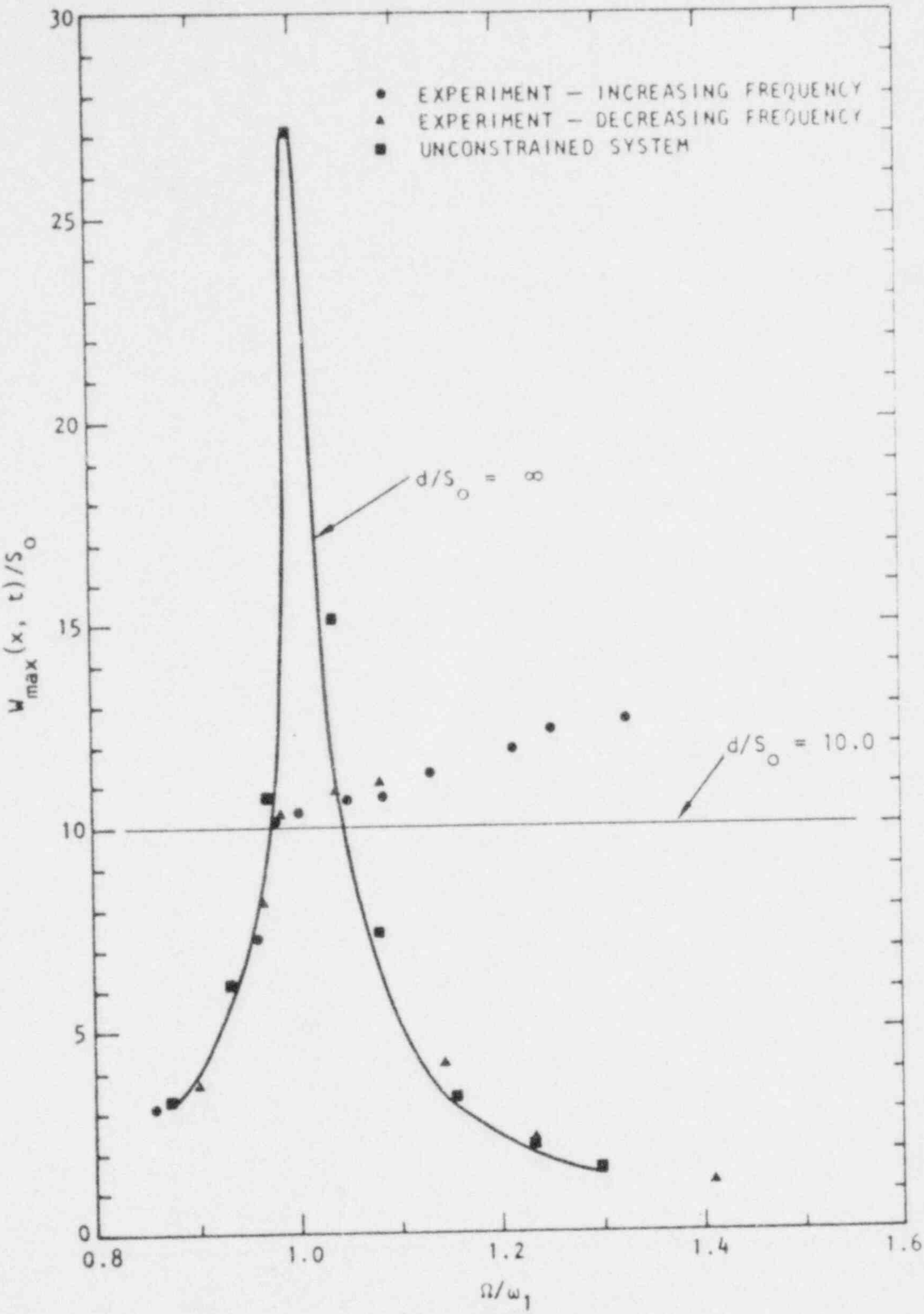

FIGURE 3.8 REDUCED VIBRATION DATA FOR $K^* = 25$, $\zeta = 0.04$, CLEARANCE RATIO $d/S_o = 10$ AND ∞

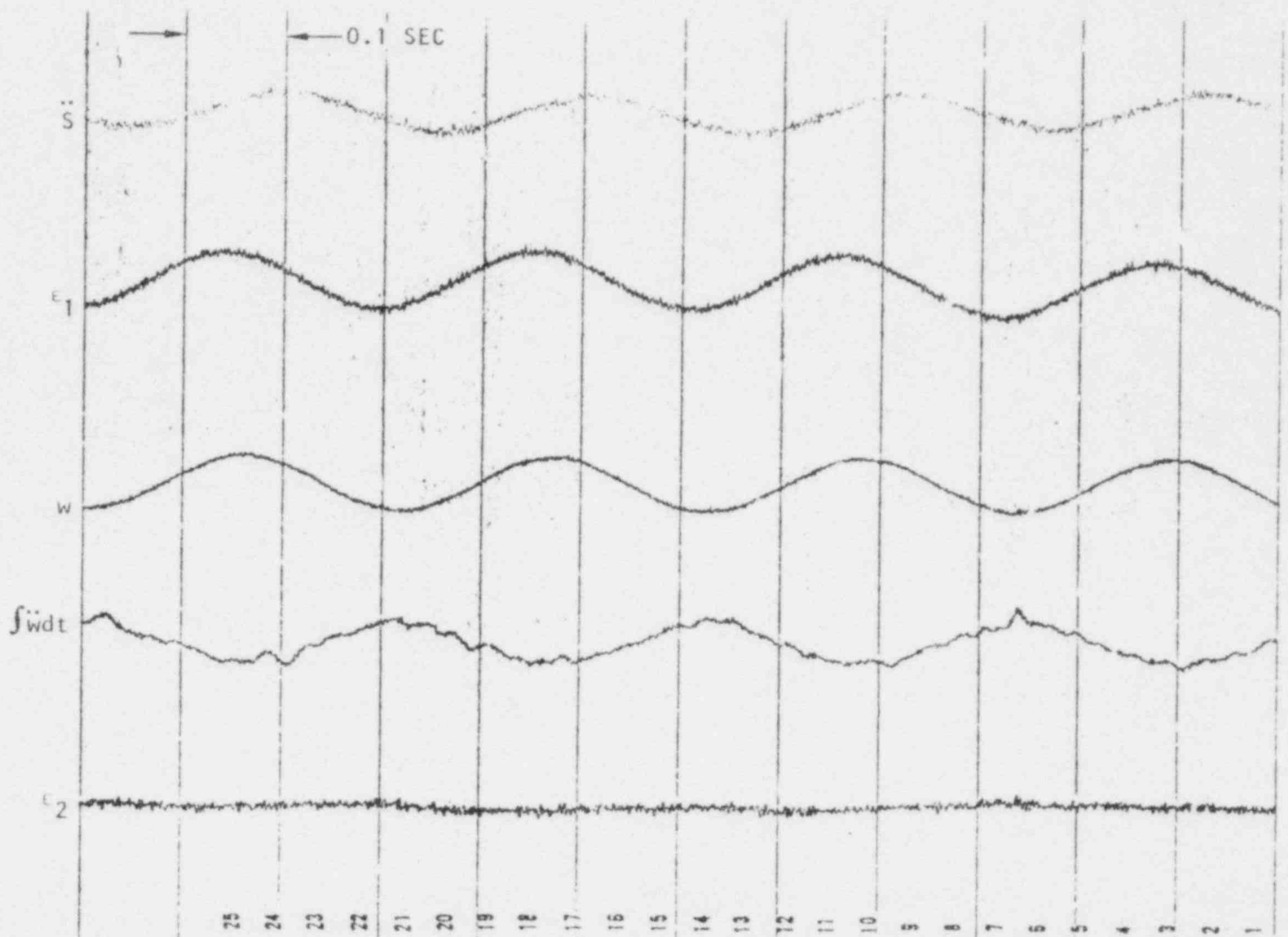

FIGURE 3.9 STEADY-STATE EXCITATION AND FORCED LINEAR (NO-IMPACT) RESPONSE OF BEAM/STRIKER SYSTEM; $\Omega/2\pi$ = 26.1 Hz; EXCITATION LEVEL $\ddot{S}_1$

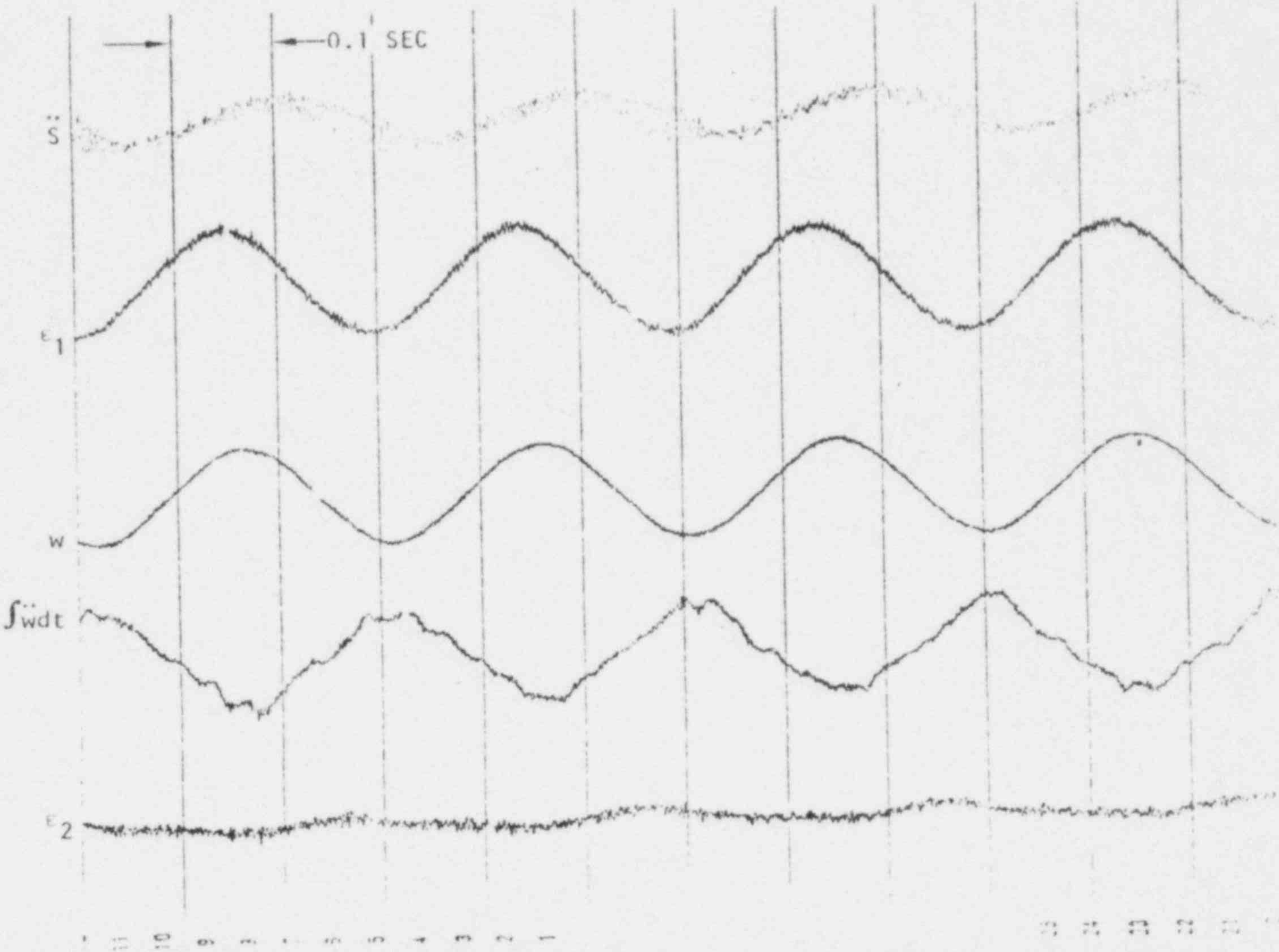

FIGURE 3.10 STEADY-STATE EXCITATION AND FORCED NONLINEAR RESPONSE OF BEAM/ STRIKER SYSTEM; $\Omega/2\pi = 27.4$; EXCITATION LEVEL $\ddot{S}_2 > \ddot{S}_1$

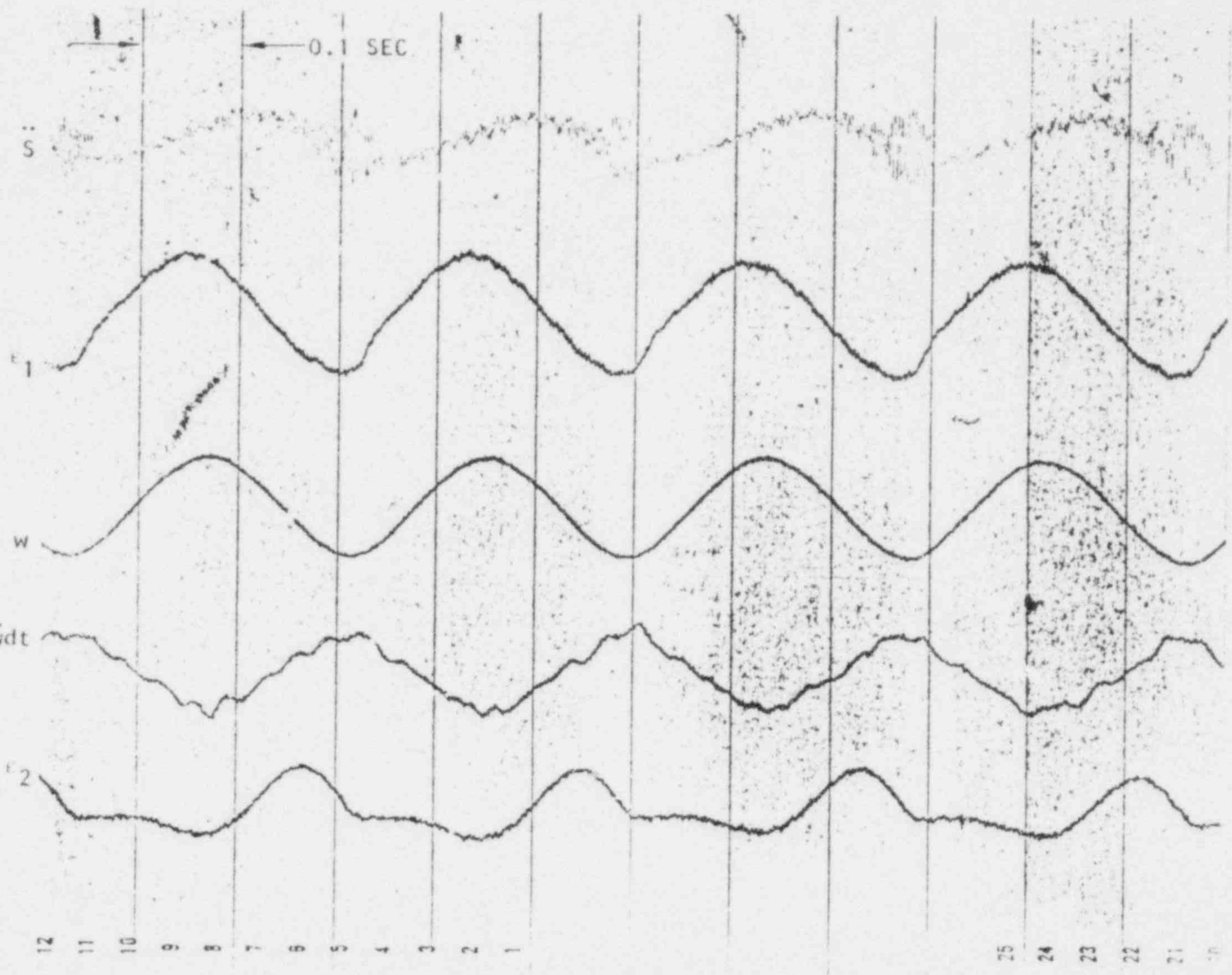

FIGURE 3.11 STEADY-STATE EXCITATION AND FORCED NONLINEAR RESPONSE OF BEAM/STRIKER SYSTEM; $\Omega/2\pi$ = 28.9 Hz; EXCITATION LEVEL $\ddot{S}_3 > \ddot{S}_2$

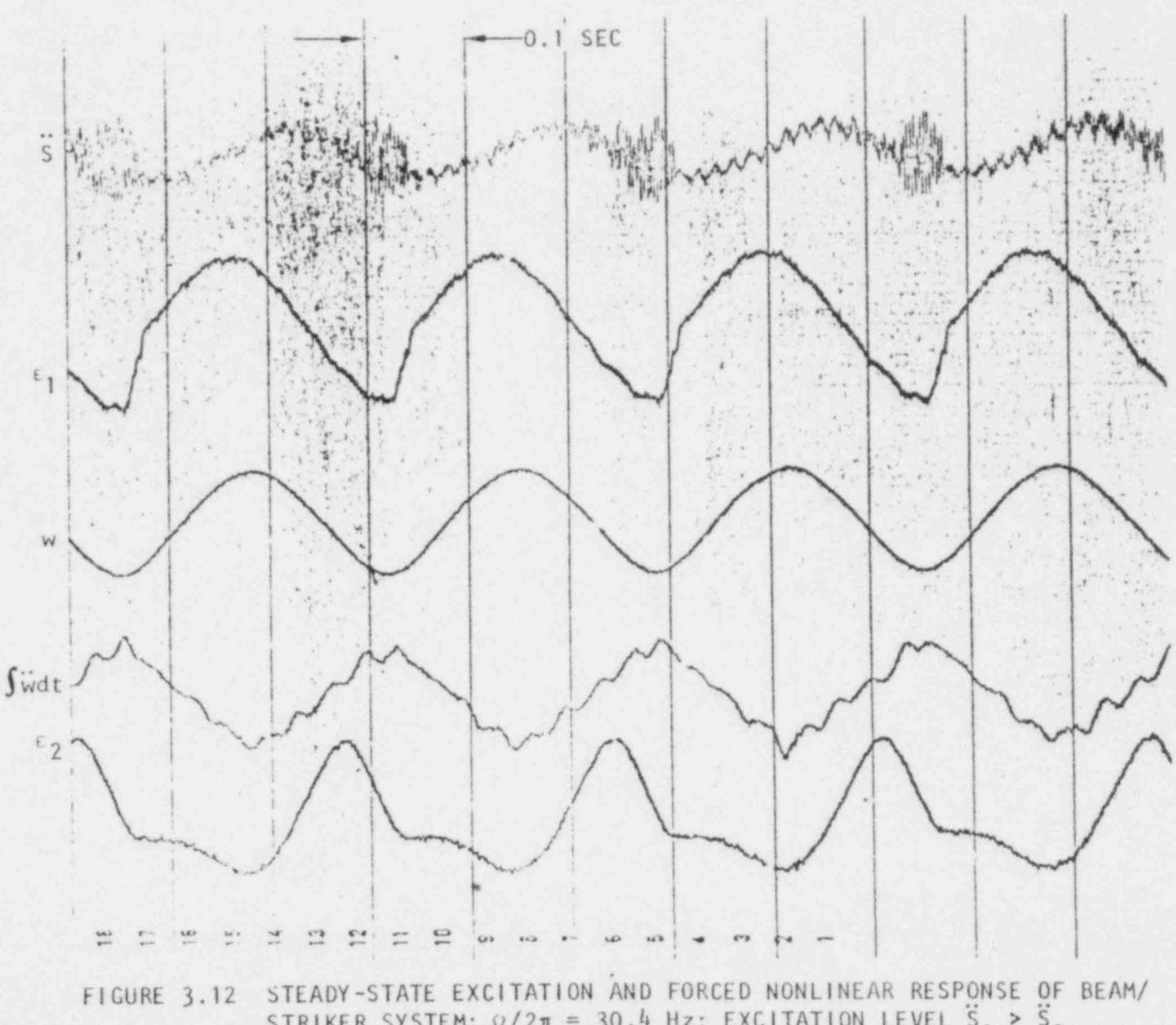

FIGURE 3.12 STEADY-STATE EXCITATION AND FORCED NONLINEAR RESPONSE OF BEAM/STRIKER SYSTEM; $\Omega/2\pi$ = 30.4 Hz; EXCITATION LEVEL $\ddot{S}_3 > \ddot{S}_2$

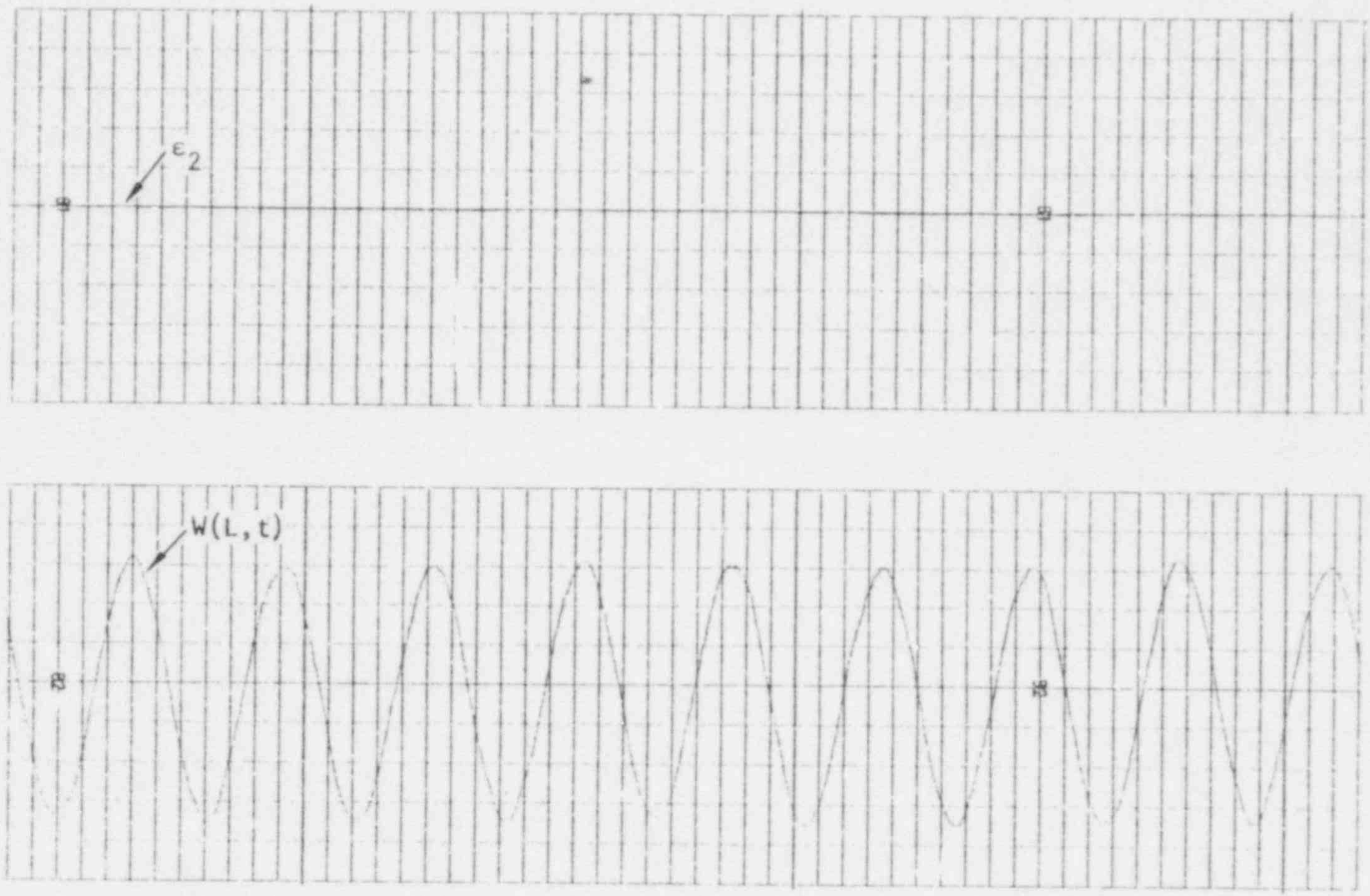

(a) ε_2, W(L, t)

FIGURE 3.13 VIBRATION RESPONSE, EXCITATION LEVEL $\ddot{S}_1$, NO IMPACT, $\Omega/2\pi$ = 26.1 Hz, SPEED = 100 CM/SEC

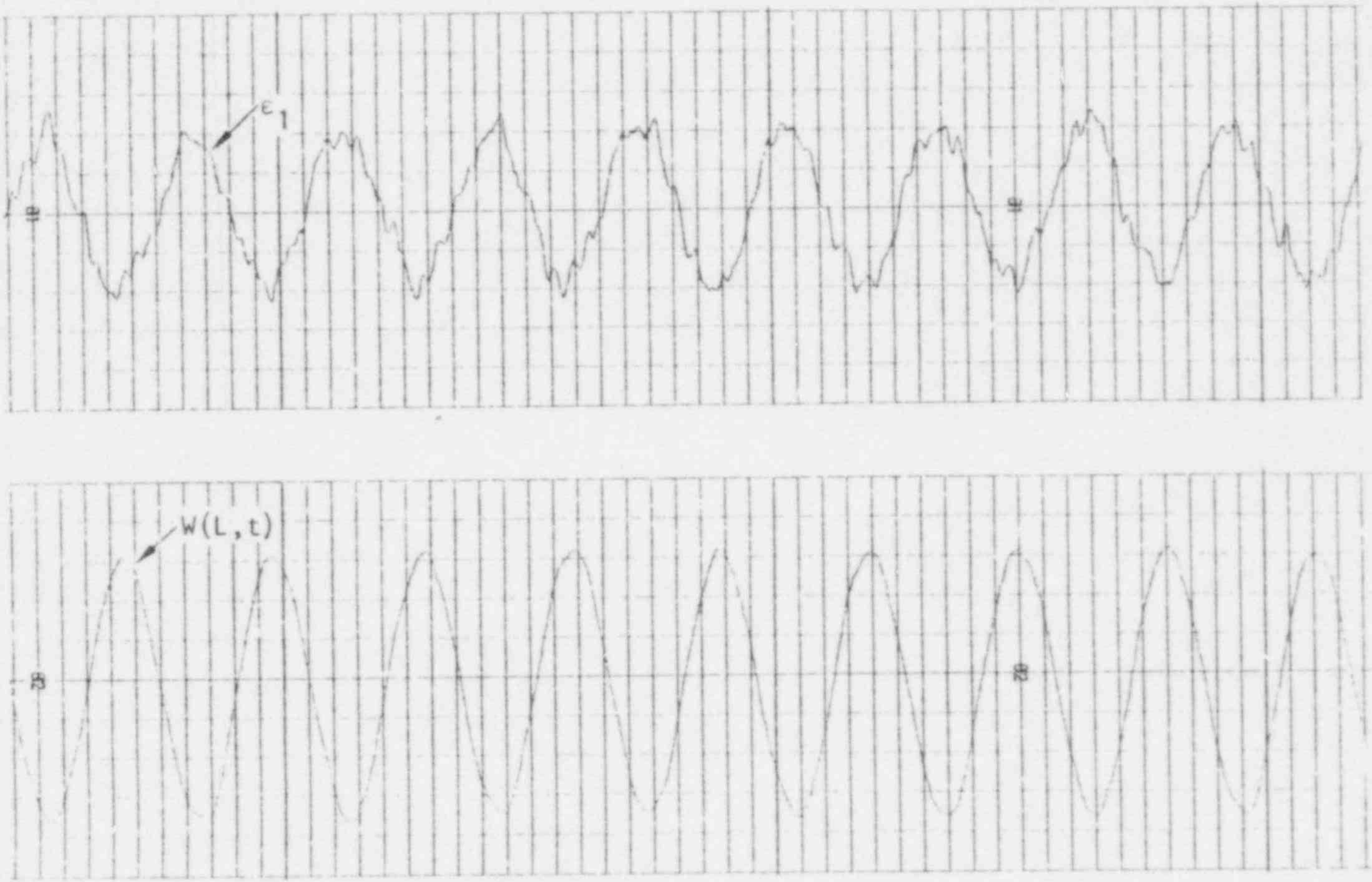

(b) ε, W(L, t)

FIGURE 3.13 VIBRATION RESPONSE, EXCITATION LEVEL $\ddot{S}_1$, NO IMPACT, $\Omega/2\pi$ = 26.1 Hz, SPEED = 100 CM/SEC

POOR ORIGINAL

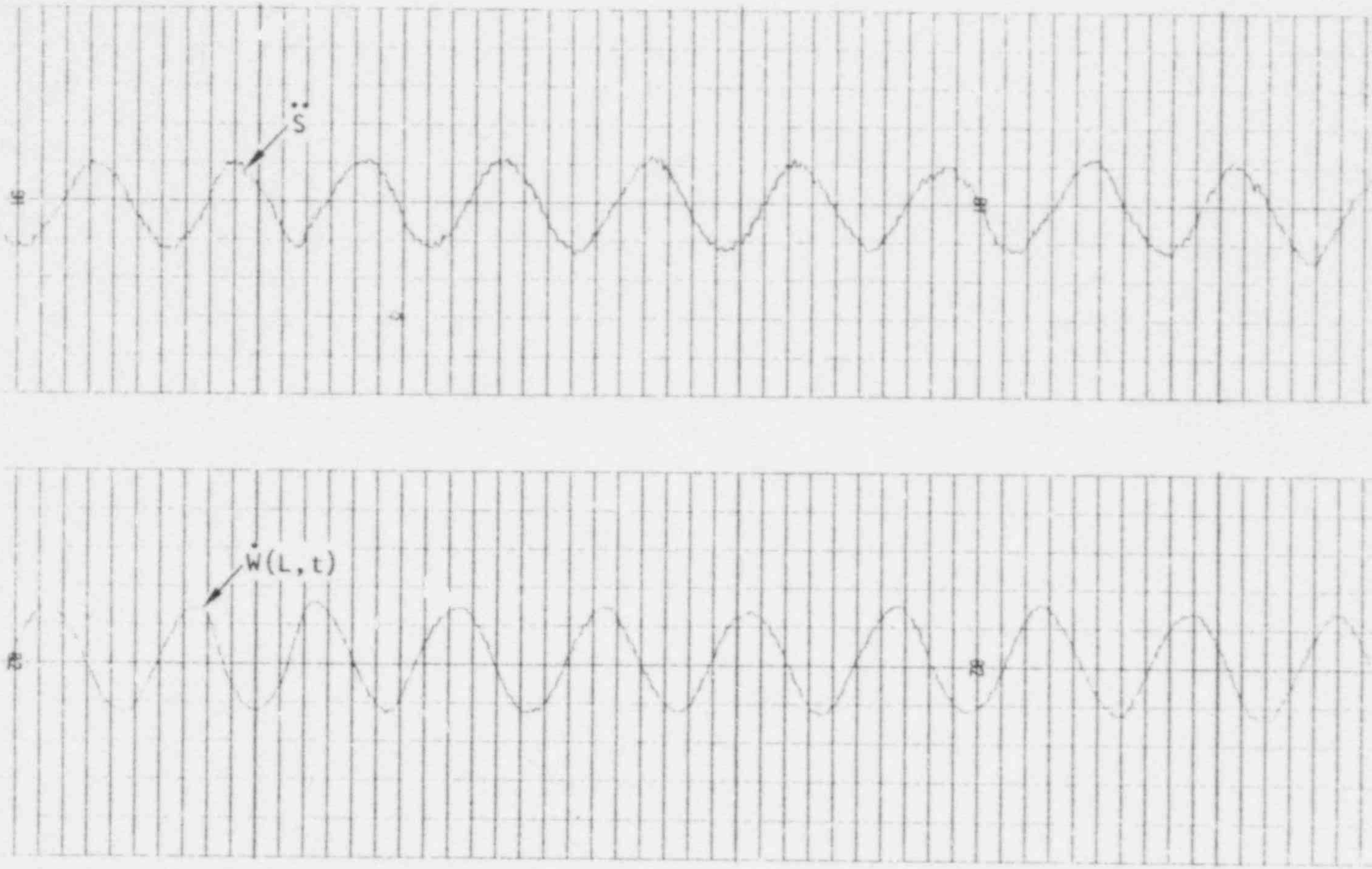

(c) $\ddot{S}$, $\dot{W}(L, t)$

FIGURE 3.13 VIBRATION RESPONSE, EXCITATION LEVEL $\ddot{S}_1$, NO IMPACT, $\Omega/2\pi$ = 26.1 Hz, SPEED = 100 CM/SEC

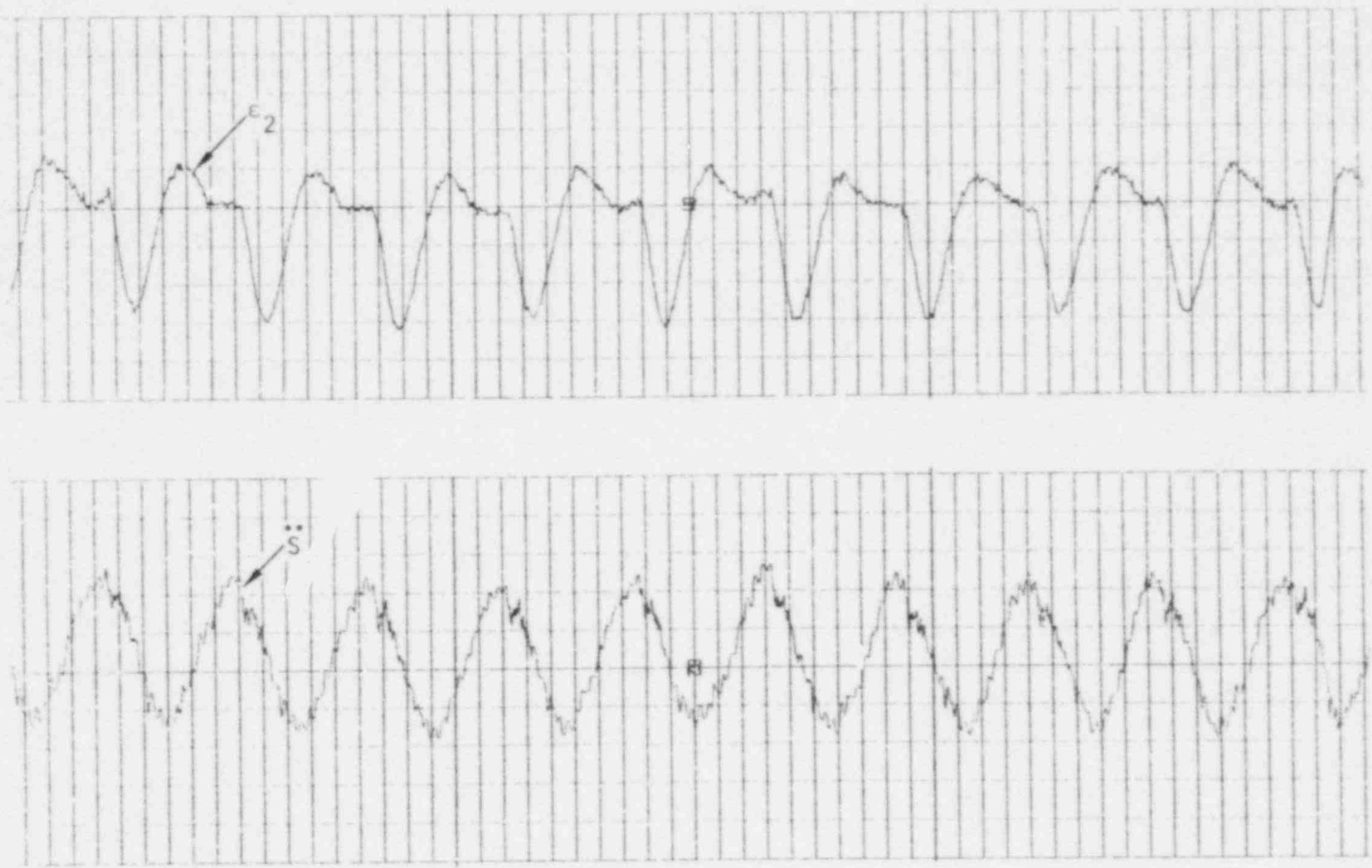

(a) ε_2, $\ddot{S}$

FIGURE 3.14 VIBRATION RESPONSE, EXCITATION LEVEL $\ddot{S}_2 > \ddot{S}_1$, IMPACT, $\Omega/2\pi$ = 27.4 Hz
SPEED = 100 CM/SEC

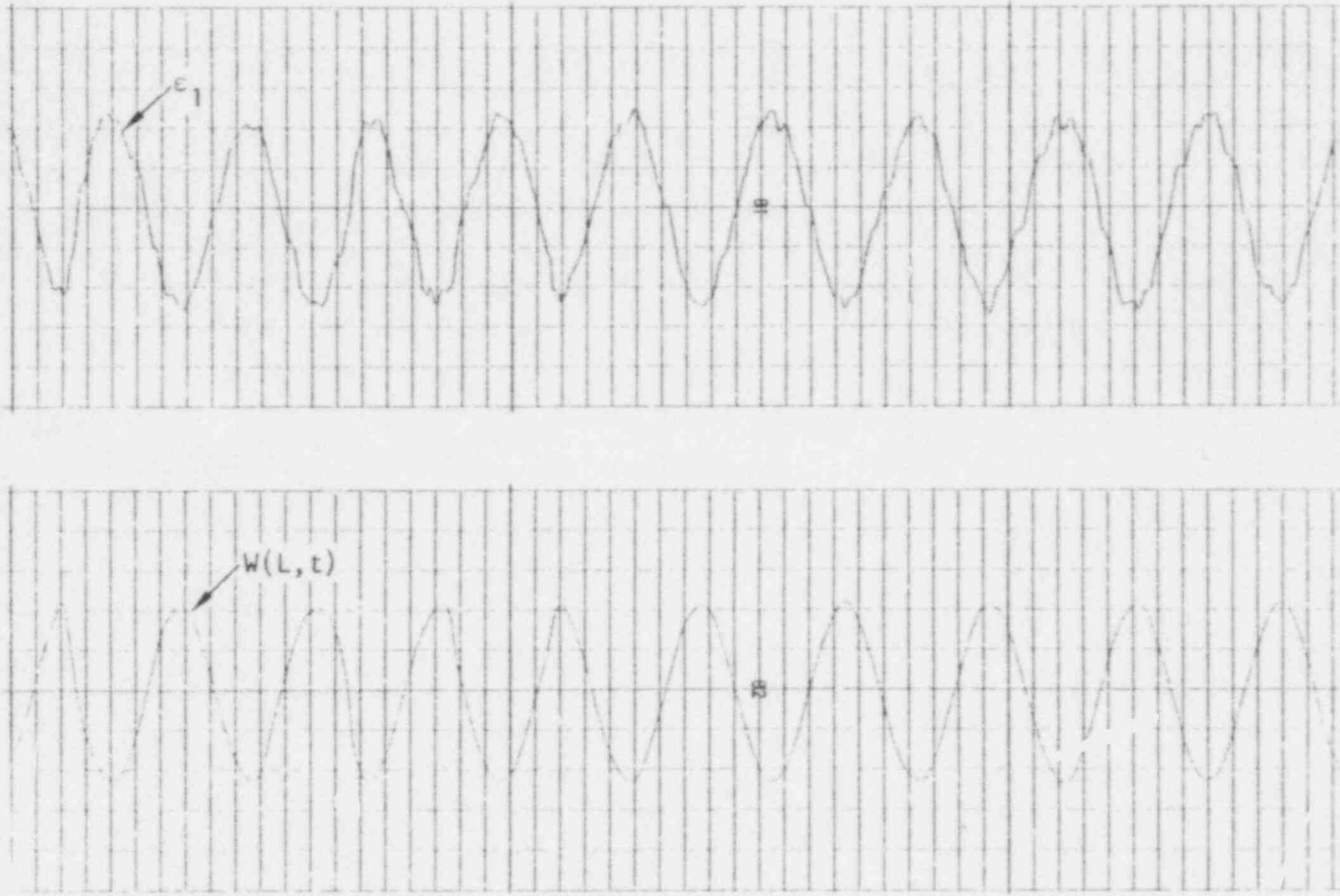

(b) ε_1, W(L, t)

FIGURE 3.14 VIBRATION RESPONSE, EXCITATION LEVEL $\ddot{S}_2 > \ddot{S}_1$, IMPACT, $\Omega/2\pi$ = 27.4 Hz, SPEED = 100 CM/SEC

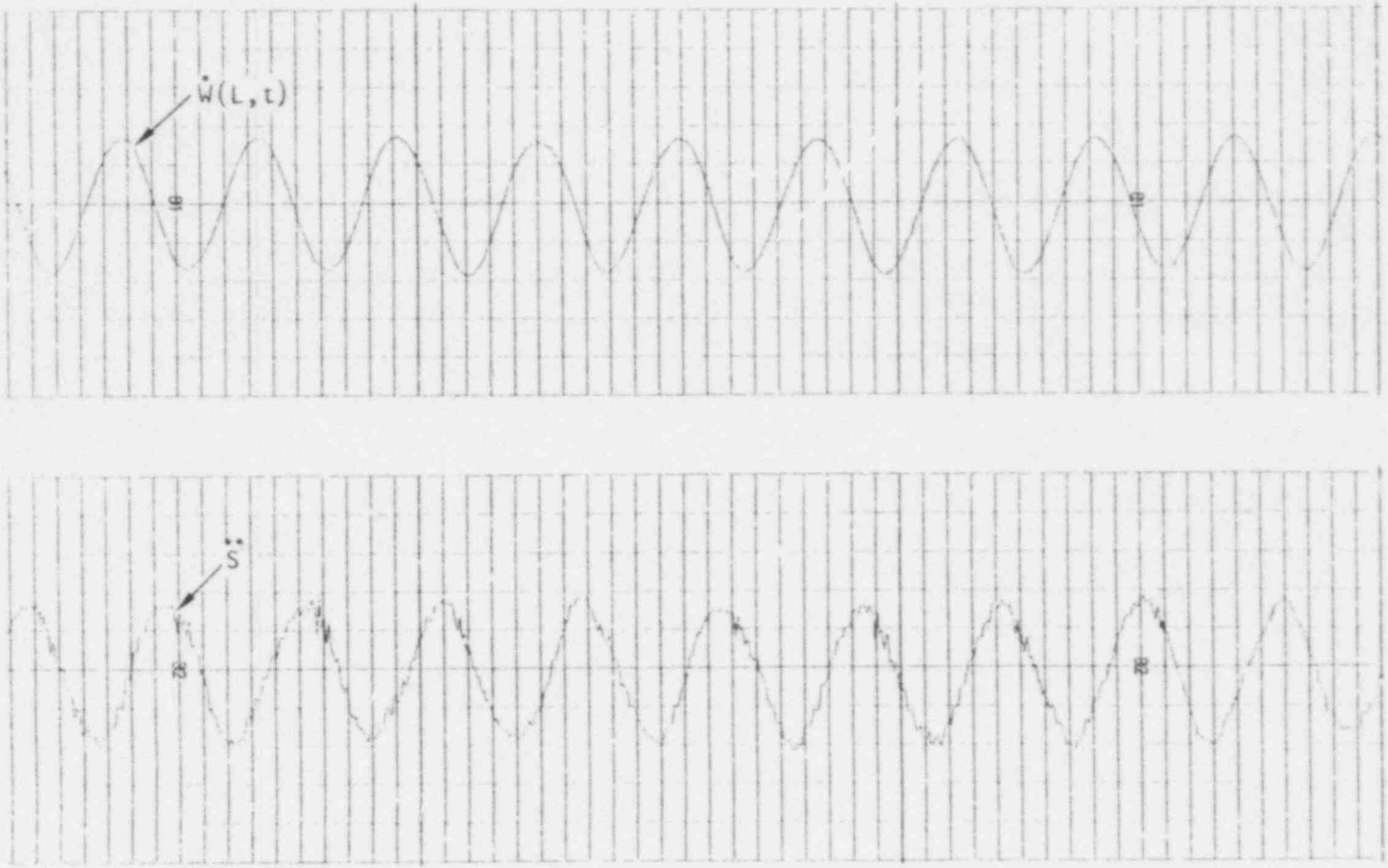

(c) $\dot{W}(L, t)$, $\ddot{S}$

FIGURE 3.14 VIBRATION RESPONSE, EXCITATION LEVEL $\ddot{S}_2 > \ddot{S}_1$, IMPACT, $\Omega/2\pi$ = 27.4 Hz, SPEED = 100 CM/SEC

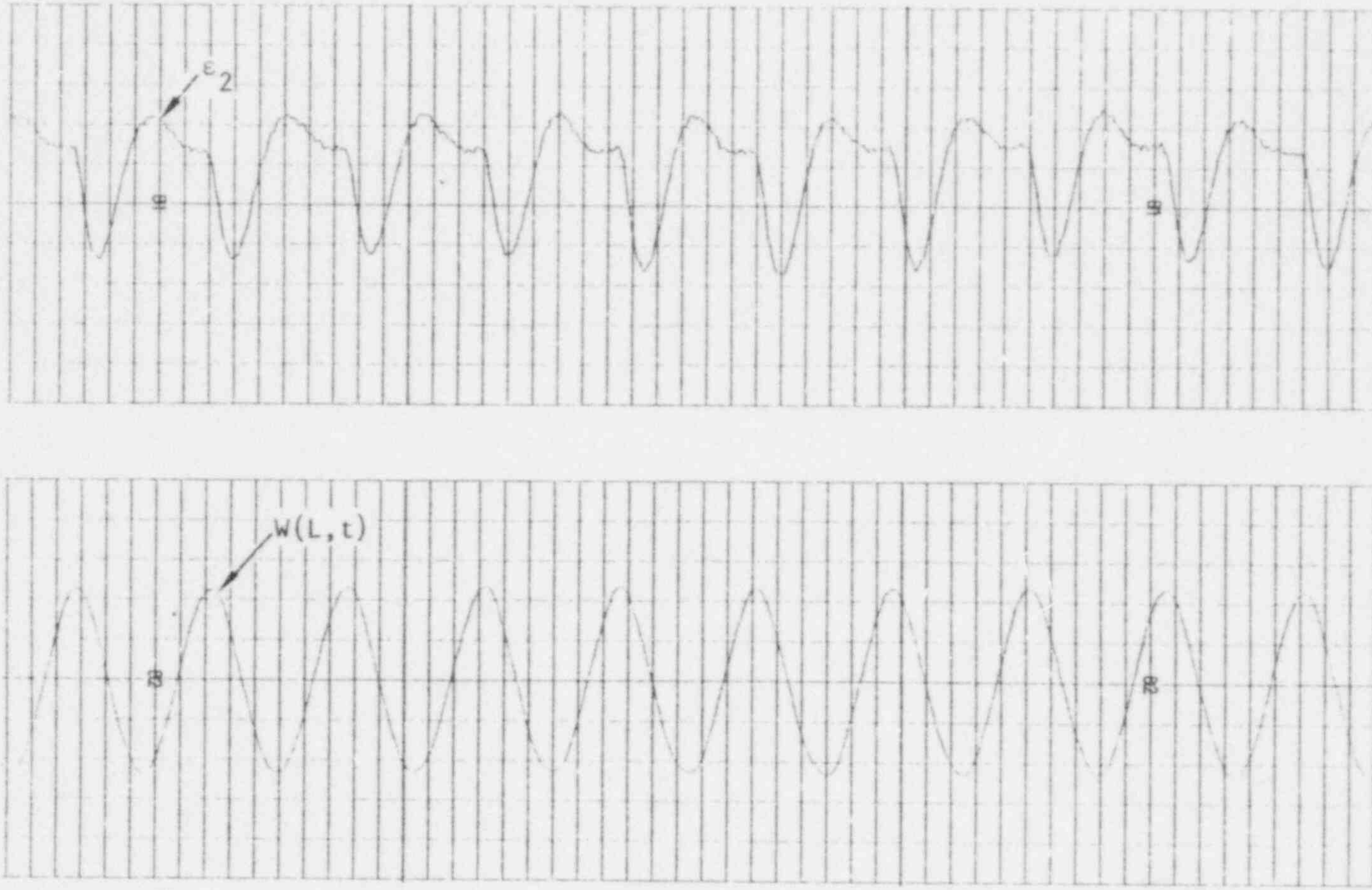

(a) ε_2, W(L, t)

FIGURE 3.15 VIBRATION RESPONSE, EXCITATION LEVEL $\ddot{S}_3 > \ddot{S}_2$, IMPACT, $\Omega/2\pi$ = 28.9 Hz, SPEED = 100 CM/SEC

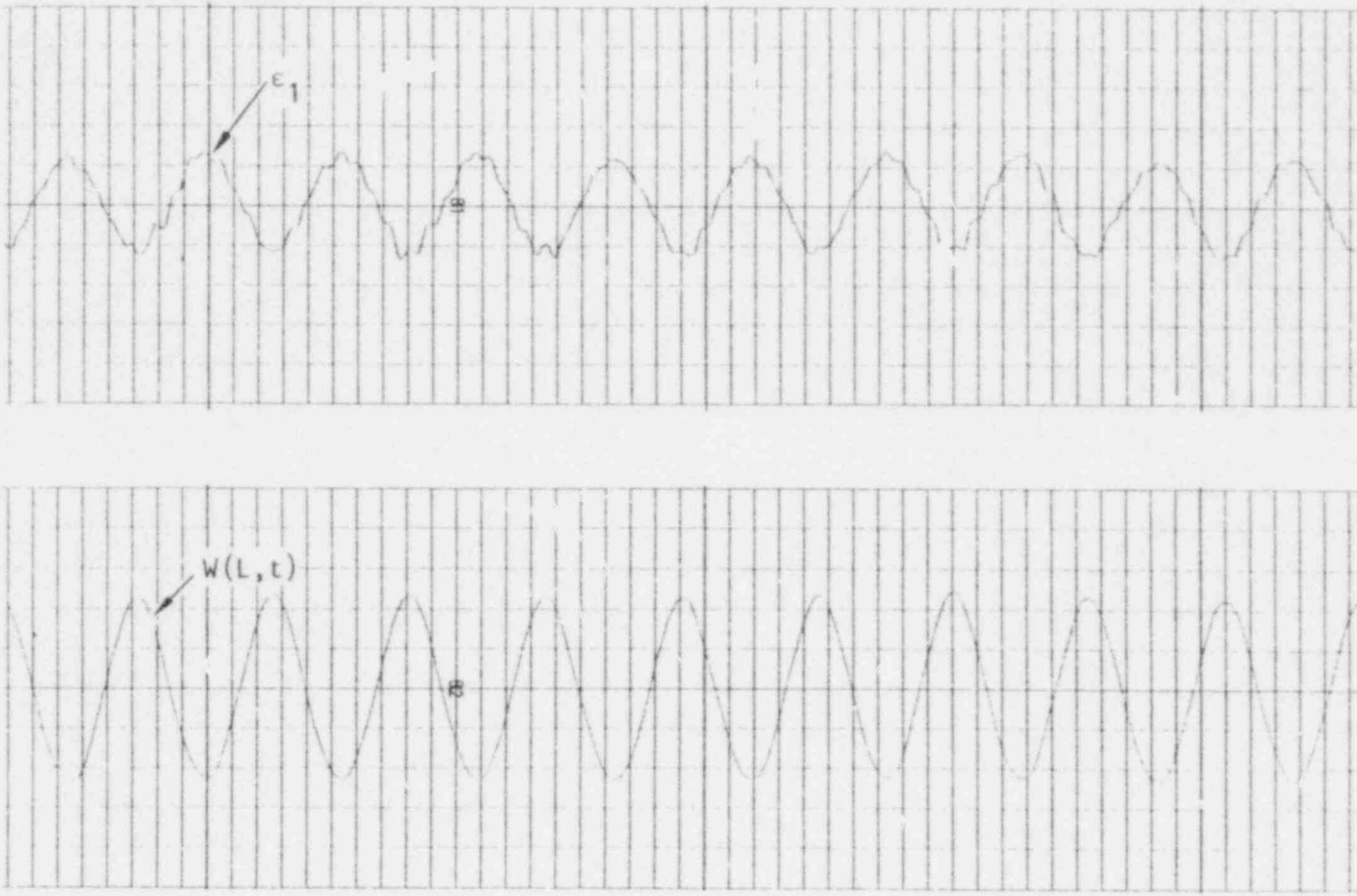

(b) ε_1, $W(L, t)$

FIGURE 3.15 VIBRATION RESPONSE, EXCITATION LEVEL $\ddot{S}_3 > \ddot{S}_2$, IMPACT, $\Omega/2\pi$ = 28.9 Hz, SPEED = 100 CM/SEC

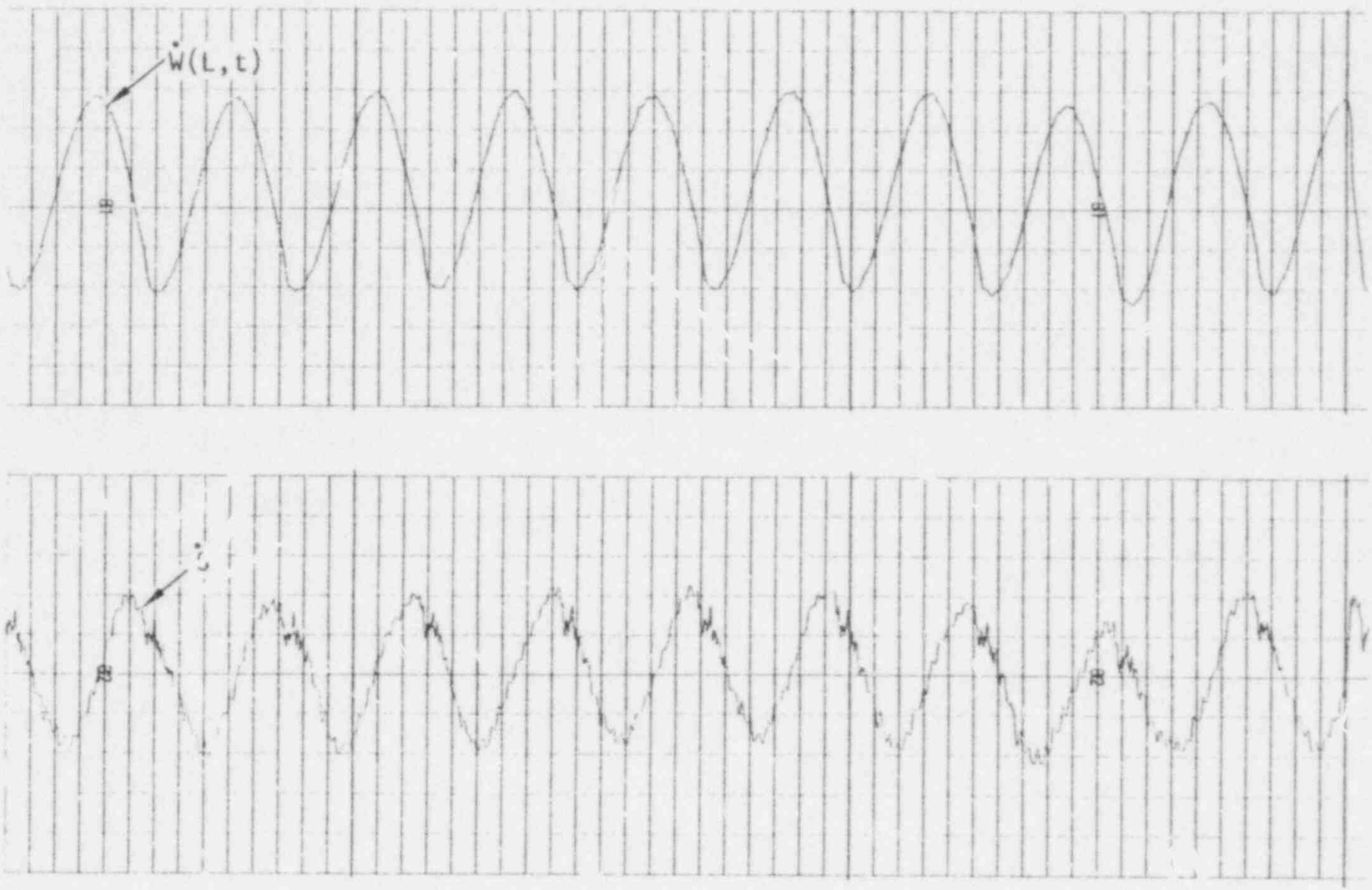

(c) $\dot{W}(L, t)$, $\ddot{S}$

FIGURE 3.15 VIBRATION RESPONSE, EXCITATION LEVEL $\ddot{S}_3 > \ddot{S}_2$, IMPACT, $\Omega/2\pi$ = 28.9 Hz, SPEED = 100 CM/SEC

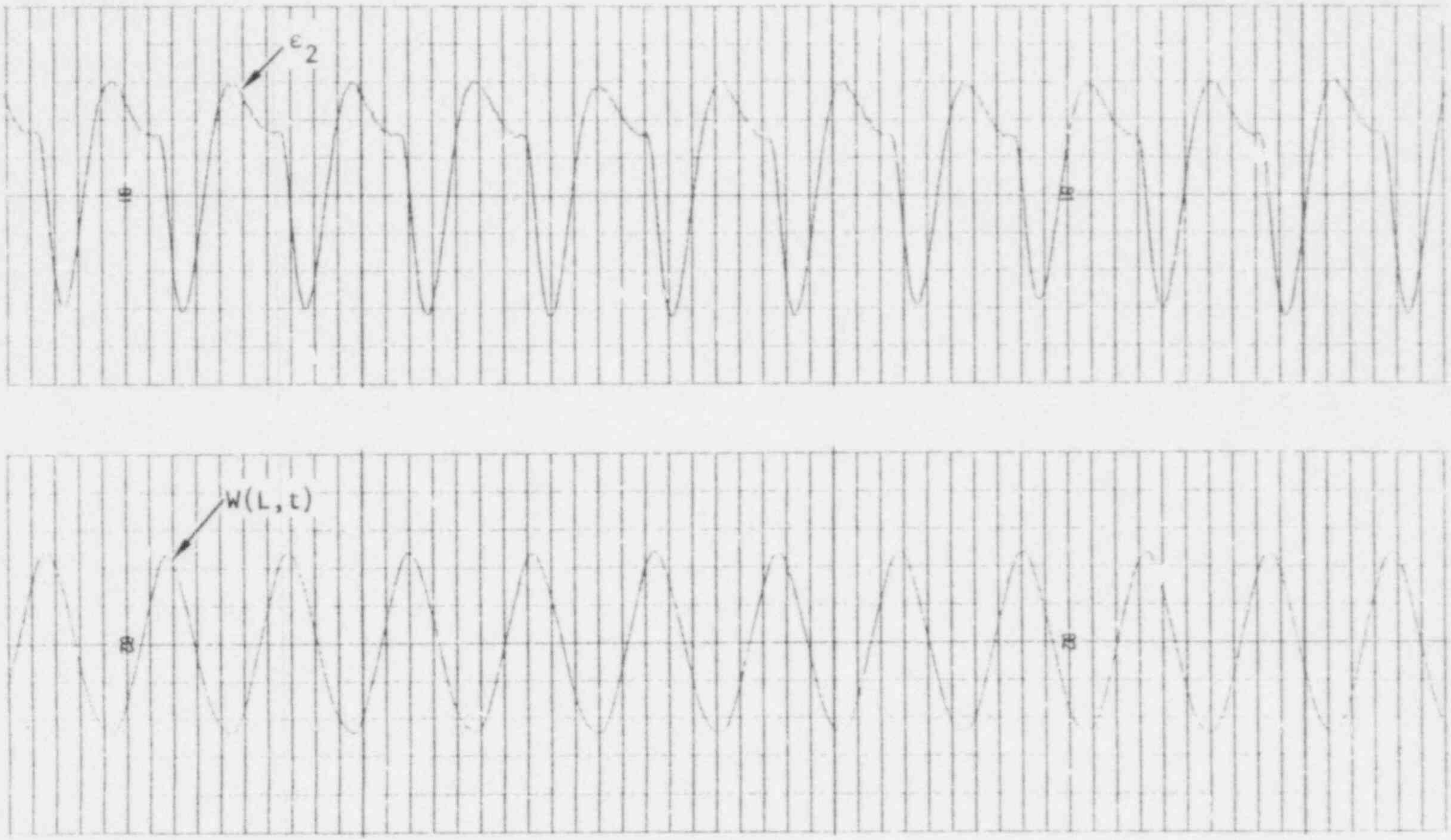

(a) ε_2, W(L, t)

FIGURE 3.16 VIBRATION RESPONSE, EXCITATION LEVEL $\ddot{S}_3 > \ddot{S}_2$, IMPACT, $\Omega/2\pi$ = 30.4 Hz, SPEED = 100 CM/SEC

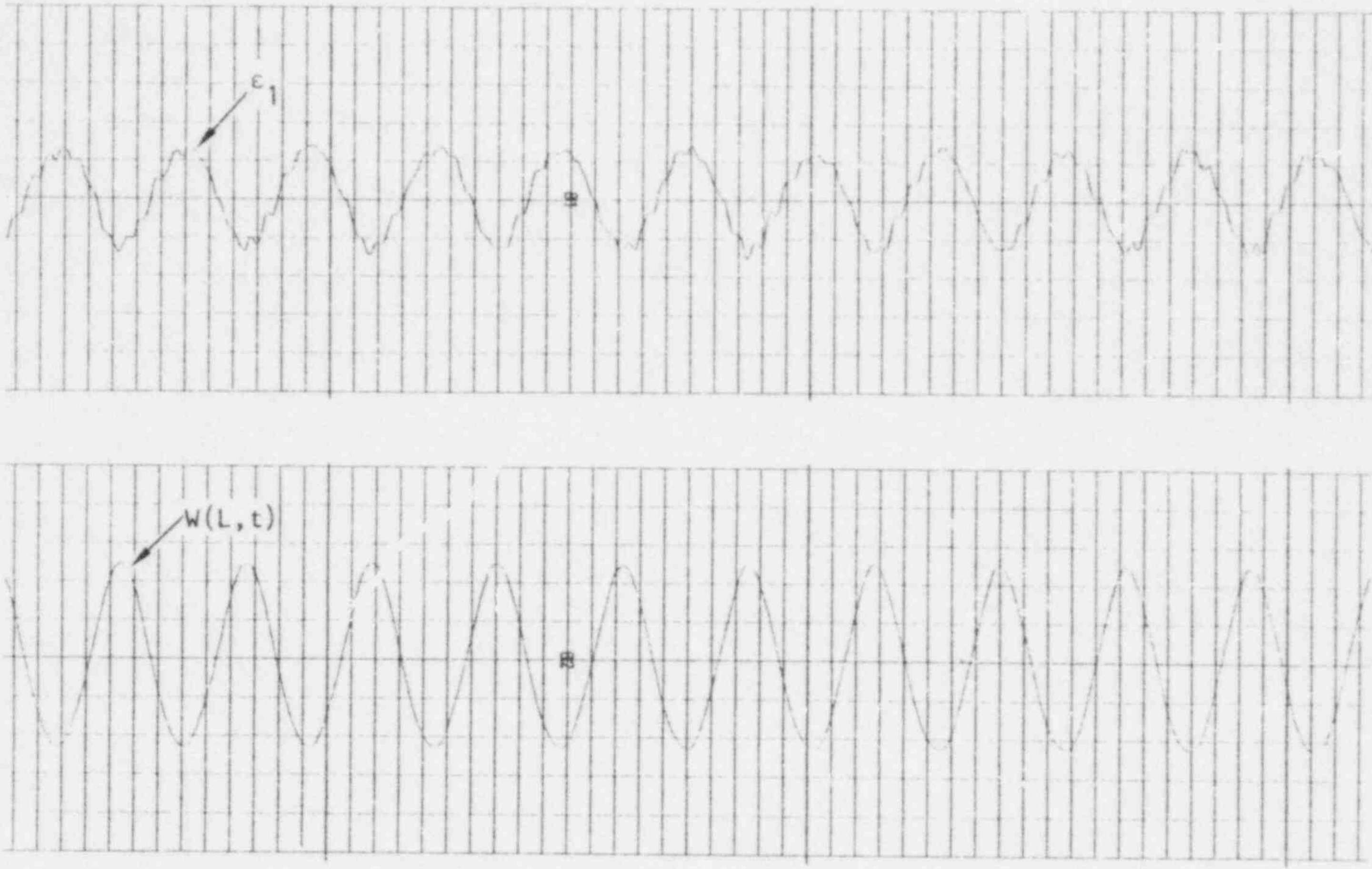

(b) ε_1, W(L, t)

FIGURE 3.16 VIBRATION RESPONSE, EXCITATION LEVE. $\ddot{S}_3 > \ddot{S}_2$, IMPACT, $\Omega/2\pi = 30.4$ Hz, SPEED = 100 CM/SEC

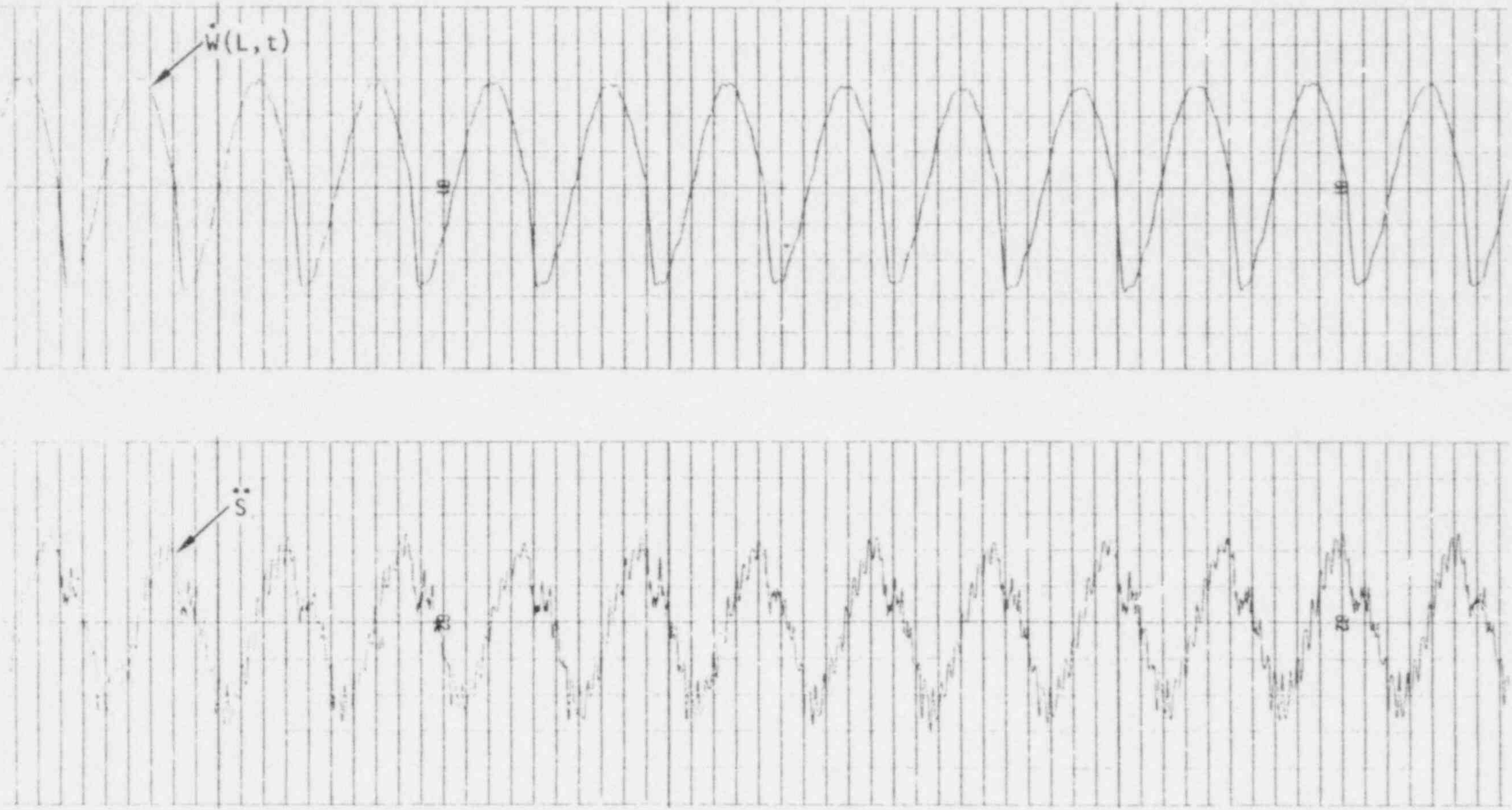

(c) $\dot{W}(L, t)$, $\ddot{S}$

FIGURE 3.16 VIBRATION RESPONSE, EXCITATION LEVEL $\ddot{S}_3 > \ddot{S}_2$, IMPACT, $\Omega/2\pi$ = 30.4 Hz, SPEED = 100 CM/SEC

Increasing the excitation level further to $\ddot{S} = \ddot{S}_3 > \ddot{S}_2$ causes the two beams to impact periodically, once per cycle of the excitation (Figures 3.11, 3.12). These impacts result in a significant contribution to the response from the higher modes of vibration of the beams, as can be seen by comparing the records of the strains ε_1 and ε_2 shown in the figures, with increasing excitation levels.

The results obtained from the experiments conducted indicate the presence of nonlinear phenomena, such as the multivalued response. This particular phenomenon is evident from the fact that the striker beam maintains impact with the target even if the increasing frequency Ω results in a linear (unconstrained) response less than the gap d (i.e., inadequate causing contact between the two beams). On the other hand, for decreasing frequency values, impacts will not be sustained until $\Omega < \Omega^*$ for which $A(\Omega^*) < d$. Note that this multivalued response behavior is characteristic of systems with hardening nonlinearities (Stoker, 1950), which is the type of system under consideration.

Chapter 4

NUMERICAL RESULTS

4.1 Application to an Example Problem

Based on the analysis presented in Section 2, a computer program was developed for the construction of a typical steady-state solution of an arbitrary example problem. The system chosen for this example is shown in Figure 4.1. It consists of a uniform cantilever beam with an elastic stop (spring) placed at its end with a clearance (gap) d. The beam is assumed to have a constant stiffness EI, a uniform cross sectional area A_s, and mass density m. The computer program was designed to solve for the unknowns of the problem discussed in Chapter 2, using the iteration scheme presented in Section 2.3.4. A brief description of the program is presented in Appendix C.

For the derivation of the damping ratio $\zeta_i^{(j)}$, the damping parameters α and β can be related to the frequencies and ratios of critical damping of two modes i and j (see, for example, Timoshenko, et al., 1974) by

$$\alpha = (2\zeta_i - \beta\omega_i)\,\omega_i \qquad (4.1)$$

and

$$\beta = 2(\zeta_j\omega_j - \zeta_i\omega_i)\,(\omega_j^2 - \omega_i^2) \qquad (4.2)$$

For the present work, the values of α and β were determined from Equations 4.1 and 4.2 so as to make the damping ratios of the first two

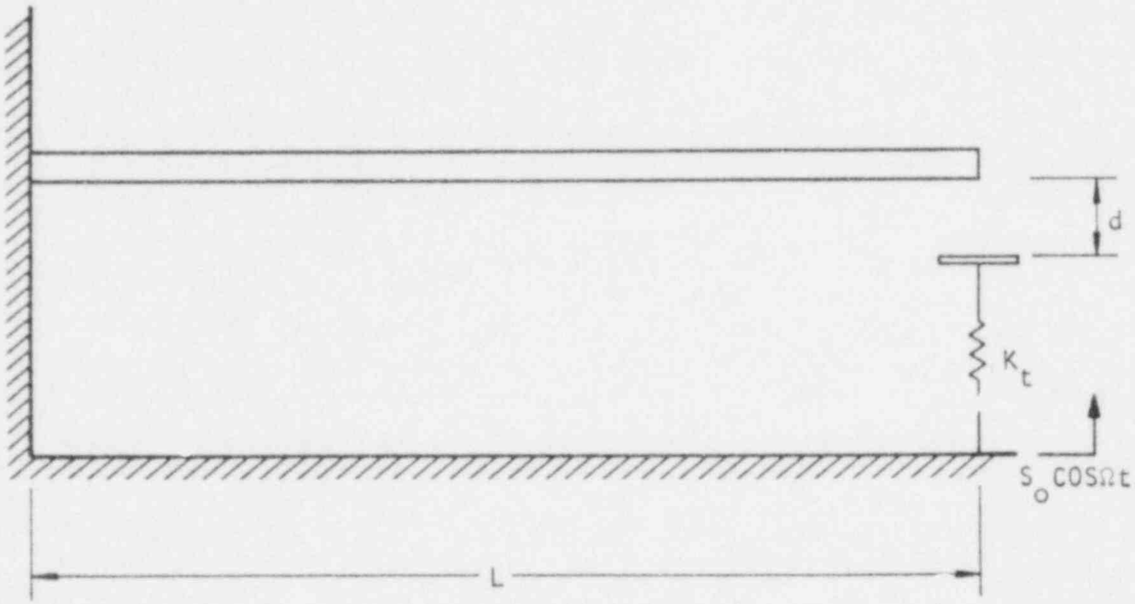

FIGURE 4.1 DYNAMIC MODEL OF THE EXAMPLE PROBLEM

modes of vibration of the unconstrained region of solution $\zeta_1 = \zeta_2 = \zeta_0$ $\equiv$ constant. The damping ratio $\zeta_i^{(j)}$ for each mode of both solution regions is then determined by using the following equation:

$$\zeta_i^{(j)} = 0.5\left[\frac{\alpha}{\omega_i^{(j)}} + \beta\omega_i^{(j)}\right] \qquad (4.3)$$

4.1.1 Present Theory

Typical steady-state solutions for different arbitrary sets of parameters are illustrated in Figures 4.2 through 4.9, where the displacement $W(x,t)$, the velocity $\dot{W}(x,t)$, and the curvature $W''(x,t)$ at different stations along the striker-beam length are shown for one period of the excitation. The contribution of the higher modes to the response is clear in all of the figures, as was the case in the experimental data discussed in Section 3.2.6.

Furthermore, it can be seen that the amount of penetration ($W(L,t)$ - d), the duration of contact, and the maximum positive peak displacement depend largely on K* (the stiffness ratio of the target to the striker beam), as well as on the damping of the striker beam and the gap size. A complete discussion of the effects of the various parameters is presented in Section 4.2.

4.1.2 Comparison between Theory and Experiment

Figure 4.10 presents a typical comparison of the theoretical and experimental results. In this figure the stiffness ratio K* is about 25 and the damping of the striker beam is about 4%. It is clear from this figure that the agreement between the theoretical and experimental results is fairly good, even though only two modes were used in the in the theoretical analysis.

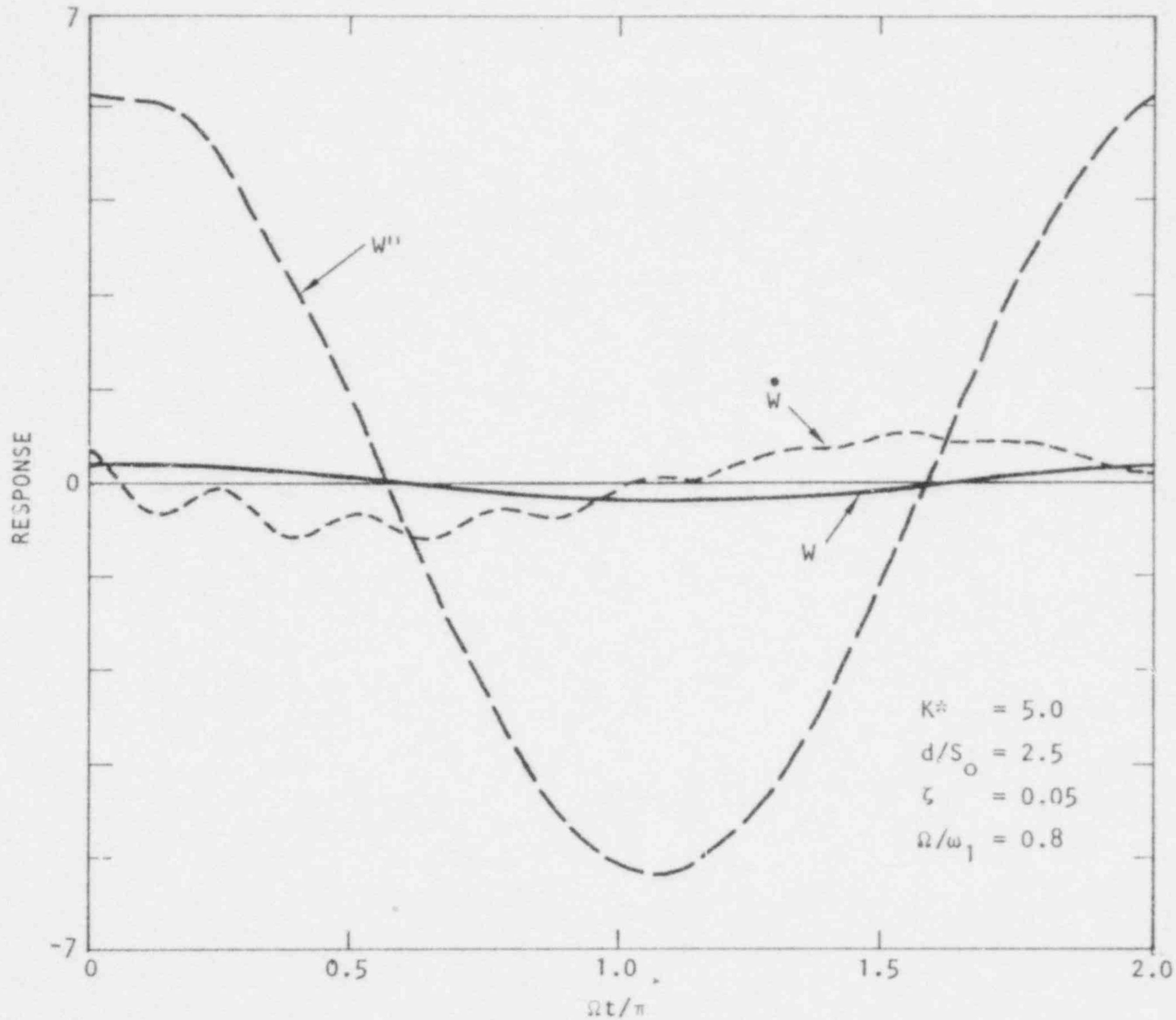

FIGURE 4.2 CONSTRUCTION OF A TYPICAL SOLUTION (DISPLACEMENT, VELOCITY, AND CURVATURE AT X = 0.25L)

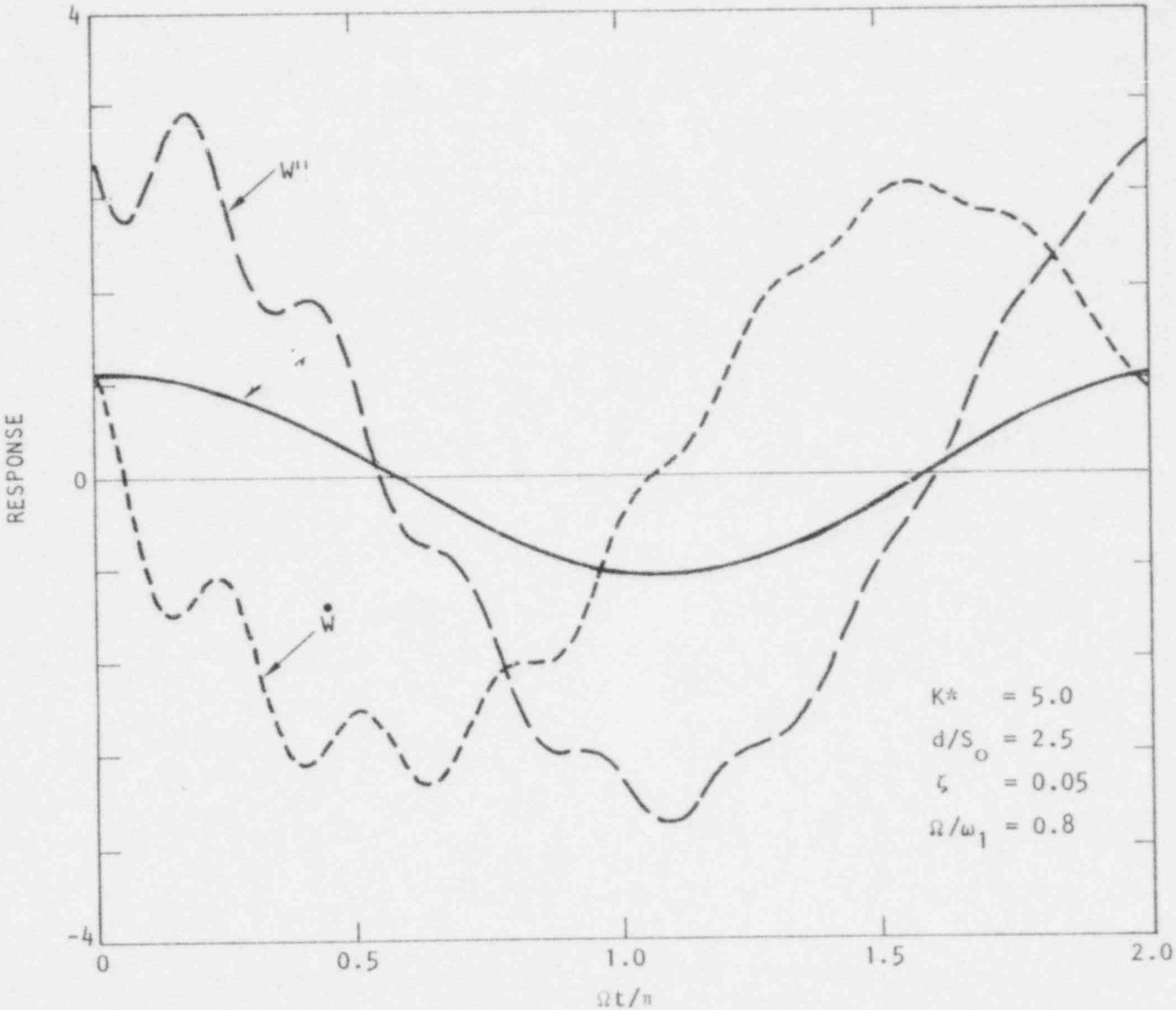

FIGURE 4.3 CONSTRUCTION OF A TYPICAL SOLUTION (DISPLACEMENT, VELOCITY, AND CURVATURE AT X = 0.5L)

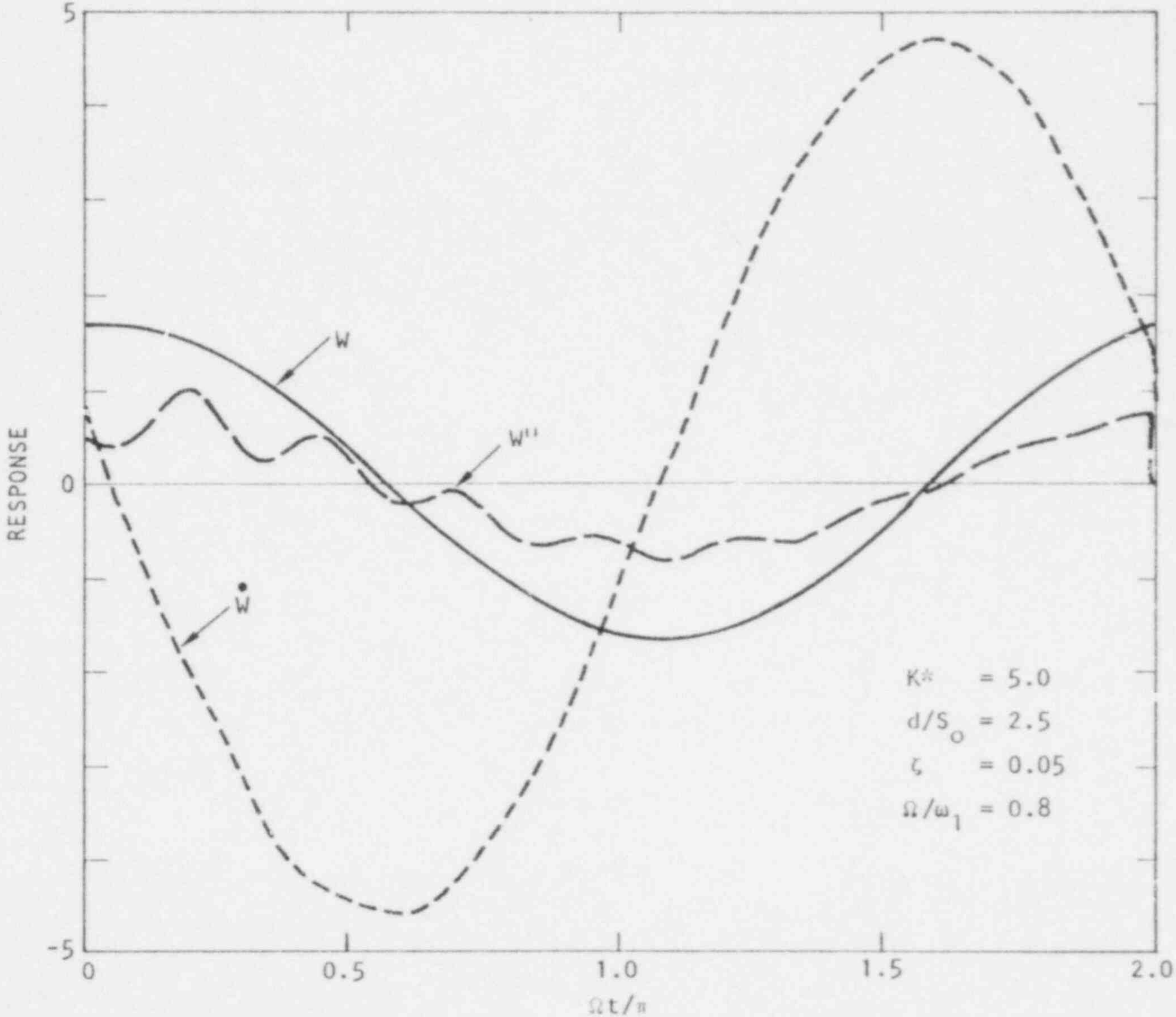

FIGURE 4.4 CONSTRUCTION OF A TYPICAL SOLUTION (DISPLACEMENT, VELOCITY, AND CURVATURE AT X = 0.75L)

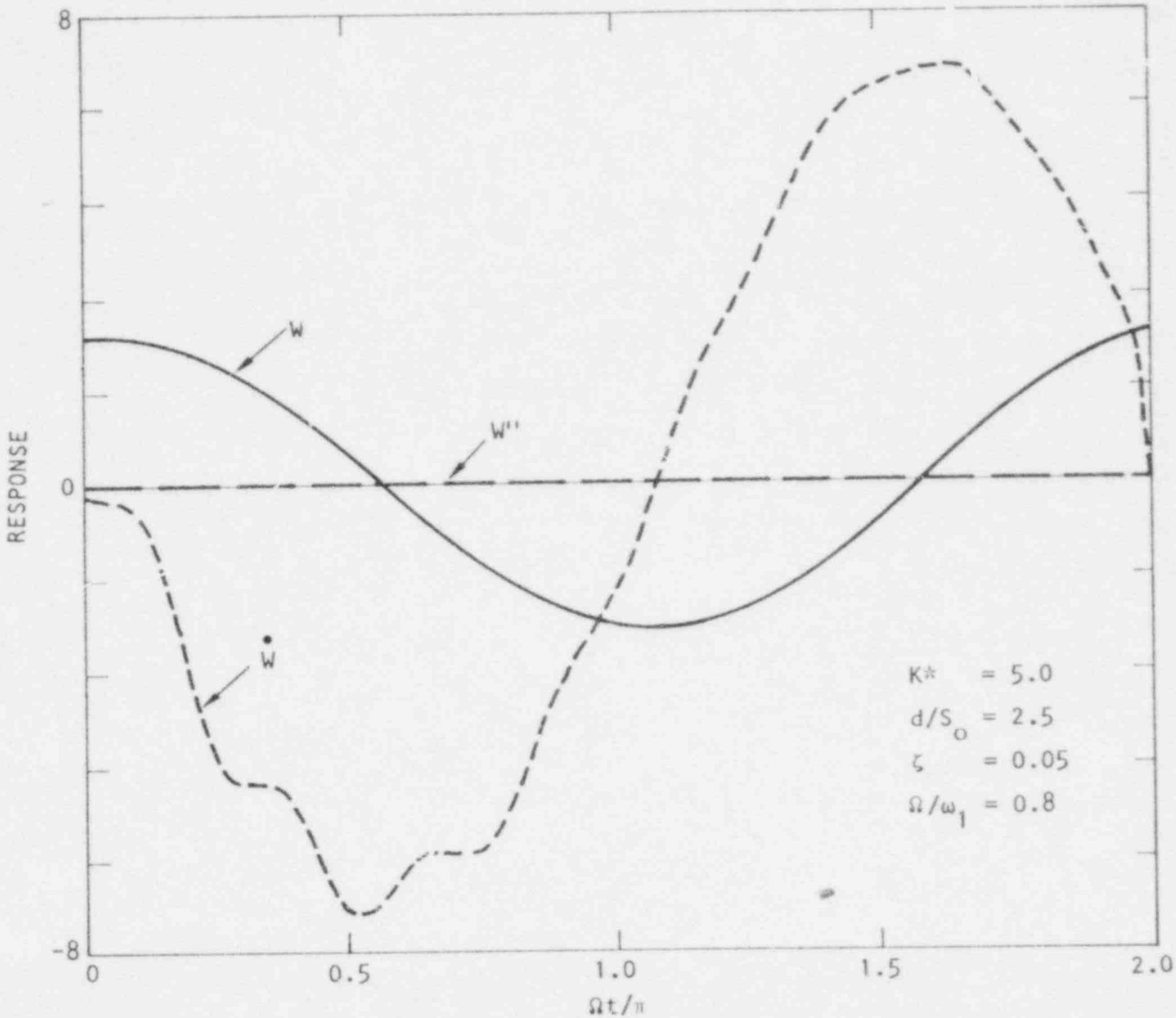

FIGURE 4.5 CONSTRUCTION OF A TYPICAL SOLUTION (DISPLACEMENT, VELOCITY, AND CURVATURE AT X = L

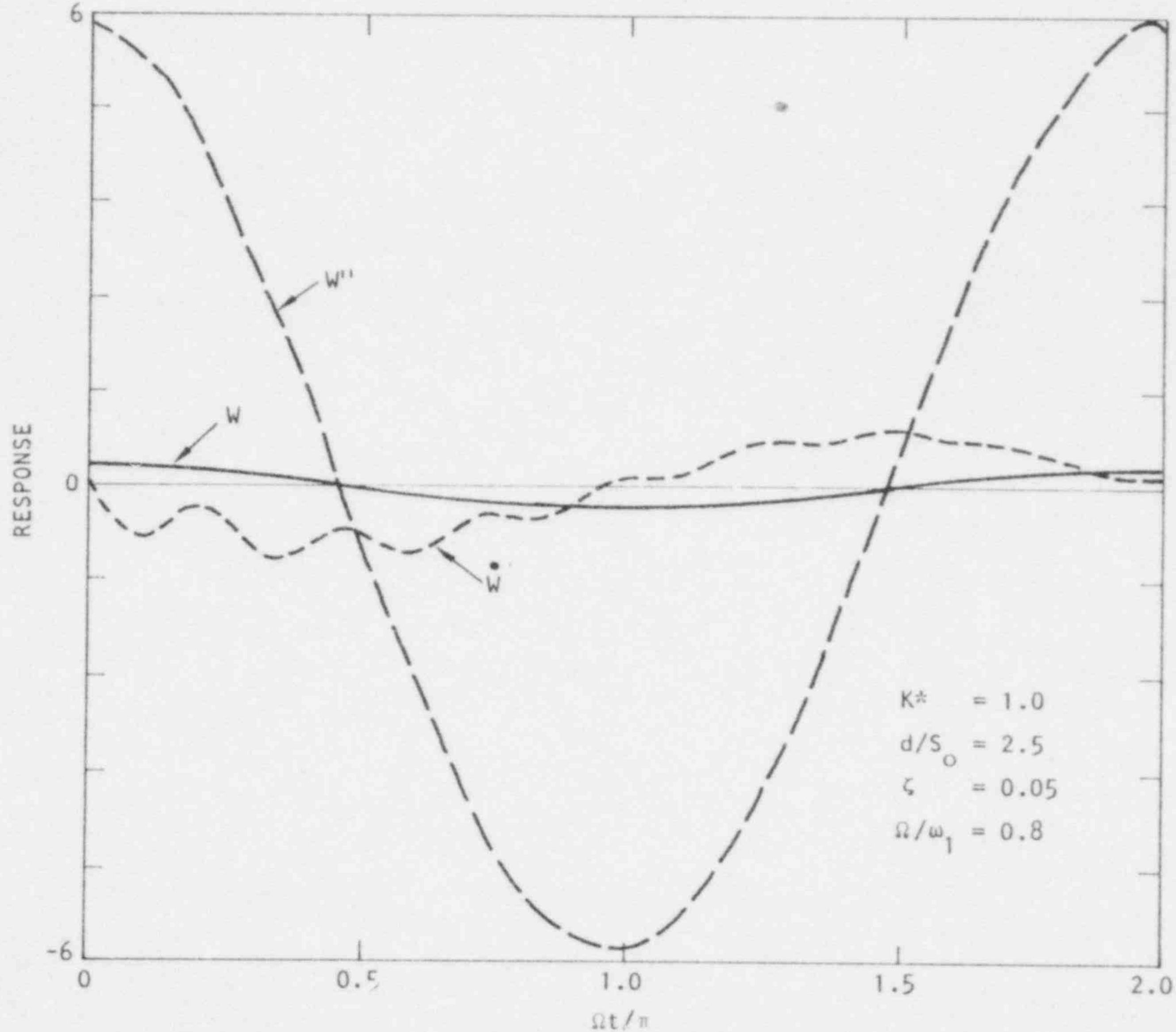

FIGURE 4.6 CONSTRUCTION OF A TYPICAL SOLUTION (DISPLACEMENT, VELOCITY, AND CURVATURE AT X = 0.25L)

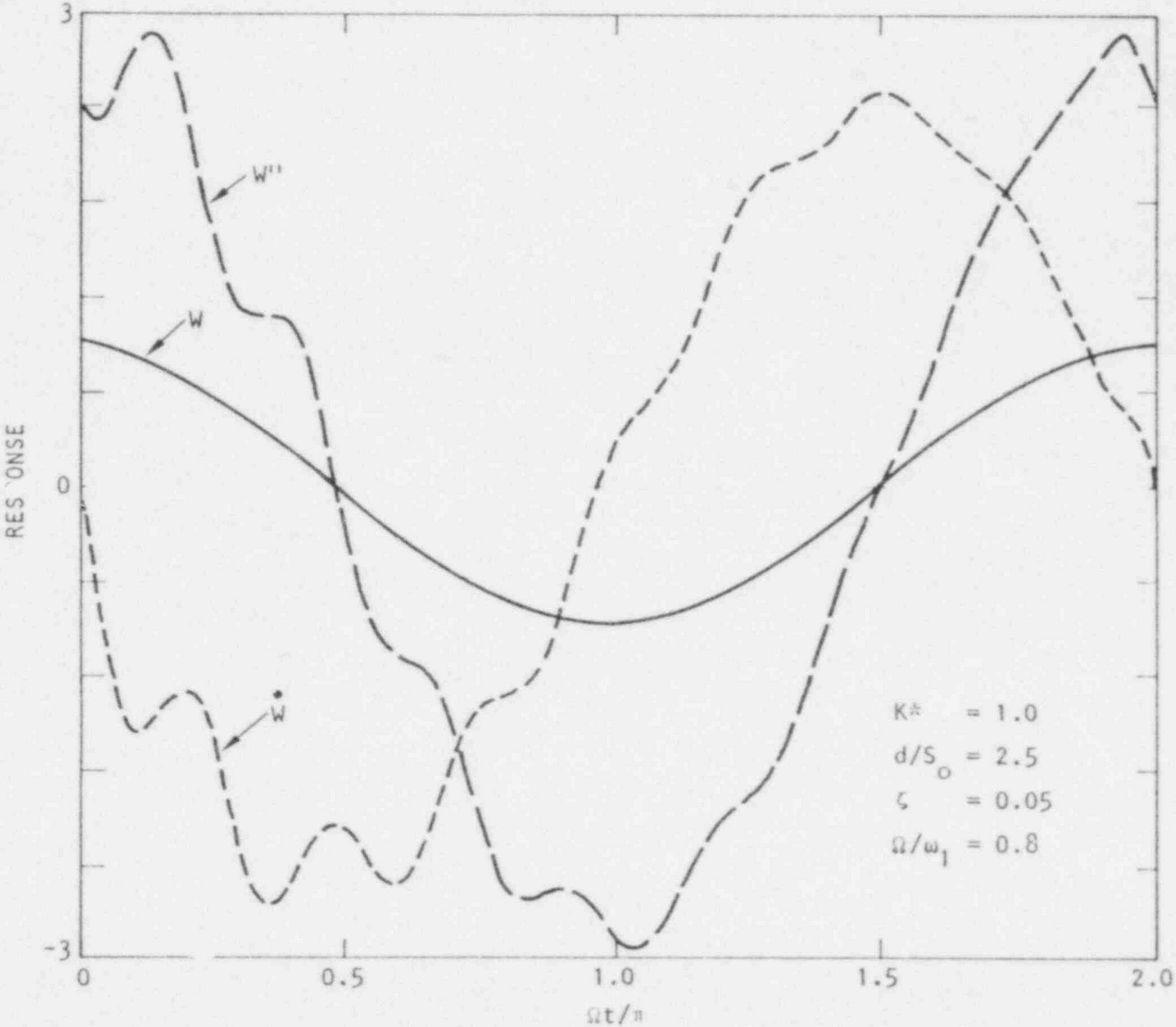

FIGURE 4.7 CONSTRUCTION OF A TYPICAL SOLUTION (DISPLACEMENT, VELOCITY, AND CURVATURE AT X = 0.5L)

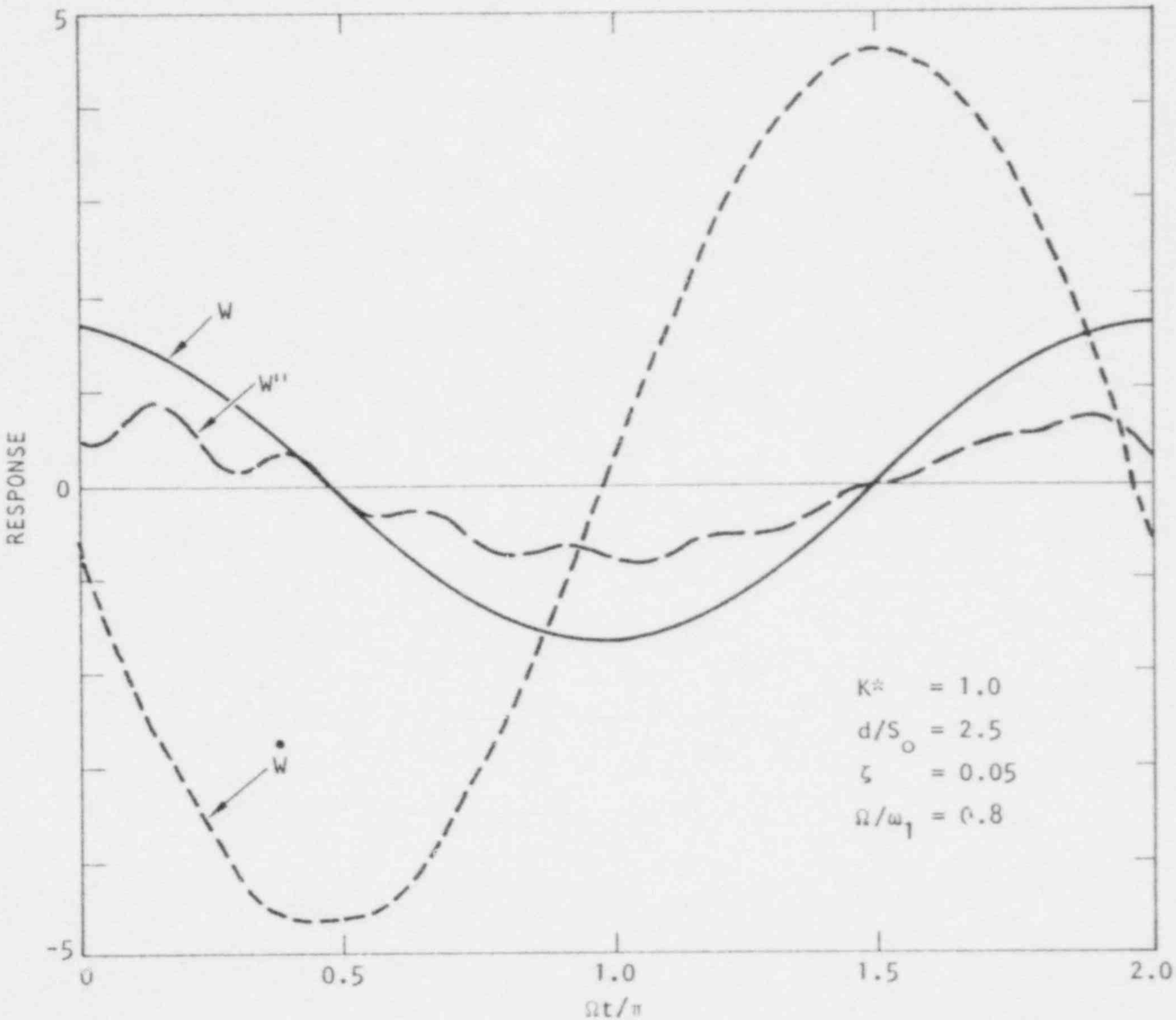

FIGURE 4.8 CONSTRUCTION OF A TYPICAL SOLUTION (DISPLACEMENT, VELOCITY, AND CURVATURE AT X = 0.75L)

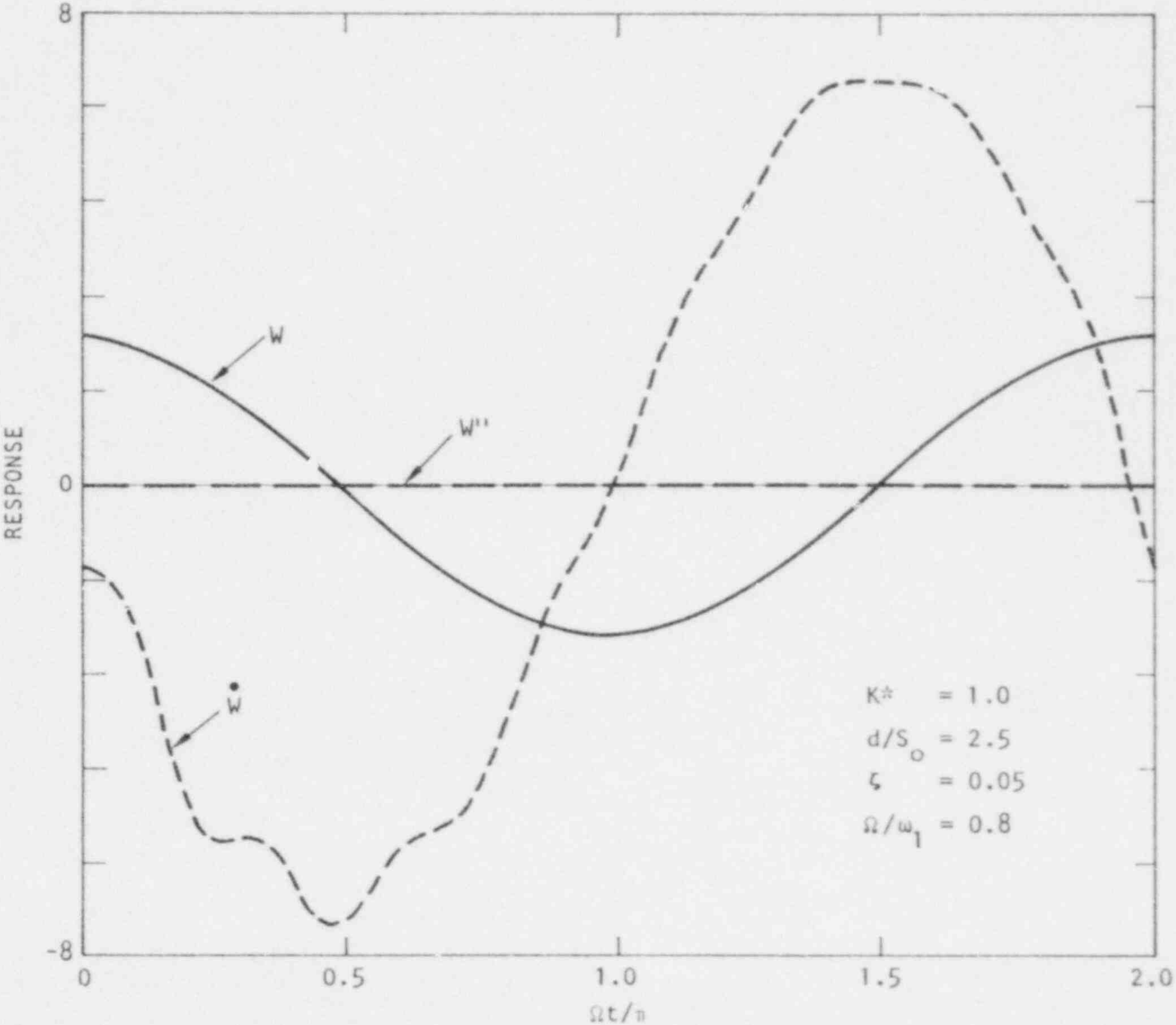

FIGURE 4.9 CONSTRUCTION OF A TYPICAL SOLUTION (DISPLACEMENT, VELOCITY, AND CURVATURE AT X = L)

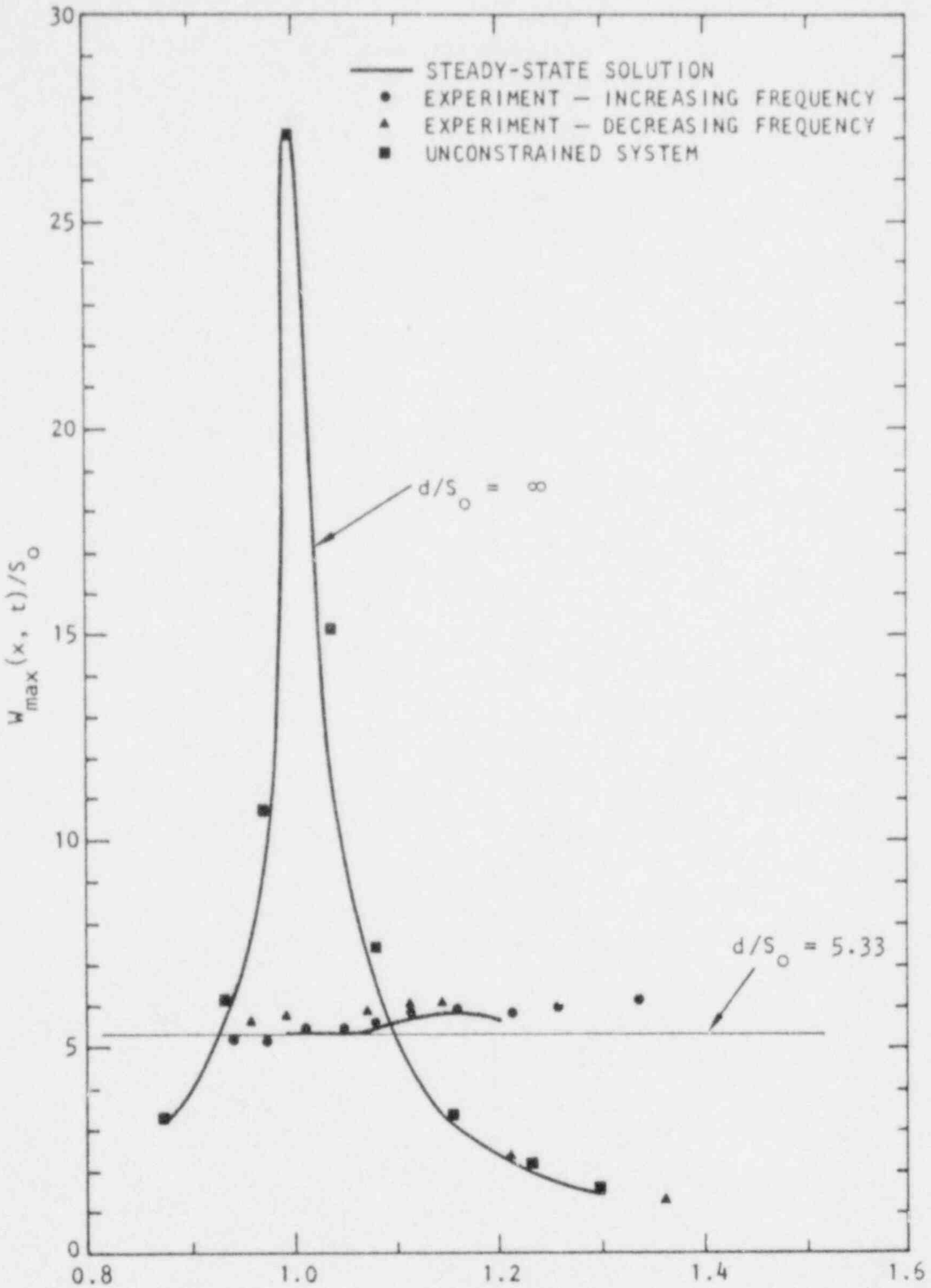

FIGURE 4.10 COMPARISON BETWEEN THEORY AND EXPERIMENT OF THE RESPONSE OF A CONTINUOUS SYSTEM WITH A GAP: $K^* = 25$, $\zeta = 0.04$, CLEARANCE RATIO $d/S_o = 5.33$

4.2 Effect of System Parameters

The effects of the system parameters were studied by varying one parameter at a time while keeping the rest constant. The graphs shown in the figures clarify the various effects. Figures 4.11 through 4.26 represent the dimensionless positive peak response W_{max}/S_o versus the dimensionless frequency ratio Ω/ω_1 for the chosen parameters, whereas Figures 4.27 through 4.38 represent the dimensionless no-contact time ratio α_2/π versus the dimensionless frequency ratio Ω/ω_1. The effect of each parameter is discussed in the following separate sections.

4.2.1 Excitation Frequency Effect

It can be seen from Figures 4.11 through 4.14 that the peak response ratio W_{max}/S_o is a nonlinear function of the excitation frequency Ω/ω_1. The maximum peak response occurs at different excitation frequencies, depending on the beam-to-spring stiffness ratio K*.

4.2.2 Damping Effect

It is found that the amount of damping ζ_i present in the primary system has a significant effect on the peak response of the system with a gap, as would be the case for the system without a gap. Generally, the peak response is reduced by increasing the amount of damping of the primary system. The amount of reduction depends on the values of the stiffness ratio K*, clearance ratio d/S_o, and excitation frequency ratio Ω/ω_1. Figures 4.15 through 4.20 show the effect of the change in the value of the damping ratio for stiffness ratios K* equal to 5, 10, and 20 and clearance ratios d/S_o equal to 1.5 and 2.5. It is clear from these figures that the maximum reduction occurs at the peak values of the response. Figure 4.16 illustrates this for the case of stiffness

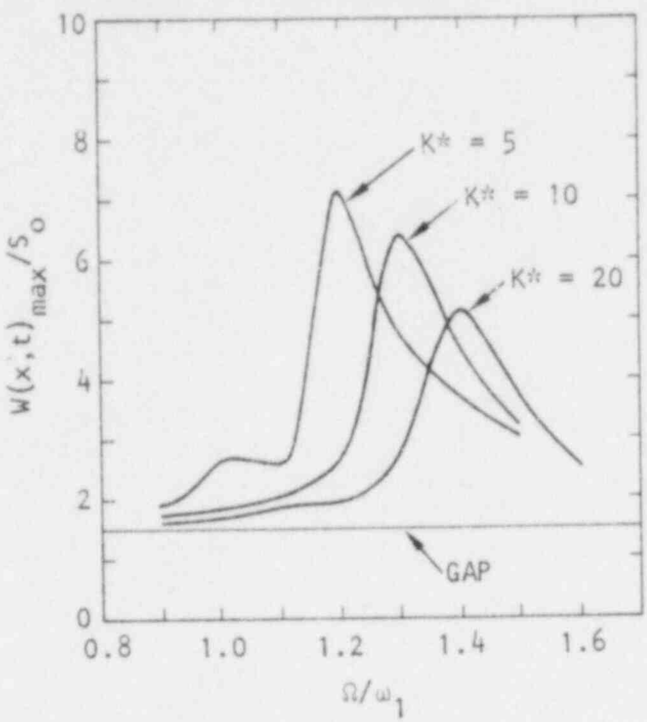

FIGURE 4.11 MAXIMUM POSITIVE PEAK RESPONSE FOR $\zeta = 0.05$, CLEARANCE RATIO $d/S_o = 1.5$, $K^* = 5, 10, 20$

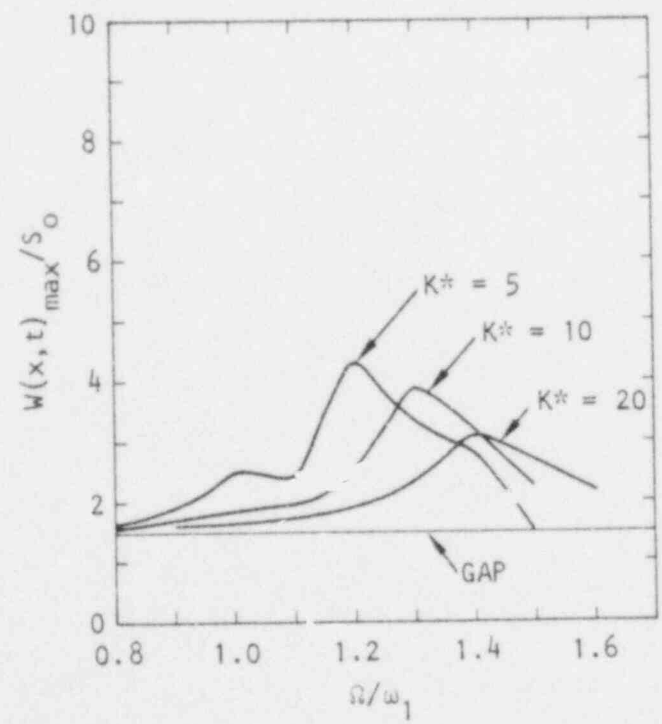

FIGURE 4.12 MAXIMUM POSITIVE PEAK RESPONSE FOR $\zeta = 0.10$, CLEARANCE RATIO $d/S_o = 1.5$, $K^* = 5, 10, 20$

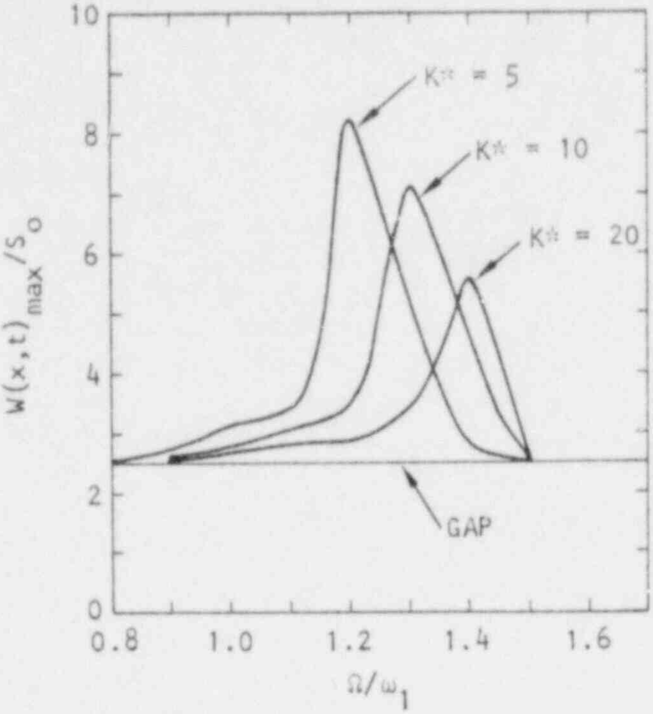

FIGURE 4.13 MAXIMUM POSITIVE PEAK RESPONSE FOR $\zeta = 0.05$, CLEARANCE RATIO $d/S_o = 2.5$, K* = 5, 10, 20

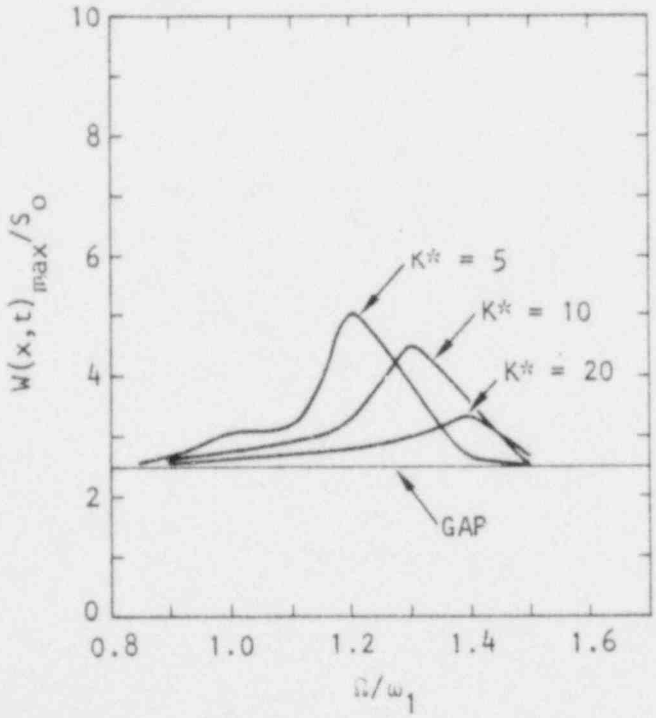

FIGURE 4.14 MAXIMUM POSITIVE PEAK RESPONSE FOR $\zeta = 0.10$, CLEARANCE RATIO $d/S_o = 2.5$, K* = 5, 10, 20

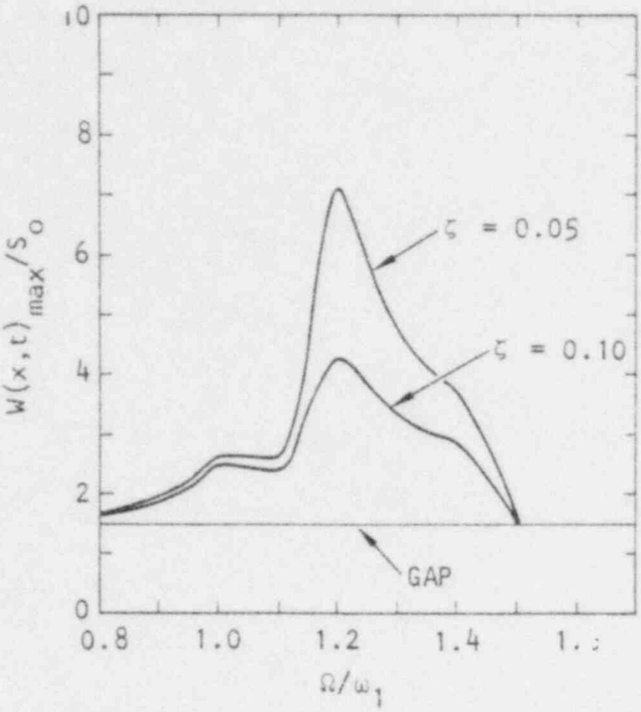

FIGURE 4.15 MAXIMUM POSITIVE PEAK RESPONSE FOR $\zeta = 0.05, 0.10$, CLEARANCE RATIO $d/S_o = 1.5$, $K^* = 5$

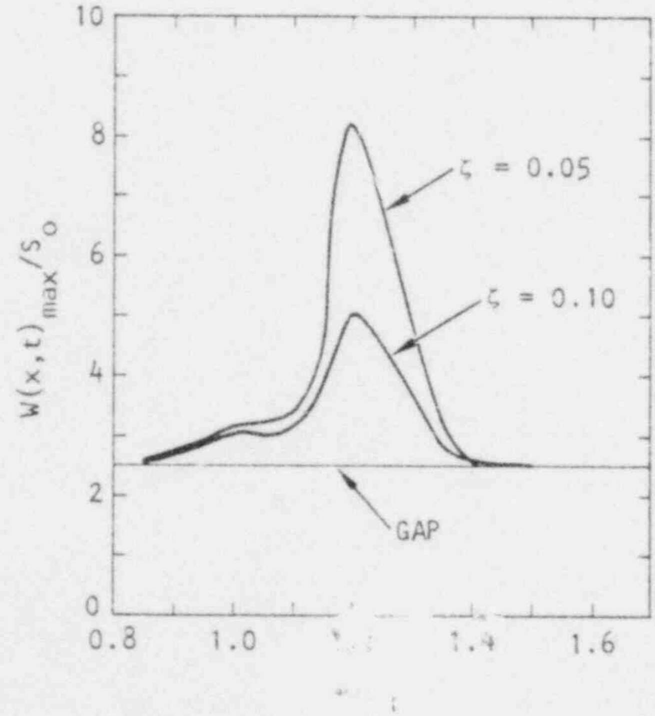

FIGURE 4.16 MAXIMUM POSITIVE PEAK RESPONSE FOR $\zeta = 0.05, 0.10$, CLEARANCE RATIO $d/S_o = 2.5$, $K^* = 5$

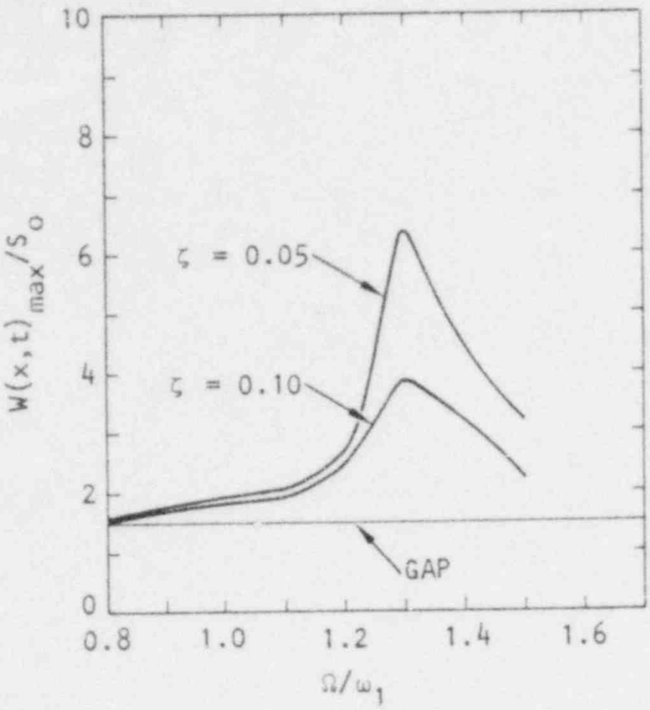

FIGURE 4.17 MAXIMUM POSITIVE PEAK RESPONSE FOR $\zeta = 0.05, 0.10$, CLEARANCE RATIO $d/S_o = 1.5$, $K^* = 10$

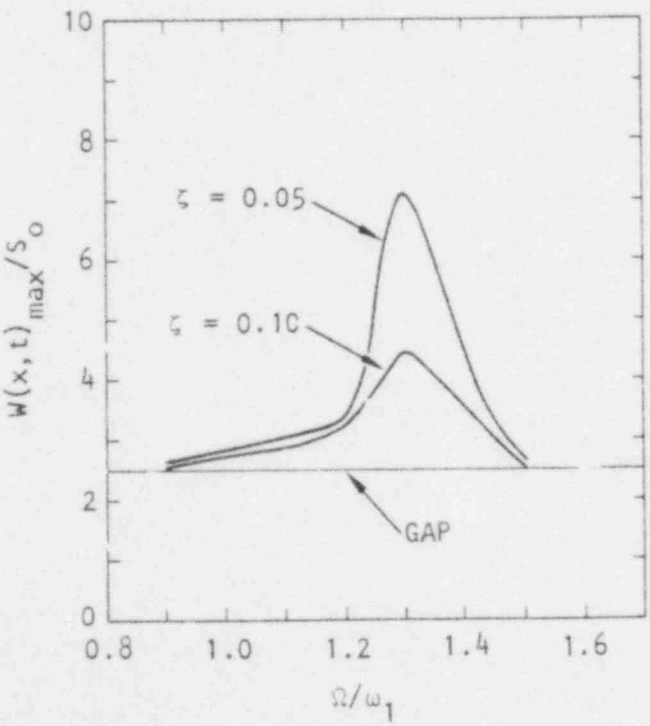

FIGURE 4.18 MAXIMUM POSITIVE PEAK RESPONSE FOR $\zeta = 0.05, 0.10$, CLEARANCE RATIO $d/S_o = 2.5$, $K^* = 10$

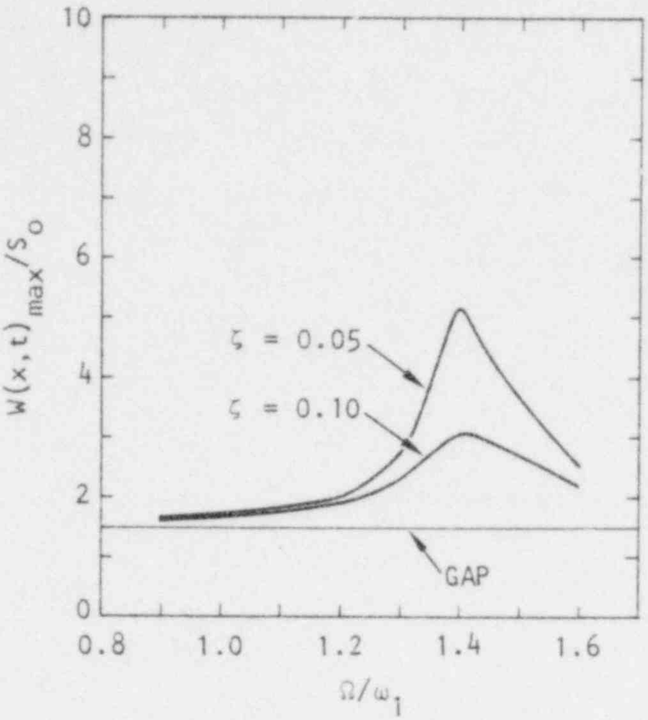

FIGURE 4.19 MAXIMUM POSITIVE PEAK RESPONSE FOR $\zeta = 0.05$, 0.10, CLEARANCE RATIO $d/S_o = 1.5$, $K^* = 20$

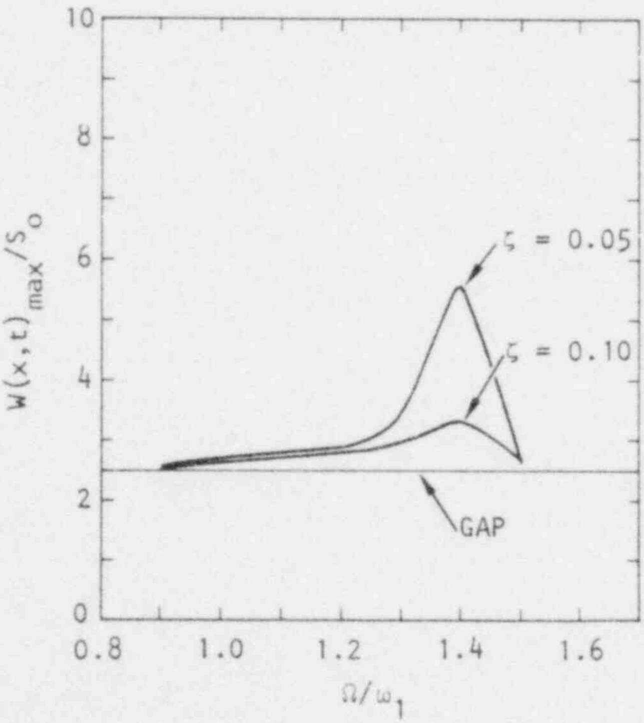

FIGURE 4.20 MAXIMUM POSITIVE PEAK RESPONSE FOR $\zeta = 0.05$, 0.10, CLEARANCE RATIO $d/S_o = 2.5$, $K^* = 20$

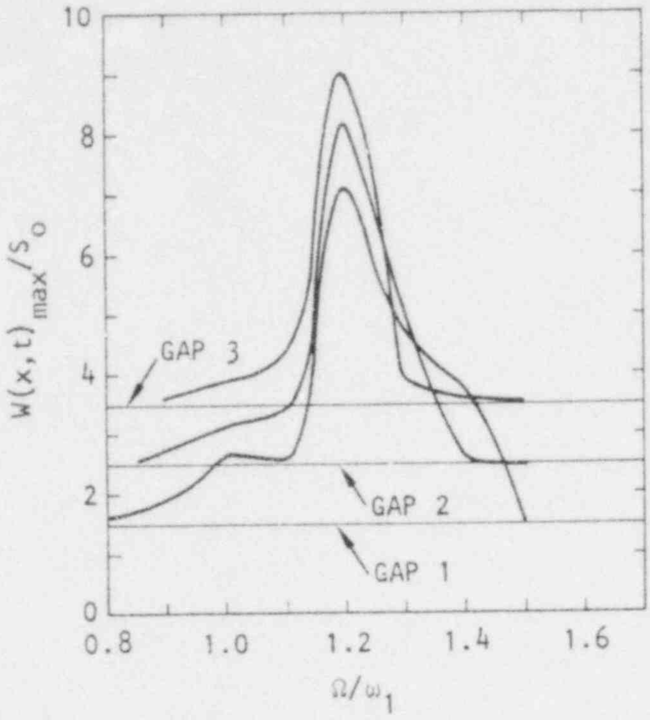

FIGURE 4.21 MAXIMUM POSITIVE PEAK RESPONSE FOR $\zeta = 0.05$, CLEARANCE RATIOS d/S_o = 1.5, 2.5, 3.5, K* = 5

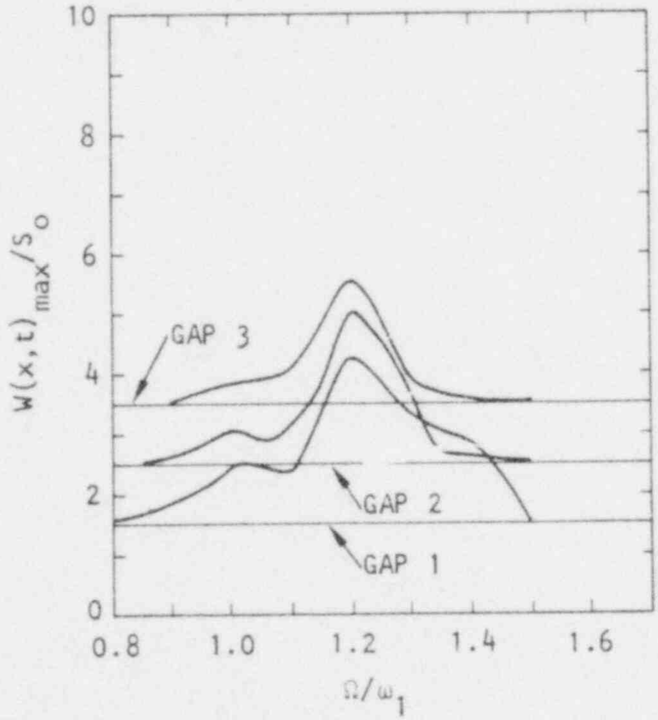

FIGURE 4.22 MAXIMUM POSITIVE PEAK RESPONSE FOR $\zeta = 0.10$, CLEARANCE RATIOS d/S_o = 1.5, 2.5, 3.5, K* = 5

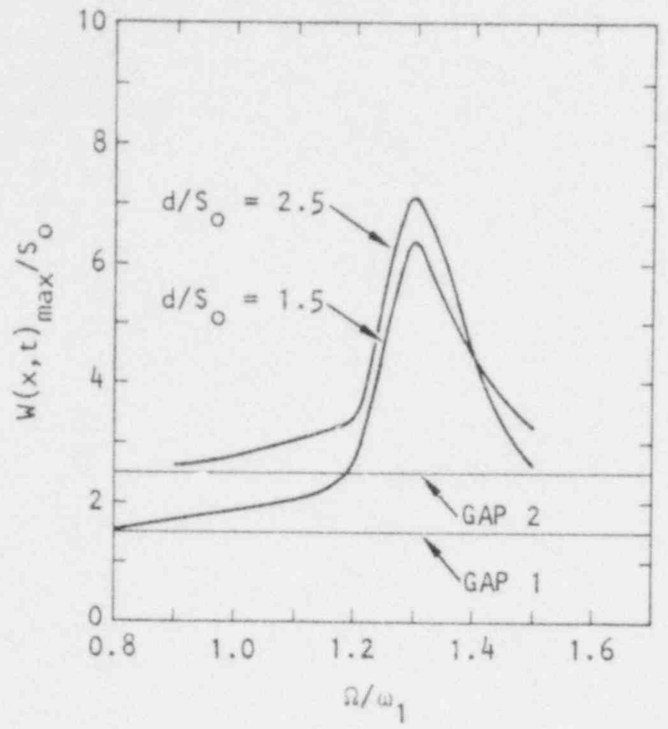

FIGURE 4.23 MAXIMUM POSITIVE PEAK RESPONSE FOR $\zeta = 0.05$, CLEARANCE RATIOS d/S_o = 1.5, 2.5, K* = 10

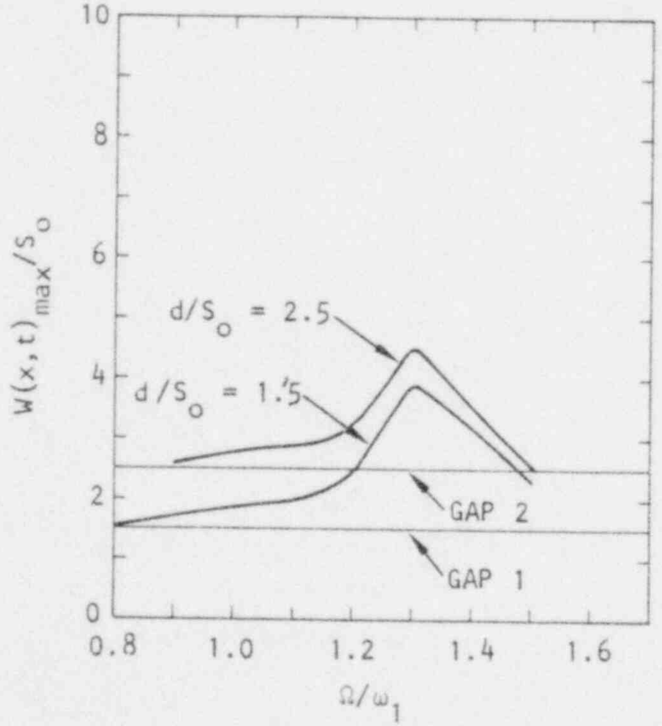

FIGURE 4.24 MAXIMUM POSITIVE PEAK RESPONSE FOR $\zeta = 0.10$, CLEARANCE RATIOS d/S_o = 1.5, 2.5, K* = 10

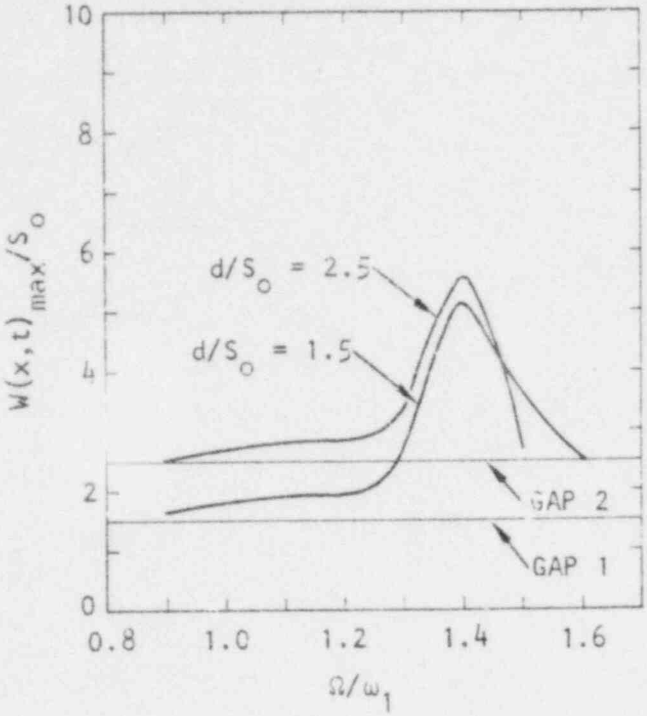

FIGURE 4.25 MAXIMUM POSITIVE PEAK RESPONSE FOR ζ = 0.05, CLEARANCE RATIOS d/S_o = 1.5, 2.5, K* = 20

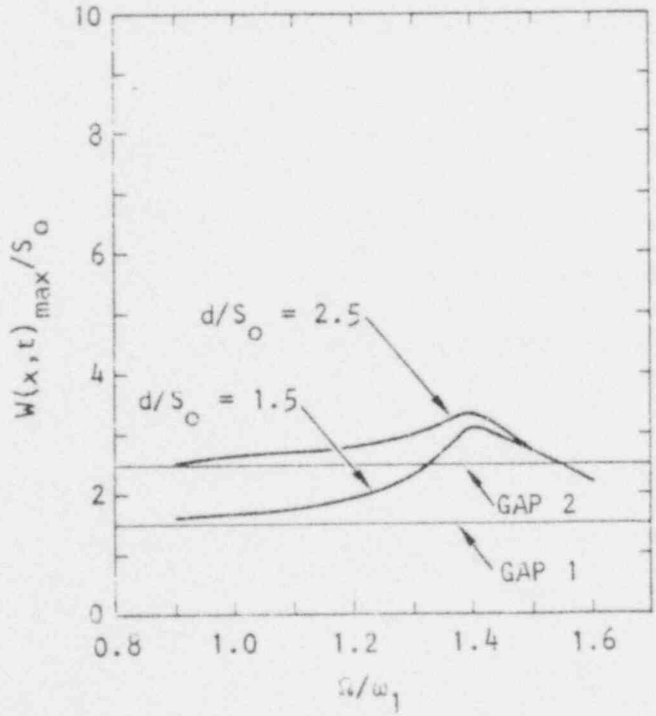

FIGURE 4.26 MAXIMUM POSITIVE PEAK RESPONSE FOR ζ = 0.10, CLEARANCE RATIOS d/S_o = 1.5, 2.5, K* = 20

ratio K^* equal to 5 and for a gap size d/S_0 equal to 2.5. An increase in the value of damping ratio ζ_i from 0.05 to 0.10 would reduce the maximum positive peak response W_{max}/S_0 by 38.5% at an excitation frequency ratio of Ω/ω_1 = 1,2, whereas the reduction is very small, if any, at the frequency ratio of 0.8.

4.2.3 Stiffness Ratio Effect

The stiffness ratio has a significant influence on the response of the system, as can be seen from Figures 4.11 through 4.14 in which all the parameters except the stiffness ratio K^* are kept constant. Note that in all of these figures, increasing the stiffness ratio alone would reduce the maximum peak response an amount dependent upon the damping ratio ζ_i and the gap size d/S_0.

The amount of peak response for a certain excitation frequency ratio Ω/ω_1 would be greater or less, depending on the range of the excitation. For example, Figure 4.11 shows that where the constant gap ratio d/S_0 is equal to 1.5, at an excitation frequency Ω/ω_1 equal to 1.2, the peak response is greater for a lower stiffness ratio K^*; whereas for an excitation frequency ratio Ω/ω_1 equal to 1.4, the peak response is greater for a higher stiffness ratio. Thus, it could be concluded that hardening of the spring does not imply a reduction in the peak response amplitude in all excitation frequency ranges. It is also seen from Figure 4.11 that a 10.5% reduction in the maximum peak response resulted from a 100% increase in the stiffness ratio K^* (from K^* = 5 to K^* = 10), although a 28.5% reduction is achieved by a 400% increase in the stiffness ratio (from K^* = 5 to K^* = 20).

4.2.4 Effect of Gap Size

It is seen from Figures 4.21 through 4.26 that decreasing the gap size generally reduced the value of the maximum peak response by an amount that depends on the stiffness ratio K* and the damping ratio ζ_i; on the other hand certain ranges of the frequency of excitation Ω/ω_1 may have an opposite effect on the peak response. For example, decreasing the gap size ratio d/S_o by 40% resulted in a 13% reduction in the value of the maximum peak response for a constant stiffness ratio K* equal to 5.0 and a constant damping ratio ζ_i equal to 0.05. The same stiffness ratio and same percentage of decreases in the gap size resulted in a 14% reduction in the maximum peak response for a constant damping ratio of 0.10. Figure 4.24 shows that the peak response is reduced about 36% at an excitation frequency ratio Ω/ω_1 equal to 0.9 for a 40% decrease in the gap size d/S_1; while a 7% reduction in peak response is achieved at a higher excitation frequency ratio equal to 1.4.

4.2.5 Contact Duration

The study of the time of contact is important in that it shows how long the primary system (the striker beam) stays in contact with the elastic stop (spring), for then the whole system is considered a constrained beam in the solution of the problem. In all of the cases of parameter permutations studied, the contact time of the primary system with the elastic stop was noted. Graphs of the variation of the non-dimensional no-contact time α_2/π versus the excitation frequency ratio Ω/ω_1 are shown in Figures 4.27 through 4.38. In Figures 4.27 through 4.29, all parameters are kept constant except the stiffness ratio K*. This was done to see the effect of the elastic stop stiffness on the contact time. It is seen in these figures that the maximum contact time

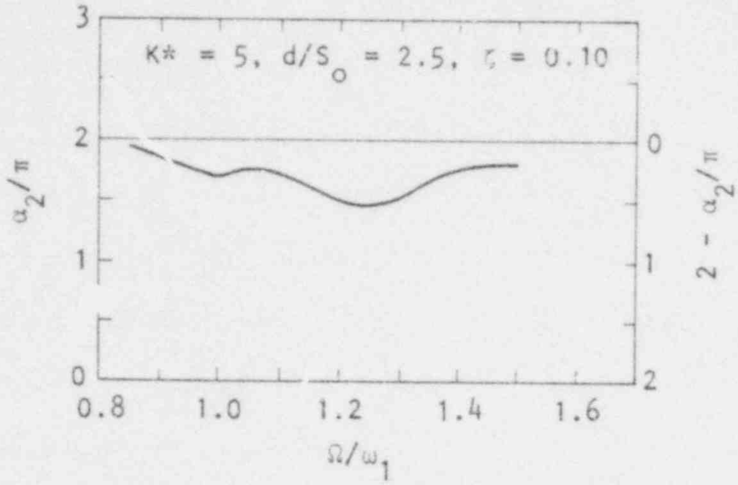

FIGURE 4.27 VARIATION OF DIMENSIONLESS CONTACT TIME WITH FREQUENCY RATIO; $K^* = 5$, $d/S_o = 2.5$, $\zeta = 0.10$

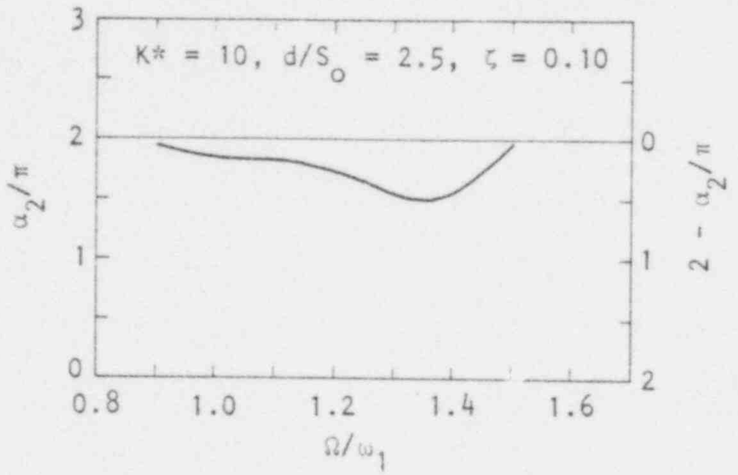

FIGURE 4.28 VARIATION OF DIMENSIONLESS CONTACT TIME WITH FREQUENCY RATIO; $K^* = 10$, $d/S_o = 2.5$, $\zeta = 0.10$

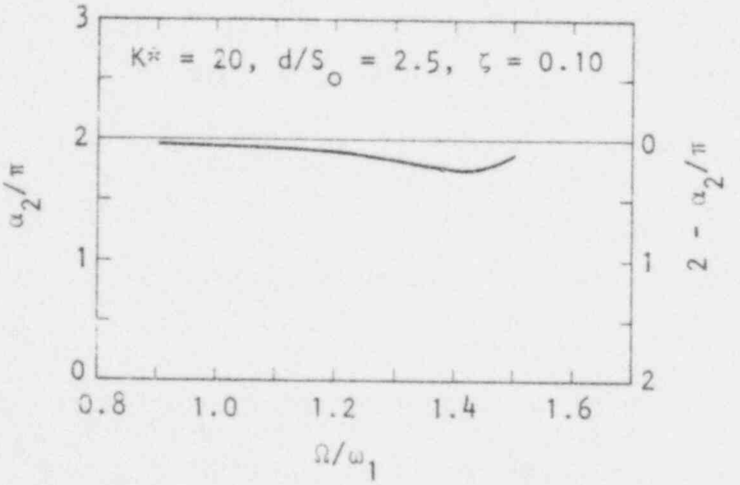

FIGURE 4.29 VARIATION OF DIMENSIONLESS CONTACT TIME WITH FREQUENCY RATIO; $K^* = 20$, $d/S_o = 2.5$, $\zeta = 0.10$

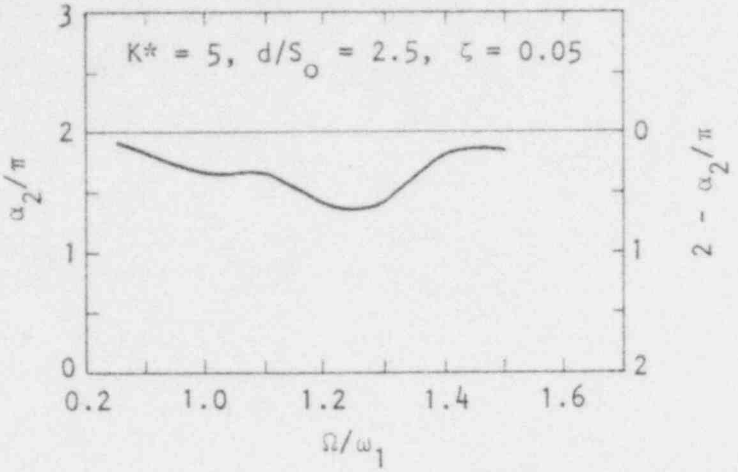

FIGURE 4.30 VARIATION OF DIMENSIONLESS CONTACT TIME WITH FREQUENCY RATIO; $K^* = 5$, $d/S_o = 2.5$, $\zeta = 0.05$

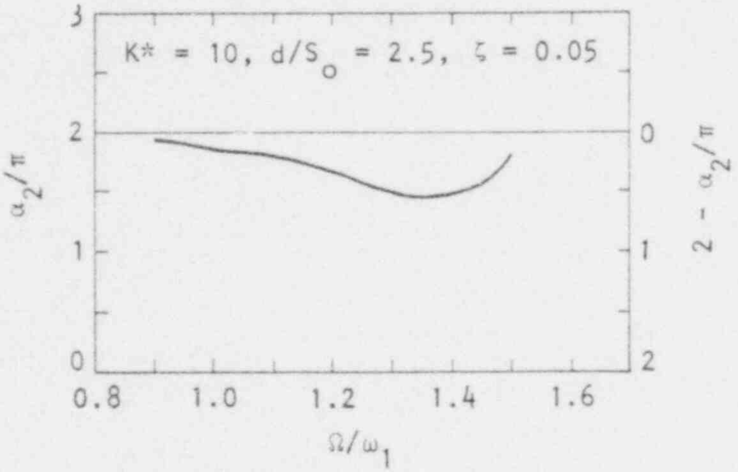

FIGURE 4.31 VARIATION OF DIMENSIONLESS CONTACT TIME WITH FREQUENCY RATIO; $K^* = 10$, $d/S_o = 2.5$, $\zeta = 0.05$

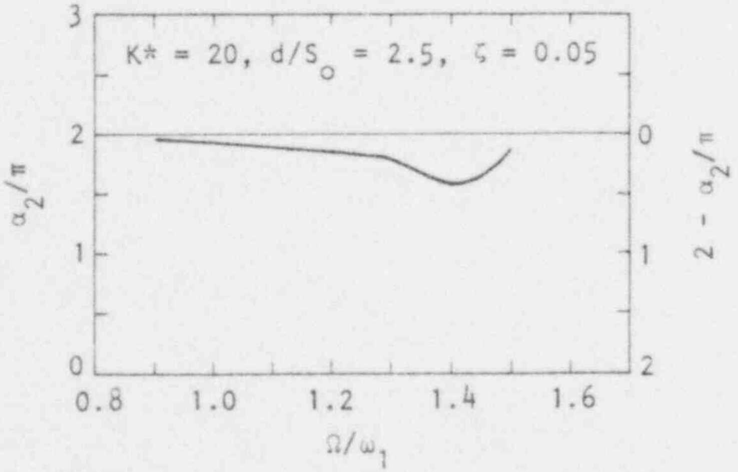

FIGURE 4.32 VARIATION OF DIMENSIONLESS CONTACT TIME WITH FREQUENCY RATIO; $K^* = 20$, $d/S_o = 2.5$, $\zeta = 0.05$

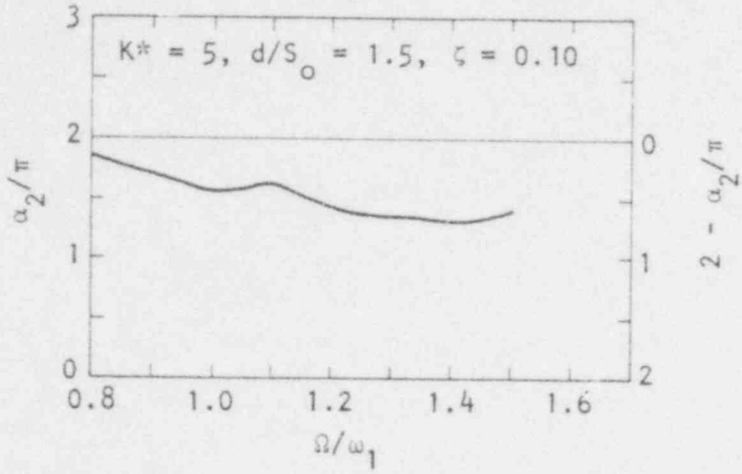

FIGURE 4.33 VARIATION OF DIMENSIONLESS CONTACT TIME WITH FREQUENCY RATIO; $K^* = 5$, $d/S_o = 1.5$, $\zeta = 0.10$

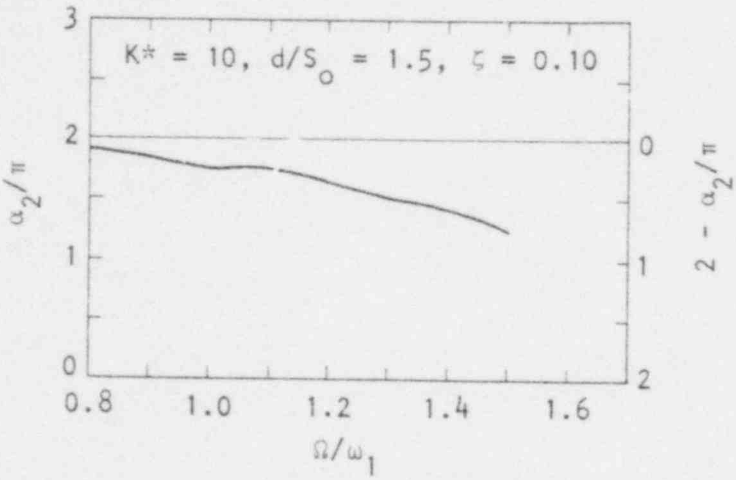

FIGURE 4.34 VARIATION OF DIMENSIONLESS CONTACT TIME WITH FREQUENCY RATIO; $K^* = 10$, $d/S_o = 1.5$, $\zeta = 0.10$

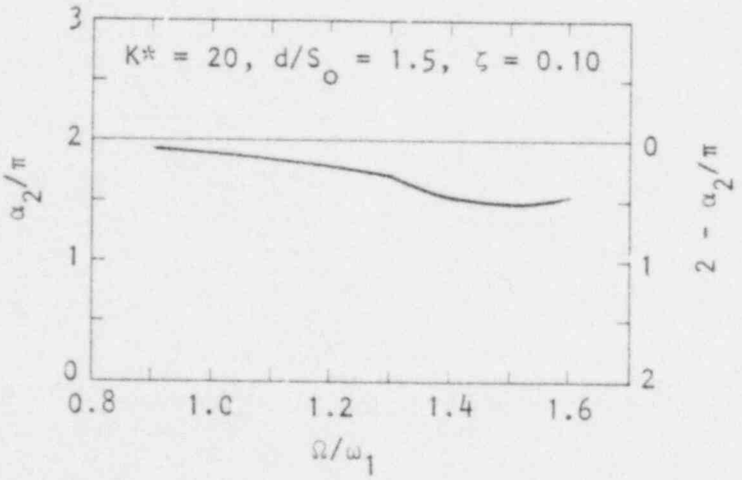

FIGURE 4.35 VARIATION OF DIMENSIONLESS CONTACT TIME WITH FREQUENCY RATIO; $K^* = 20$, $d/S_o = 1.5$, $\zeta = 0.10$

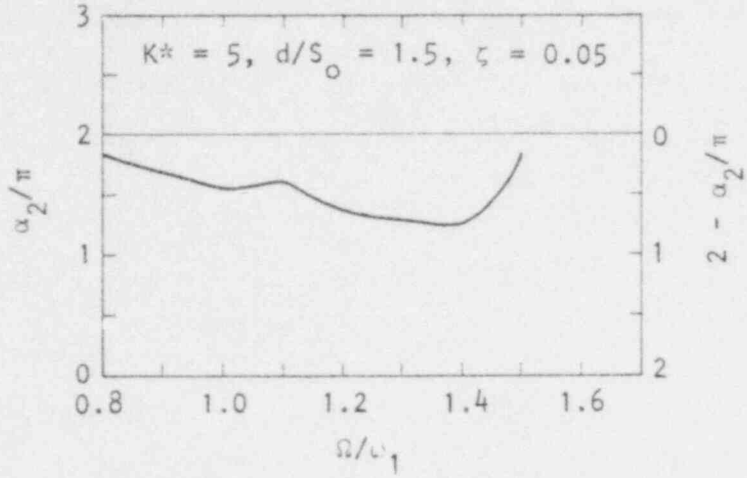

FIGURE 4.36 VARIATION OF DIMENSIONLESS CONTACT TIME WITH FREQUENCY RATIO; $K^* = 5$, $d/S_o = 1.5$, $\zeta = 0.05$

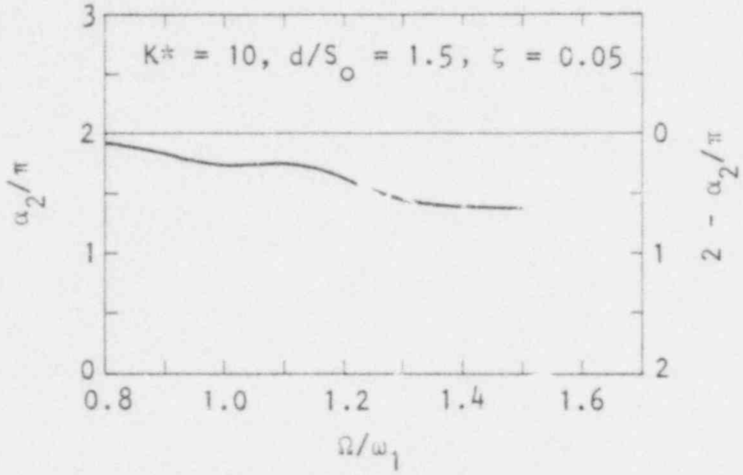

FIGURE 4.37 VARIATION OF DIMENSIONLESS CONTACT TIME WITH FREQUENCY RATIO; $K^* = 10$, $d/S_o = 1.5$, $\zeta = 0.05$

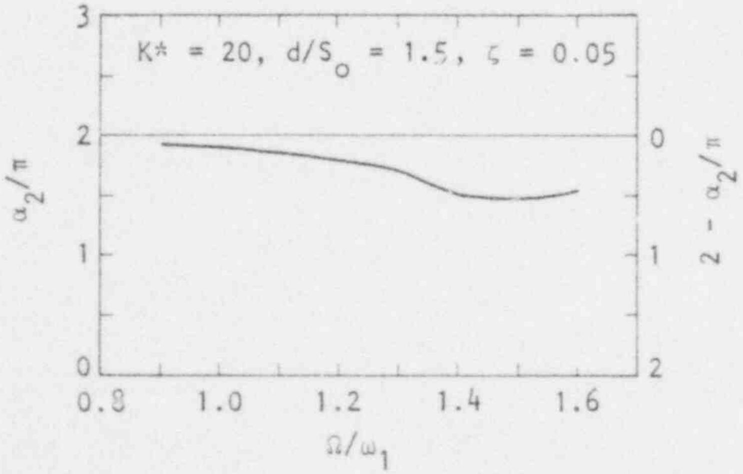

FIGURE 4.38 VARIATION OF DIMENSIONLESS CONTACT TIME WITH FREQUENCY RATIO; $K^* = 20$, $d/S_o = 1.5$, $\zeta = 0.05$

is reduced by increasing the stiffness ratio K*, depending on the excitation frequency range. For example, by increasing the stiffness ratio from 5 to 10, the maximum contact time is reduced 13% at excitation frequency ratios Ω/ω_1 = 1.25 and Ω/ω_1 = 1.35, respectively. This illustrates that the percentage of decrease is not linear. Figures 4.30 through 4.32 are similar to Figures 4.27 through 4.29 except the damping is reduced to 0.05. This reduction affects the contact time ratio α_2/π by increasing the contact time, the amount of increase depending on the stiffness ratio and the excitation frequency ratio. Increasing the damping of the primary system from 0.05 to 0.10 causes a decrease in the maximum contact time of about 5.5% for a stiffness ratio K* equal to 5.0. Figures 4.33 through 4.38 are similar to those of 4.27 through 4.32 except the clearance ratio d/S_0 is reduced about 40%. This was done to see the effect of the gap size on the contact duration. Comparison between Figures 4.27 and 4.33 shows that a 40% reduction in the gap size ratio for a constant stiffness ratio of 5.0 and a 0.10 damping ratio caused an increase of the contact time by at least 7.6% at an excitation frequency ratio Ω/ω_1 = 1.25 and by at most 21% at Ω/ω_1 = 1.42.

Chapter 5

SUMMARY AND CONCLUSIONS

An exact closed-form analytical solution for the steady-state motion of a viscously damped Bernoulli-Euler beam with an unsymmetric geometric nonlinearity was derived using the normal-mode approach. The elastic beam was assumed to have uniform properties and arbitrary boundary conditions, and was subjected to a harmonic excitation. The geometric nonlinearity consists of an elastic spring, placed at some arbitrary location within the span of the beam and separated from the beam by a certain gap.

A computer program was developed for the construction of a typical steady-state solution of an arbitrary example problem based on the formulation presented. The program was designed to solve for the unknowns of the problem using an iteration scheme presented in Section 2.3.4. The program also allowed the use of an arbitrary number of modes. A typical steady-state solution of an arbitrary example problem was presented, as well as a study of the effect of various system parameters.

Experimental studies with a mechanical model were performed to verify the validity of the analytical solution and also to investigate the effect of system parameters. A fairly good agreement between the theoretical and experimental results was achieved.

From the analytical/experimental work carried out in this study, it was found that:

(a) The analytical solution presented herein provided a model for the understanding of the dynamic response of realistic nonlinear structural systems having components that can be modeled as continuous beams with geometric nonlinearity.

(b) The parametric study performed provided useful information regarding the amount of penetration, the duration of contact, and the maximum positive peak displacement.

Additional studies along similar lines are needed. For example, the effect of other types of loads, such as blast or earthquake loads should be considered; and more sophisticated models should be constructed by adding a mass and a dashpot to the elastic stop, or, better yet, by considering the elastic stop as a beam.

Chapter 6

REFERENCES

Anderson, J.C., and Masri, S.F., Analytical/Experimental Correlation of a Nonlinear System Subjected to a Dynamic Load, Report No. CE 79-07, University of Southern California, Los Angeles, June 1979.

Anderson, J.C., and Singh, A.K., "Inelastic Response of Nuclear Piping Subjected to Rupture Forces," Journal of Pressure Vessel Technology, Trans. ASME, Vol. 98, Series J, No. 2, May 1976.

Beaufait, F.W., Basic Concepts of Structural Analysis, Prentice-Hall, Englewood, New Jersey, 1977.

Clough, R.W., and Penzien, J., Dynamics of Structures, McGraw-Hill, New York, 1975.

Den Hartog, J.P., and Heiles, R.M., "Forced Vibrations with Nonlinear Spring Constants," Journal of Applied Mechanics, Vol. 3, Trans. ASME, Vol. 58, 1936, pp. 127-130.

Gorman, D.J., Free Vibration Analysis of Beams and Shafts, John Wiley, New York, 1975.

Iwan, W.D., "Steady-State Dynamic Response of a Limited Slip System," Journal of Applied Mechanics, Vol. 35, Trans. ASME, Vol. 90, 1968, pp. 322-326.

Kotwicki, P.J., Chang, K.C., and Johnson, E.R., "Effects of Restraint Stiffness and Gap on the Dynamic Response of Piping Systems," Third U.S. National Congress on Pressure Vessels and Piping, ASME, San Francisco, June 25-29, 1979.

Lee, W.F.Z., and Saibel, E., "Free Vibrations of Constrained Beams," Journal of Applied Mechanics, Trans. ASME, 1952.

Masri, S.F., Analytical and Experimental Studies of Nonlinear System Modeling and Scaling: First Annual Progress Report, NUREG-0192-1, Nuclear Regulatory Commission, Washington, D.C., November 1976.*

Masri, S.F., "Analytical and Experimental Studies of a Dynamic System With a Gap," Journal of Mechanical Design, Vol. 100, Trans. ASME, July 1978, pp. 480-486.

McBride, E.J., and Jeannette, P.A., "The Free Lateral Vibrations of a Cantilever Beam with a Terminal Dashpot," Journal of Applied Mechanics, Vol. 65, Trans. ASME, September 1943, pp. A168-A172.

Moreadith, F.L., et al., "Structural Analysis and Design of Pipe Whip Restraints," Structural Design of Nuclear Power Plants, Vol. 2, ASCE, December 1973.

Norris, C.H., and Wilbur, J.B., Elementary Structural Analysis, McGraw-Hill, New York, 1960.

Onesto, A.T., "A Snubber Response Sensitivity Study," Third U.S. National Congress on Pressure Vessels and Piping, ASME, San Francisco, California, June 25-29, 1979.

Stoker, J.J., "Nonlinear Vibration in Mechanical and Electrical Systems," Interscience, New York, 1950.

Timoshenko, S., and Young, D.H., Theory of Structures, McGraw-Hill, New York, 1965.

Timoshenko, S., Young, D.H., and Weaver, W., Jr., Vibration Problems in Engineering, John Wiley, New York, 1974.

Watanabe, T., "Forced Vibration of Continuous Systems with Nonlinear Boundary Conditions," Journal of Mechanical Design, Vol. 100, No. 3, Trans. ASME, July 1978, pp. 487-491.

Young, D., "Vibration of a Beam with Concentrated Mass, Spring, and Dashpot," Journal of Applied Mechanics, Vol. 70, Trans. ASME, March 1948, pp. 65-72.

*Available for purchase from the National Technical Information Service, Springfield, VA 22161.

APPENDIX A

DERIVATION OF FREQUENCIES AND MODE SHAPES

A.1 The Governing Differential Equation of Free Vibration

There are two commonly used methods for obtaining solutions to the problem of free vibration of beams. The method most frequently used, where possible, is to solve the beam differential equation that expresses equilibrium between inertia forces and elastic restoring forces, subject to prescribed boundary conditions. The second method is an energy method, which consists essentially of utilizing the fact that in free vibration the sum of the beam's potential energy, due to its departure from a static equilibrium configuration, and the kinetic energy, due to the motion of its particles, is constant.

The differential equation governing the free vibration of uniform beams is

$$\frac{\partial^2 W(x,t)}{\partial t^2} + \frac{EI}{\rho A}\frac{\partial^4 W(x,t)}{\partial x^4} = 0 \qquad (A.1)$$

where $W(x,t)$ is the transverse displacement of the beam; E, I, A, and ρ are the modulus of elasticity, moment of inertia, cross-sectional area and density of the beam, respectively; and t is the time.

In Equation A.1, the effect of shear strain and rotary inertia are neglected. Using the first method mentioned above, Equation A.1 can be solved by means of separation of variables. This can be done by expressing the displacement $W(x,t)$ as

$$W(x,t) = X(x) \cdot T(t) \tag{A.2}$$

where $X(x)$ is a function of x only and $T(t)$ is a function of t only. Substitution of Equation A.2 into Equation A.1 yields the following two ordinary differential equations:

$$\frac{d^2T(t)}{dt^2} + \omega^2 T(t) = 0 \tag{A.3}$$

and

$$\frac{d^4X(x)}{dx^4} - \beta^4 X(x) = 0 \tag{A.4}$$

where

$$\beta^4 = \rho \frac{A}{EI}^2 \tag{A.5}$$

and ω is the circular frequency of the beam vibration.

The solutions for these equations are

$$X(x) = A \sin \beta x + B \cos \beta x + C \sinh \beta x + D \cosh \beta x \tag{A.6}$$

and

$$T(t) = \cos (\omega t + \alpha) \tag{A.7}$$

where α is a phase angle depending on the initial conditions.

The four constants A, B, C, and D in Equation A.6 define the shape and amplitude of the beam vibration. These constants must be evaluated by consideration of the boundary conditions at the ends of the beam segment. Two conditions expressing the displacement, slope, moment, or shear force will be defined at each end of the beam segment. These may be used to express three of the four constants in terms of the fourth and will also provide the frequency equation from which the frequency parameter β, and hence the value of ω, can be evaluated. The fourth constant cannot be evaluated directly in a free vibration analysis. This constant defines the amplitude of motion, which depends on the initial conditions.

A.2 Boundary Conditions

Beams may be subjected to two types of boundary conditions: classical and nonclassical.

A.2.1 Classical Boundary Conditions

These types of boundary conditions involve only the shape of the beam deflection curve at its boundaries. They consist of the following:

1. Free Boundary Conditions

   These conditions specify that the moment as well as the shear force at the beam boundary are equal to zero, i.e.,

$$\left.\frac{d^2X(x)}{dx^2} = \frac{d^3X(x)}{dx^3}\right|_{\text{boundary}} = 0 \qquad (A.8)$$

2. Clamped Boundary Conditions

   Clamped boundary conditions specify that the displacement as well as the slope of the beam should equal zero, i.e.,

$$X(x) = \left.\frac{dX(x)}{dx}\right|_{\text{boundary}} \qquad \text{(A.9)}$$

3. Simple Boundary Conditions

This case of boundary conditions states that the displacement as well as the curvature of the beam boundary should equal zero, i.e.,

$$X(x) = \left.\frac{d^2X(x)}{dx^2}\right|_{\text{boundary}} \qquad \text{(A.10)}$$

A.2.2 Nonclassicial Boundary Conditions

Only one kind of nonclassical boundary conditions will be mentioned here -- the lateral coil spring. It is the type that may be used for the solution of the problem of concern. This condition states that at the position of the spring, the shear force on the beam is equal to the spring restoring force or

$$EI\frac{d^3X(x)}{dx^3} = KX(x) \qquad \text{(A.11)}$$

A.3 Formulation of the Solution

Two cases will be considered here, the clamped-free beam and the clamped-constrained beam (i.e., the cantilever beam with a coil spring at its end). Other combinations could be similarly derived.

A.3.1 Clamped-Free Beam

For the case of the clamped-free (cantilever) beam, Figure A.1a, the boundary conditions are as follows. At the end $x = 0$, the boundary conditions are of the type 2, i.e., Equation A.9 or

$$X(x)\Big|_{x=0} = \frac{dX(x)}{dx}\Big|_{x=0} = 0 \qquad (A.12)$$

whereas at the end $x = L$, the boundary conditions are of type 1, i.e., Equation A.8 or

$$\frac{d^2X(x)}{dx^2}\Big|_{x=t} = \frac{d^3X(x)}{dx^3}\Big|_{x=L} \qquad (A.13)$$

These boundary conditions, when substituted in Equation A.6, yields

$$\begin{bmatrix} \sin \beta L + \sinh \beta L & \cos \beta L + \cosh \beta L \\ \cos \beta L + \cosh \beta L & \sinh \beta L - \sin \beta L \end{bmatrix} \begin{Bmatrix} A \\ B \end{Bmatrix} = \begin{Bmatrix} 0 \\ 0 \end{Bmatrix} \qquad (A.14)$$

For the coefficients to be nonzero, this equation requires that the determinant of the square matrix vanish; setting this determinant equal to zero provides the frequency equation

$$1 + \cos \beta L \cosh \beta L = 0 \qquad (A.15)$$

The solution of this transcendental equation then provides the values of βL which represents the frequencies of vibration of the cantilever beam.

From the two equations in the matrix expression of A.14 and the relationships from the first two boundary conditions, Equation A.6 can

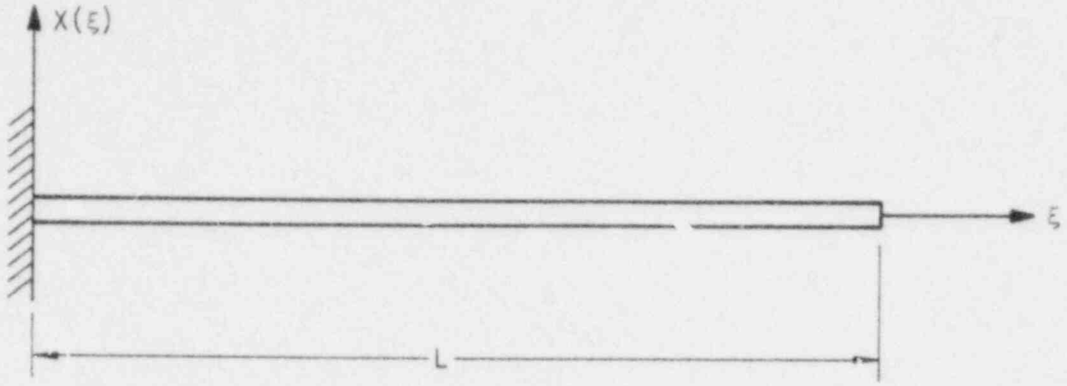

(a) CLAMPED-FREE BEAM

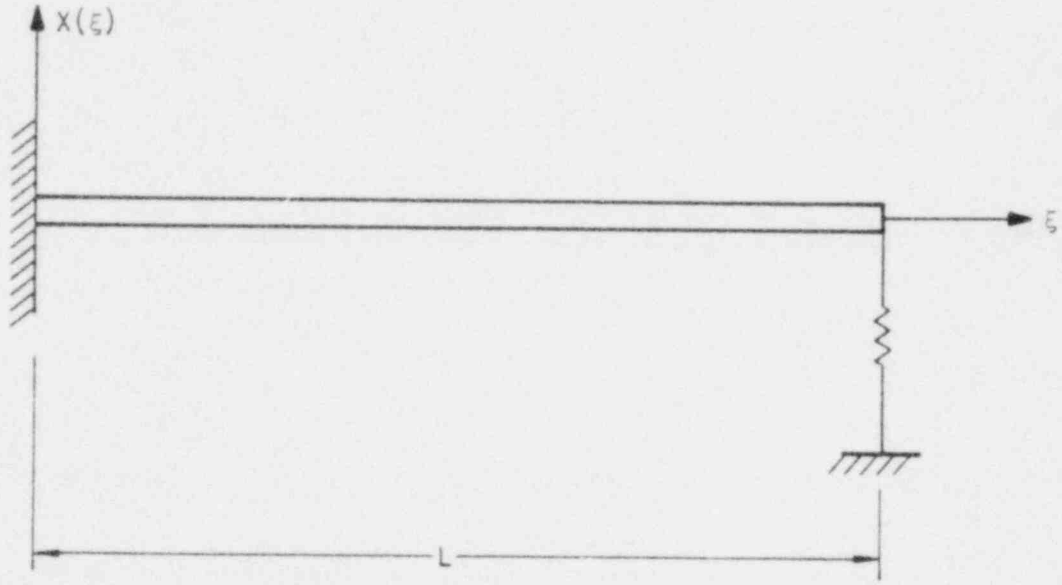

(b) CLAMPED-CONSTRAINED BEAM

FIGURE A-1 TWO BEAM CONDITIONS

be written as

$$X(x) = A\left[\sin \beta x - \sinh \beta x + \ (\cosh \beta x - \cos \beta x)\right] \qquad (A.16)$$

where

$$\gamma = \frac{\sin \beta L + \sinh \beta L}{\cos \beta L + \cosh \beta L} \qquad (A.17)$$

Then the mode shapes can be found by substituting the value of βL that is obtained from the frequency Equation A.15 into the Equation A.16.

A.3.2 Clamped-Constrained Beam

In the case of a cantilever beam supported at its end with a transverse linear coil spring (Figure A.1b), there are three classical boundary conditions to be imposed:

$$X(x)\Big|_{x=0} = 0; \quad \frac{dX(x)}{dx}\Big|_{x=0} \quad \text{and} \quad \frac{d^2X(x)}{dx^2}\Big|_{x=\ell} = 0 \qquad (A.18)$$

The fourth boundary condition is the nonclassical one:

$$EI\,\frac{d^3X(x)}{dx^3} = KX(x)\Big|_{x=L} \qquad (A.19)$$

On substituting Equations A.18 and A.19 into Equation A.6, it is found that $A = -C$, $B = -D$, and the solution for the vibration frequencies requires finding those values of β that satisfy the determinant equation

$$\begin{vmatrix} \sin \beta L + \sinh \beta L & \cos \beta L + \cosh \beta L \\ \cos \beta L + \text{soch } \beta L & (\sin \beta L + \sinh \beta L) \\ + \frac{\bar{K}^*}{3} (\sin \beta L - \sinh \beta L) & + \frac{\bar{K}^*}{3} (\cos \beta L - \cosh \beta L) \end{vmatrix} = \begin{Bmatrix} 0 \end{Bmatrix}$$

(A.20)

where

$$\bar{K}^* = \frac{K}{EI} \tag{A.21}$$

It can be seen from Equation A.20 that as $\bar{K}^*$ approaches zero the equation approaches that of the vibration of a clamped-free beam.

Simplifying Equation A.20 yields

$$\bar{K}^* (\sinh \beta L \cos \beta L - \sin \beta L \cosh \beta L) - \beta^3(1 - \cos \beta L \cosh \beta L) = 0$$

(A.22)

The solution of the characteristic Equation A.22 then provides the values of the frequency of vibration of the system.

In a way similar to the previous case considered, the mode shapes can be obtained as

$$X(x) = \sinh \beta x - \sin \beta x + (\cosh \beta x - \cos \beta x) \tag{A.23}$$

where

$$\gamma = \frac{-(\sin \beta L + \sinh \beta L)}{\cosh \beta L + \cos \beta L}$$

APPENDIX B

DEFINITION OF SYMBOLS

$$\phi_i^{(j)} = \frac{\eta_i^{(j)}}{r_i^{(j)}} (\alpha_{j+1} - \alpha_j)$$

$$\phi_i^{(1)} = \frac{\eta_i^{(1)}}{r_i^{(1)}} (\alpha_2 - \alpha_1) = \frac{\eta_i^{(1)}}{r_i^{(1)}} \alpha_2$$

$$\phi_i^{(2)} = \frac{\eta_i^{(2)}}{r_i^{(2)}} (\alpha_3 - \alpha_2) = \frac{\eta_i^{(2)}}{r_i^{(2)}} (2\pi - \alpha_2)$$

$$E_i^{(j)} = \exp \left[- \frac{\zeta_i^{(j)}}{r_i^{(j)}} (\alpha_{j+1} - \alpha_j) \right]$$

$$E_i^{(1)} = \exp \left[- \frac{\zeta_i^{(1)}}{r_i^{(1)}} (\alpha_2 - \alpha_1) \right] = \exp \left(- \frac{\zeta_i^{(1)}}{r_i^{(1)}} \alpha_2 \right)$$

$$E_i^{(2)} = \exp \left[- \frac{\zeta_i^{(2)}}{r_i^{(2)}} (\alpha_3 - \alpha_2) \right] = \exp \left[- \frac{\zeta_i^{(2)}}{r_i^{(2)}} (2\pi - \alpha_2) \right]$$

$$C11_i^{(j)} = E_i^{(j)} \sin \phi_i^{(j)}$$

$$C12_i^{(j)} = E_i^{(j)} \cos \phi_i^{(j)}$$

$$C13_i^{(j)} = \omega_i^{(j)} \left(\zeta_i^{(j)} \, C12_i^{(j)} - \xi_i^{(j)} \, C11_i^{(j)} \right)$$

$$C14_i^{(j)} = -\omega_i^{(j)} \left(\xi_i^{(j)} \, C12_i^{(j)} + \eta_i^{(j)} \, C11_i^{(j)} \right)$$

$$S1_i^{(j)} = \left(\zeta_i^{(j)} \, C11_i^{(j)} + \xi_i^{(j)} \, C12_i^{(j)} \right) \Big/ \eta_i^{(j)}$$

$$S2_i^{(j)} = \left(1 \Big/ \omega_i^{(j)} \, \eta_i^{(j)} \right) * C11_i^{(j)}$$

$$S3_i^{(j)} = \frac{\omega_i^{(j)}}{\eta_i^{(j)}} \, C11_i^{(j)}$$

$$S4_i^{(j)} = \frac{1}{\omega_i^{(j)} \, \eta_i^{(j)}} \, C13_i^{(j)}$$

$$S5_i^{(j)} = \Omega \, A_i^{(j)} \, S2_i^{(j)}$$

$$S6_i^{(j)} = -A_i^{(j)} \, S1_i^{(j)}$$

$$S7_i^{(j)} = A_i^{(j)}$$

$$S8_i^{(j)} = \Omega \, A_i^{(j)} \, S4_i^{(j)}$$

$$S9_i^{(j)} = -A_i^{(j)} \, S3_i^{(j)}$$

$$S10_i^{(j)} = -A_i^{(j)}$$

$$GO_{\ell m} = \int_0^L \phi_\ell^{(2)}(x)\ M(x)\ \phi_m^{(1)}(x)\ dx$$

$$CO_{\ell k} = \int_0^L \phi_\ell^{(1)}(x)\ M(x)\ \phi_k^{(2)}(x)\ dx$$

$$C1_{\ell m} = GO_{\ell m}\ S3_m^{(1)}$$

$$C2_{\ell m} = GO_{\ell m}\ S4_m^{(1)}$$

$$C3_{\ell m} = GO_{\ell m}\ S8_m^{(1)}$$

$$C4_{\ell m} = GO_{2m}\ S9_m^{(1)}$$

$$C5_{\ell m} = GO_{\ell m}\ S10_m^{(1)}$$

$$C6_{\ell i} = GO_{\ell i}\ S1_i^{(1)}$$

$$C7_{\ell i} = GO_{\ell i}\ S2_i^{(1)}$$

$$C8_{\ell i} = GO_{\ell i}\ S5_i^{(1)}$$

$$C9_{\ell i} = GO_{\ell i}\ S6_i^{(1)}$$

$$C10_{\ell i} = GO_{\ell i}\ S7_i^{(1)}$$

$$h1_j = C75_j + C51_j$$

$$h2_j = C67_j + C52_j$$

$$h3_j = C77_j + C53_j$$

$$h4_j = C78_j + C54_j$$

$$h5_j = C79_j$$

$$h6_j = C55_j$$

$$h7_j = C56_j$$

$$h8_j = C57_j$$

$$h9_j = C58_j$$

$$h10_p = C80_p + C59_p$$

$$h11_p = C81_p + C60_p$$

$$h12_p = C82_p + C61_p$$

$$h13_p = C83_p + C62_p$$

$$h14_p = C84_p$$

$$h15_p = C63_p$$

$$h16_p = C64_p$$

$$h17_p = C65_p$$

$$h18_p = C66_p$$

$$h19_k = C85_k + C67_k$$

$$h20_k = C86_k + C68_k$$

$$h21_k = C87_k + C69_k$$

$$h22_k = C88_k + C70_k$$

$$h23_k = C89_k$$

$$h24_k = C71_k$$

$$h25_k = C72_k$$

$$h26_k = C73_k$$

$$h27_k = C74_k$$

$$h28_i = \phi_i^{(1)}(h)\ S1_i^{(1)}$$

$$h29_i = \phi_i^{(1)}(h)\ S2_i^{(1)}$$

$$h30_i = \phi_i^{(1)}(h)\ S5_i^{(1)}$$

$$h31_i = \phi_i^{(1)}(h)\ S6_i^{(1)}$$

$$h32_i = \phi_i^{(1)}(h)\ S7_i^{(1)}$$

$$h^{(j)}40_i = \cos\left(\alpha_j - \gamma_i^{(j)}\right)$$

$$h^{(j)}41_i = \sin\left(\alpha_j - \gamma_i^{(j)}\right)$$

$$j^{(j)}42_i = \cos\left(\alpha_{j+1} - \gamma_i^{(j)}\right)$$

$$h^{(j)}43_i = \sin\left(\alpha_{j+1} - \gamma_i^{(j)}\right)$$

$$h44_i^{(2)} = \cos \gamma_i^{(2)}$$

$$h45_i^{(2)} = \sin \gamma_i^{(2)}$$

$$h50_j = h3_j h40_j^{(1)} - h4_j h41_j^{(1)} - h5_j h43_j^{(1)} + h6_j h42_j^{(1)}$$
$$+ h7_j h40_j^{(2)} - h8_j h41_j^{(2)} + h9_j h45_j^{(2)}$$

$$h51_j = h3_j h41_j^{(1)} + h4_j h40_j^{(1)} + h5_j h42_j^{(1)} + h6_j h43_j^{(1)}$$
$$+ h7_j h41_j^{(2)} + h8_j h40_j^{(2)} + h9_j h44_j^{(2)}$$

$$h52_p = h12_p h40_p^{(1)} + h13_p h41_p^{(1)} - h14_p h43_p^{(1)} + h15_p h42_p^{(1)}$$
$$+ h16_p h40_p^{(2)} - h17_p h41_p^{(2)} + h18_p h44_p^{(2)}$$

$$h53_p = h12_p h41_p^{(1)} + h13_p h40_p^{(1)} + h14_p h42_p^{(1)} + h15_p h43_p^{(1)}$$
$$+ h16_p h41_p^{(2)} + h17_p h40_p^{(2)} - h18_p h45_p^{(2)}$$

$$h60_k = h21_k h40_k^{(1)} - h22_k h41_k^{(1)} + h23_k h43_k^{(1)} + h24_k h42_k^{(1)}$$
$$+ h25_k h40_k^{(2)} - h26_k h41_k^{(2)} + h27_k h45_k^{(2)}$$

$$h61_k = h21_k h41_k^{(1)} + h22_k h40_k^{(1)} + h23_k h42_k^{(1)} + h24_k h43_k^{(1)}$$
$$+ h25_k h41_k^{(2)} - h26_k h40_k^{(2)} + h27_k h44_k^{(2)}$$

$$h62_i = h30_i h40_i^{(1)} - h31_i h41_i^{(1)} + h32_i h43_i^{(1)}$$

$$h62_i = h30_i h41_i^{(1)} = h31_i h40_i^{(1)} + h32_i h42_i^{(1)}$$

$$C51_m = \sum_i \frac{1}{M_i^{(2)}} \phi_i^{(2)}(x) \; S2_i^{(2)} \; C1_{im}$$

$$C52_m = \sum_i \frac{1}{M_i^{(2)}} \phi_i^{(2)}(x) \; S2_i^{(2)} \; C2_{im}$$

$$C53_m = \sum_i \frac{1}{M_i^{(2)}} \phi_i^{(2)}(x) \; S2_i^{(2)} \; C3_{im}$$

$$C54_m = \sum_i \frac{1}{M_i^{(2)}} \phi_i^{(2)}(x) \; S2_i^{(2)} \; C4_{im}$$

$$C55_m = \sum_i \frac{1}{M_i^{(2)}} \phi_i^{(2)}(x) \; S2_i^{(2)} \; C5_{im}$$

$$C56_i = \phi_i^{(2)}(x) \; S5_i^{(2)}$$

$$C57_i = \phi_i^{(2)}(x) \; S6_i^{(2)}$$

$$C58_i = \phi_i^{(2)}(x) \; S7_i^{(2)}$$

$$C59_m = \sum_i \frac{1}{M_i^{(2)}} \phi_i^{(2)}(x) \; S4_i^{(2)} \; C1_{im}$$

$$C60_m = \sum_i \frac{1}{M_i^{(2)}} \phi_i^{(2)}(x) \; S4_i^{(2)} \; C2_{im}$$

$$C61_m = \sum_i \frac{1}{M_i^{(2)}} \phi_i^{(2)}(x)\; S4_i^{(2)}\; C3_{im}$$

$$C62_m = \sum_i \frac{1}{M_i^{(2)}} \phi_i^{(2)}(x)\; S4_i^{(2)}\; C4_{im}$$

$$C63_m = \sum_i \frac{1}{M_i^{(2)}} \phi_i^{(2)}(x)\; S4_i^{(2)}\; C5_{im}$$

$$C64_i = \phi_i^{(2)}(x)\; S8_i^{(2)}$$

$$C65_i = \phi_i^{(2)}(x)\; S9_i^{(2)}$$

$$C66_i = \phi_i^{(2)}(x)\; S10_i^{(2)}$$

$$C67_m = \sum_i \frac{1}{M_i^{(2)}} \phi_i^{(2)}(h)\; S1_g^{(2)}\; C1_{im}$$

$$C68_m = \sum_i \frac{1}{M_i^{(2)}} \phi_i^{(2)}(h)\; S2_i^{(2)}\; C2_{im}$$

$$C69_m = \sum_i \frac{1}{M_i^{(2)}} \phi_i^{(2)}(h)\; S2_i^{(2)}\; C3_{im}$$

$$C70_m = \sum_i \frac{1}{M_i^{(2)}} \phi_i^{(2)}(h)\; S2_i^{(2)}\; C4_{im}$$

$$C71_m = \sum_i \frac{1}{M_i^{(2)}} \phi_i^{(2)}(h)\; S2_i^{(2)}\; C5_{im}$$

$$C72_i = \phi_i^{(2)}(h)\; S5_i^{(2)}$$

$$C73_i = \phi_i^{(2)}(h)\ S6_i^{(2)}$$

$$C74_i = \phi_i^{(2)}(h)\ S7_i^{(2)}$$

$$C75_i = \sum_k \frac{1}{M_k^{(2)}}\ \phi_k^{(2)}(x)\ S1_k^{(2)}\ C6_{ki}$$

$$C76_i = \sum_k \frac{1}{M_k^{(2)}}\ \phi_k^{(2)}(x)\ S1_k^{(2)}\ C7_{ki}$$

$$C77_i = \sum_k \frac{1}{M_k^{(2)}}\ \phi_k^{(2)}(x)\ S1_k^{(2)}\ C8_{ki}$$

$$C78_i = \sum_k \frac{1}{M_k^{(2)}}\ \phi_k^{(2)}(x)\ S1_k^{(2)}\ C9_{ki}$$

$$C79_i = \sum_k \frac{1}{M_k^{(2)}}\ \phi_k^{(2)}(x)\ S1_k^{(2)}\ C10_{ki}$$

$$C80_i = \sum_n \frac{1}{M_n^{(2)}}\ \phi_n^{(2)}(x)\ S3_n^{(2)}\ C6_{ni}$$

$$C81_i = \sum_n \frac{1}{M_n^{(2)}}\ \phi_n^{(2)}(x)\ S3_n^{(2)}\ C7_{ni}$$

$$C82_i = \sum_n \frac{1}{M_n^{(2)}}\ \phi_n^{(2)}(x)\ S3_n^{(2)}\ C8_{ni}$$

$$C83_i = \sum_n \frac{1}{M_n^{(2)}}\ \phi_n^{(2)}(x)\ S3_n^{(2)}\ C9_{ni}$$

$$C84_i = \sum_n \frac{1}{M_n^{(2)}}\ \phi_n^{(2)}(x)\ S3_n^{(2)}\ C10_{ni}$$

$$C85_i = \sum_r \frac{1}{M_r^{(2)}} \phi_r^{(2)}(h)\ S1_r^{(2)}\ C6_{ri}$$

$$C86_i = \sum_r \frac{1}{M_r^{(2)}} \phi_r^{(2)}(h)\ S1_r^{(2)}\ C7_{ri}$$

$$C87_i = \sum_r \frac{1}{M_r^{(2)}} \phi_r^{(2)}(h)\ S1_r^{(2)}\ C8_{ri}$$

$$C88_i = \sum_r \frac{1}{M_r^{(2)}} \phi_r^{(2)}(h)\ S1_r^{(2)}\ C9_{ri}$$

$$C89_i = \sum_r \frac{1}{M_r^{(2)}} \phi_r^{(2)}(h)\ S1_r^{(2)}\ C10_{ri}$$

$$Q1_{\ell j} = \sum_k \frac{1}{M_k^{(2)}} CO_{\ell k}\ S1_k^{(2)}\ C6_{kj}$$

$$Q2_{\ell j} = \sum_i \frac{1}{M_i^{(2)}} CO_{\ell i}\ S2_i^{(2)}\ C1_{ij}$$

$$Q3_{\ell j} = \sum_i \frac{1}{M_i^{(2)}} CO_{\ell i}\ S1_i^{(2)}\ C7_{ij}$$

$$Q4_{\ell j} = \sum_i \frac{1}{M_i^{(2)}} CO_{\ell i}\ S2_i^{(2)}\ C2_{ij}$$

$$Q5_{\ell j} = \sum_i \frac{1}{M_i^{(2)}} CO_{\ell i}\ S1_k^{(2)}\ C8_{kj}$$

$$Q6_{\ell j} = \sum_i \frac{1}{M_i^{(2)}} CO_{\ell i}\ S2_i^{(2)}\ C3_{ij}$$

$$Q7_{\ell j} = \sum_k \frac{1}{M_k^{(2)}} CO_{\ell k}\ S1_k^{(2)}\ C9_{kj}$$

$$Q8_{\ell j} = \sum_i \frac{1}{M_i^{(2)}} CO_{\ell i} \; S2_i^{(2)} \; C4_{ij}$$

$$Q9_{\ell j} = \sum_k \frac{1}{M_k^{(2)}} CO_{\ell k} \; S1_k^{(2)} \; C10_{kj}$$

$$Q10_{\ell j} = \sum_i \frac{1}{M_i^{(2)}} CO_{\ell i} \; S2_i^{(2)} \; C5_{ij}$$

$$Q11_{\ell j} = CO_{ij} \; S5_j^{(2)}$$

$$Q12_{\ell j} = CO_{\ell j} \; S6_j^{(2)}$$

$$Q13_{\ell j} = CO_{\ell j} \; S6_j^{(2)}$$

$$Q14_{mp} = \sum_n \frac{1}{M_n^{(2)}} CO_{mn} \; S3_n^{(2)} \; C6_{np}$$

$$Q15_{mp} = \sum_i \frac{1}{M_i^{(2)}} CO_{mi} \; S4_i^{(2)} \; C1_{ip}$$

$$Q16_{mp} = \sum_n \frac{1}{M_n^{(2)}} CO_{mn} \; S3_m^{(2)} \; C7_{np}$$

$$Q17_{mp} = \sum_i \frac{1}{M_i^{(2)}} CO_{mi} \; S4_i^{(2)} \; C2_{ip}$$

$$Q18_{mp} = \sum_n \frac{1}{M_n^{(2)}} CO_{mn} \; S3_n^{(2)} \; C8_{mp}$$

$$Q19_{mp} = \sum_i \frac{1}{M_i^{(2)}} CO_{mi} \; S4_i^{(2)} \; C3_{ip}$$

$$U6_{\ell j} = Q12_{\ell j}$$

$$U7_{\ell j} = Q13_{\ell j}$$

$$H1_{\ell j} = Q1_{\ell j} + Q2_{\ell j}$$

$$H2_{\ell j} = Q3_{\ell j} + Q4_{\ell j}$$

$$H3_{\ell j} = U1_{\ell j}h40_j^{(1)} - U2_{\ell j}h41_j^{(1)} - U3_{\ell j}h43_j^{(1)} + U4_{\ell j}h42_j^{(1)}$$
$$+ U5_{\ell j}h40_j^{(2)} - U6_{\ell j}h41_j^{(1)} + U7_{\ell j}h45_j^{(2)}$$

$$H4_{\ell j} = U1_{\ell j}h41^{(1)} + U2_{\ell j}h40_j^{(1)} + U3_{\ell j}h42_j^{(1)} + U4_{\ell j}h43_j^{(1)}$$
$$+ U5_{\ell j}h41_j^{(2)} + U6_{\ell j}h40_j^{(2)} + U7_{\ell j}h44_j^{(2)}$$

$$H5_{mp} = Q14_{mp} + Q15_{mp}$$

$$H6_{mp} = Q16_{mp} + Q17_{mp}$$

$$H7_{mp} = U8_{mp}h40_p^{(1)} - U9_{mp}h41_p^{(1)} - U10_{mp}h43_p^{(1)} + U11_{mp}h42_p^{(1)}$$
$$+ U12_{mp}h40_p^{(2)} - U13_{mp}h41_p^{(2)} + U14_{mp}h44_p^{(2)}$$

$$Q20_{mp} = \sum_n \frac{1}{M_n^{(2)}} CO_{mn} \; S3_n^{(2)} \; C9_{np}$$

$$Q21_{mp} = \sum_i \frac{1}{M_i^{(2)}} CO_{mi} \; S4_i^{(2)} \; C4_{ip}$$

$$Q22_{mp} = \sum_n \frac{1}{M_n^{(2)}} CO_{mn} \; S3_n^{(2)} \; C10_{np}$$

$$Q23_{mp} = \sum_i \frac{1}{M_i^{(2)}} CO_{mi} \; S4_i^{(2)} \; C5_{ip}$$

$$Q24_{mp} = CO_{mp} \; S8_p^{(2)}$$

$$Q25_{mp} = CO_{mp} \; S9_p^{(2)}$$

$$Q26_{mp} = CO_{mp} \; S10_p^{(2)}$$

$$U1_{\ell j} = Q5_{\ell j} + Q6_{\ell j}$$

$$U2_{\ell j} = Q7_{\ell j} + Q8_{\ell j}$$

$$U3_{\ell j} = Q9_{\ell j}$$

$$U4_{\ell j} = Q10_{\ell j}$$

$$U5_{\ell j} = Q11_{\ell j}$$

$$H8_{mp} = U8_{mp}h41_p^{(1)} + U9_{mp}h40_p^{(1)} + U10_{mp}h42_p^{(1)} + U11_{mp}h42_p^{(1)}$$

$$+ U12_{mp}h41_p^{(2)} + U13_{mp}h40_p^{(2)} - U14_{mp}h45_p^{(2)}$$

APPENDIX C

COMPUTER PROGRAM

The computer program used for the solution of the problem was developed based on the formulation presented in Chapter 2. The program was designed to solve for the unknowns of the problem, α_2, α_0, q_{i1}, and $\dot{q}_{i1}$, using the iteration scheme presented in Section 4.3.4 and admitting an arbitrary number of modes. The rest of the unknowns, q_{i2} and $\dot{q}_{i2}$, are then found by back substitution, and the time variables, $q_i^j(t)$ and $\dot{q}_i^j(t)$ are computed. The response, velocity, and curvature as functions of time are then easily computed using the proper formulas. A flow chart showing the steps involved for the solution of the problem is given in Figure C.1. The flow chart entries are explained as follows:

1. Input data. The data related to the program are explained below.

E = EE =	Young's modulus of elasticity of the striker beam.
E * I = EI =	Striker beam stiffness (Young's modulus E multiplied by the moment of inertia I.)
L = EL =	Length of the striker beam.
M(x) = DNSTY =	Striker beam mass density per unit length.
$\frac{\Omega}{S_0}$ =	Excitation amplitude level.

d = DS =	Gap size.
$\zeta(1)$ = ZETAI(1) =	First mode damping ratio.
$\zeta(2)$ = ZETAI(2) =	Second mode damping ratio.
$\frac{\Omega}{\omega_1}$ = OMGFAC =	Value of the exciting frequency ratio.
$(\alpha_2)_{initial}$ = AINTLP =	Initial value of α_2/π for iteration.
$(\alpha_2)_{final}$ = AFNLP =	Final value of α_2/π for iteration.
Tolerance $\Delta\left(\frac{\alpha_2}{\pi}\right)$ =	Tolerance level for α_2/π.
(Iteration increment) = INC =	The number of increments for iteration.
(Function tolerance) = EPFMIN =	Iteration tolerance level.
(Maximum number of modes) = MAXNOM =	The maximum number of modes chosen for the solution.
$\Delta\left(\frac{\Omega}{\omega_1}\right)$ = OMGINC =	Increment of the exciting frequency ratio.
$\frac{d}{S_o}$ = GAPFAC	Increment in gap size ratio.
(Maximum iterations) = ITRMAX =	The maximum number of iterations to be used.

2. Frequencies of the free and constrained beams.

   Two different subroutines for the evaluation of the frequencies of each beam constitute part of the program. These subroutines evaluate the required number of frequencies stored and used in other parts of the program, such as the computation of the mode shapes.

3. Mode shapes for the free and constrained beam.

A separate function subroutine for each case is provided to compute the mode shapes where needed.

4. Second derivatives of the mode shapes of the free and constrained beams.

   As with the evaluation of the mode shapes, two function subroutines are available for the computation of the second derivatives of the mode shapes for the free and constrained beams. These second derivatives will be used later in the computation of the curvatures of the beam under consideration.

5. Problem parameters.

   A subroutine was written to compute the following parameters: β and α, the damping parameters that can be related to the frequencies and ratios of critical damping of two modes i and j :

$$\alpha = (2\zeta_1^{(1)} - \beta\omega_1)\omega_1 \tag{C.1}$$

and

$$\beta = \frac{2(\zeta_2^{(1)}\omega_2 - \zeta_1^{(1)}\omega_1)}{(\omega_2^2 - \omega_1^2)} \tag{C.2}$$

$r_i^{(j)} = \frac{\Omega}{\omega_i^{(j)}}$ = Frequency ratio.

$\gamma_i^{(j)} = \frac{\tan^{-1} 2\zeta_i^{(j)} r_i^{(j)}}{(1 - r_i^{(j)})^2}$ = Phase angle.

6. Generalized parameters.

A subroutine for computing the following generalized parameters was written:

a) Generalized mass = $\int_0^L M(x)\left[\phi_i^{(j)}(x)\right]^2 dx = M_i^{(j)}$

b) Generalized stiffness = $M_i^{(j)} * \left[\omega_i^{(j)}\right]^2$

c) Generalized force = $\int_0^L F_0\left[\phi_i^{(j)}(x)\right]^2 dx$

where

$$F_0 = So*\Omega^2*m(x) \qquad (C.3)$$

d) Amplitude ratio = $A_i^{(j)} = \dfrac{(f_i^{(j)}/k_i^{(j)})}{\sqrt{\left(1 - \left[r_i^{(j)}\right]^2\right)^2 + \left[2\zeta_i^{(j)}\, r_i^{(j)}\right]^2}}$

e) The two constant coefficients GO and CO where

$$GO_{ij} = \int_0^\ell \phi_i^{(2)}(x)\, M(x)\, \phi_j^{(1)}(x)\, dx \qquad (C.4)$$

$$CO_{ij} = \int_0^\ell \phi_i^{(1)}(x)\, M(x)\, \phi_j^{(2)}(x)\, dx \qquad (C.5)$$

A subroutine that utilizes the Simpson rule is available for the computation of all the integrations involved.

7. At this point, all the quantities that are independent of the unknowns of the problem, viz., α_2, α_0, q_{i1} and $\dot{q}_{i1}$, are computed

and an iteration scheme is started by assuming a value for the unknown α_2. This iteration scheme was presented in Section 2.3.4.

8. Using the assumed value of α_2, the coefficients of the unknowns q_{i1}, $\dot{q}_{i1}$, $\sin \alpha_0$, and $\cos \alpha_0$ are evaluated using a subroutine (COFIM) written for this purpose.
9. A matrix of the computed coefficients of previously mentioned unknowns is formed using a subroutine (COFMAT). This subroutine also forms the right hand side vector of the equations of the problem unknowns (Equations 2.37 through 2.40).
10. Using matrix inversion (used in this program) or any simultaneous equations solution technique, the equations are solved for the unknowns using the first assumed value of α_2.
11. At this point, the values of $\sin \alpha_0$ and $\cos \alpha_0$ found from this solution is checked for a unique value of α_2 using the formula

$$\text{Test} = \sin \alpha_0 \pm \sqrt{1 - \cos^2\alpha_0} \qquad (C.6)$$

If the test value is within a certain acceptable range, depending on the accuracy required, then the required solution for the unknowns is already achieved; otherwise, the next value of α_2, which is equal to $(\alpha_2 + \Delta\alpha_2)$, is to be used and steps 7, 8, 9 and 10 are repeated again. This iteration procedure should be continued until an acceptable solution is reached.
12. After solving Equations 2.37 through 2.40 for unknowns

q_{i1}, $\dot{q}_{i1}$, α_2, and α_0, the solution for the unknowns $\dot{q}_{\ell 2}$, and $q_{\ell 2}$ is achieved by back substitution into Equations 2.28 and 2.29, respectively. A check of the equations at the different steps of the solution is then carried out to estimate the accuracy of the computations.

13. Computation of the time-dependent variables $q_i^{j}(t)$ and $\dot{q}_i^{j}(t)$, which constitutes the remaining part of the solution, is then carried out using a subroutine designed for computing these quantities through Equations 3.8 and 3.9.

14. Computation of the response $W^{(j)}(x,t)$, the velocity $\dot{W}^{(j)}(x,t)$, and the curvature $\varepsilon(x,t)$ is then carried out in a separate subroutine utilizing Equation 3.6 and the equations

$$\dot{W}^{(j)}(x,t) = \sum_{i=1} \phi_i^{(j)}(x)\, \dot{q}_i^{(j)}(t) \qquad (C.7)$$

and

$$\varepsilon = W''^{(j)}(x,t) = \sum_{i=1} \phi_i''^{(j)}(x)\, q_i^{(j)}(t) \qquad (C.8)$$

15. The peak values of the response are then computed using subroutine MINMAX.

16. Two different plotting routines are used when required to plot the displacement, the velocity, and the curvature. One of these two routines draws the required curves on computer paper. This routine shows only specified symbols such as dots or x's at the points where the response is computed. The second rou-

tine draws curves and symbols on draft paper, calling a system routine written for this purpose.

17. The program is designed to solve the problem for different values of the excitation frequency ratio Ω/ω_1 by adding specified increments of the exciting frequency ratio if desired. This is achieved by specifying a starting value, an increment, and a maximum value of the excitation frequency ratio Ω/ω_1.

18. At this step an increment $\Delta(d/S_o)$ of the clearance ratio d/S_o may be added and the program is repeated again for the new value of the gap size.

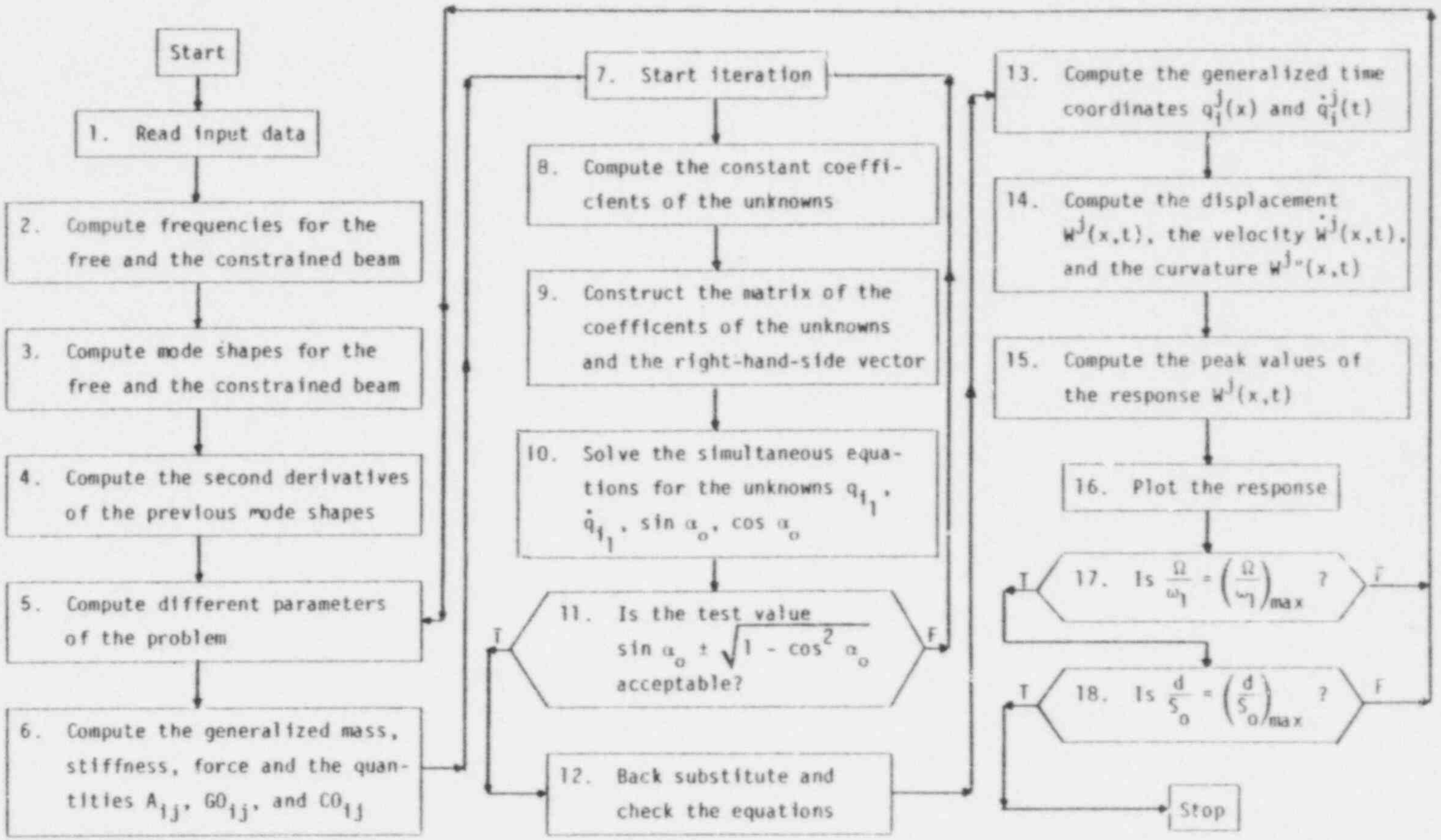

FIGURE C-1 COMPUTER PROGRAM FLOW CHART

NRC FORM 335 (7-77) U.S. NUCLEAR REGULATORY COMMISSION

BIBLIOGRAPHIC DATA SHEET

1. REPORT NUMBER (Assigned by DDC): NUREG/CR-1318

4. TITLE AND SUBTITLE (Add Volume No., if appropriate)

ANALYTICAL AND EXPERIMENTAL STUDIES OF A BEAM WITH A GEOMETRIC NONLINEARITY

2. (Leave blank)

3. RECIPIENT'S ACCESSION NO.

7. AUTHOR(S)

Y.A. Mariamy. S.F. Masri, J.C. Anderson

5. DATE REPORT COMPLETED

MONTH	YEAR
June	1980

9. PERFORMING ORGANIZATION NAME AND MAILING ADDRESS (Include Zip Code)

University of Southern California
Department of Civil Engineering
University Park
Los Angeles, California 90007

DATE REPORT ISSUED

MONTH	YEAR
November	1980

6. (Leave blank)

8. (Leave blank)

12. SPONSORING ORGANIZATION NAME AND MAILING ADDRESS (Include Zip Code)

Office of Nuclear Regulatory Research
U.S. Nuclear Regulatory Commission
Washington, D.C. 20555

10. PROJECT/TASK/WORK UNIT NO.

11. CONTRACT NO.

FIN No. B5976

13. TYPE OF REPORT: TOPICAL

PERIOD COVERED (Inclusive dates): 10/1/78 - 9/30/79

15. SUPPLEMENTARY NOTES

14. (Leave blank)

16. ABSTRACT (200 words or less)

Analytical and experimental studies of the dynamic response of a system with a geometric nonlinearity that is encountered in many practical engineering applications are described. An exact solution for the steady-state motion of a viscously damped Bernoulli-Euler beam with an unsymmetric geometric nonlinearity, under the action of harmonic excitation, is derived. Experimental measurements with a mechanical model verify the analytical findings. The effect of various parameters on the system response is determined. Major conclusions based on this investigation are presented.

17. KEY WORDS AND DOCUMENT ANALYSIS

17a. DESCRIPTORS

17b. IDENTIFIERS/OPEN-ENDED TERMS

18. AVAILABILITY STATEMENT

Unlimited

19. SECURITY CLASS (This report): Unclassified

20. SECURITY CLASS (This page): Unlcassified

21. NO. OF PAGES

22. PRICE: $